Inaugural-Dissertation zur Erlangung der Doktorwürde der Philosophischen Fakultät II (Psychologie, Pädagogik und Sportwissenschaft) der Universität Regensburg

DISSERTATION THESIS

Neuronal dynamics of visual movement processing areas

A fMRI investigation of the connectivity of visual processing areas for motion processing and attention in the human brain.

Dipl. psych. Ferenc Acs, Regensburg, Germany

2009

Supervised by: Prof. Dr. rer. nat. Mark W. Greenlee
Reviewed by: Prof. Dr. rer. nat. Elmar W. Lang

Contents

List of Tables

List of Figures

Part I.

Foundations

1. Introduction

1.1. Aim of this work

The work presented here can be seen as a documentation of a project that took nearly five years to complete. At the end of this project we got a much clearer idea about the interplay of different brain areas during visual motion processing . The statistical methods used for this work are new developments in the area of functional brain imaging (fMRI) , which was made possible by the discovery of the BOLD response by Prof. Seiji Ogawa (Ogawa, Lee, Kay, & Tank, 1990). In the following decade it was possible to compare the level of oxygen in the blood circulating through the human brain between different processing states, this was achieved by comparing the blood oxygen level dependent response (BOLD response).

However, this simple comparison of activity states is an over-simplified approach to a deeper insight in the complex nonlinear dynamics of a network of interacting brain areas. If a analysis of system dynamics is necessary, as was assumed here for a complex analysis of eye movements and attention processing, then the underlying statistical methods should provide more than simple state comparisons. Models that are founded in General

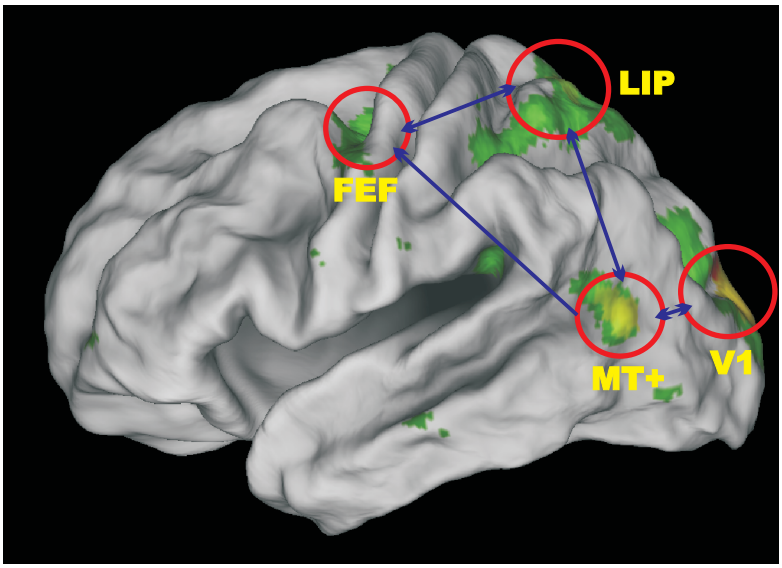

Figure 1.1.: A computer generated activity map of the left hemisphere of a human brain during a visual processing task for eye movements. The brain areas with a significant higher activity during the processing task are colored. These high activity areas are named according their functional properties for the human visual system, i.E. V1 = primary visual cortex, MT+ = middle temporal area, LIP = lateral intraparietal area, FEF = frontal eye fields. These areas form a interconnected system for the processing of eye movements. (see section 1.2.1)

Systems Theory seemed most promising for this kind of approach (Stephan, 2004).

So new methods emerged, which could give us a more sophisticated insight in the processing of the human brain. The method used in this work was the method of dynamic causal modeling (DCM), which makes it possible to investigate the interaction between brain regions (Friston, Harrison, & Penny, 2003). With this method it is possible to construct networks of interacting brain regions (see figure 1.1) and to evaluate the effects of experimental conditions on the network in question (see figure 1.2). Based on these methods we get an insight in the dynamics of the human brain in action and get a clearer idea how different visual processing areas are interacting in the human brain.

The other approach considered here was the theoretical discipline of mathematical modeling of biological neural networks. What DCM measures can be seen as the interaction of very large scale neural networks (i.e. brain regions), this work shows that meaningful conclusions from fMRI experiments, combined with the method of DCM analysis can be drawn to support or falsify assumptions for certain mathematical models. These models are called neural mass models and are one of the later classes of models that come from the discipline of mathematical modeling of biological neural networks (Trappenberg, 2002; Herz, Gollisch, Machens, & Jaeger, 2006; Deco, Jirsa, Robinson, Breakspear, & Friston, 2008).
The interaction of these different approaches leads to a method of analysis for fMRI data, which gives us deeper insights in the human brain, allowing us to see in a much wider scope that is defined in it fundamentals by General Systems Theory (Stephan, 2004).

1.2. Eye movements

A major part of this work was the investigation of the neuronal dynamics involved in the control of eye movements. So far there is a distinction between two major classes of eye

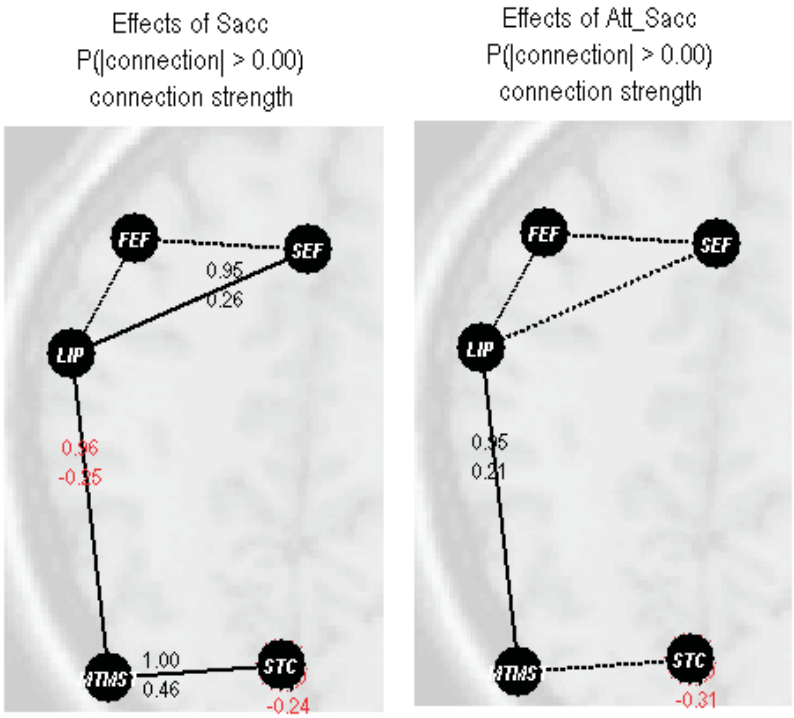

Figure 1.2.: A graphical depiction of the result of a single subject DCM analysis. The interaction of five different brain regions was modeled and measured for a eye movement paradigm. The brain regions can be seen as very large biological neural networks that influence each other, depending on the experimental condition the subject is performing. The left side shows the system state while the subject made saccadic eye movements, the right side shows the system state while the subject attending to the saccade target while a fixation cross was fixated, this is called a covert attention task.

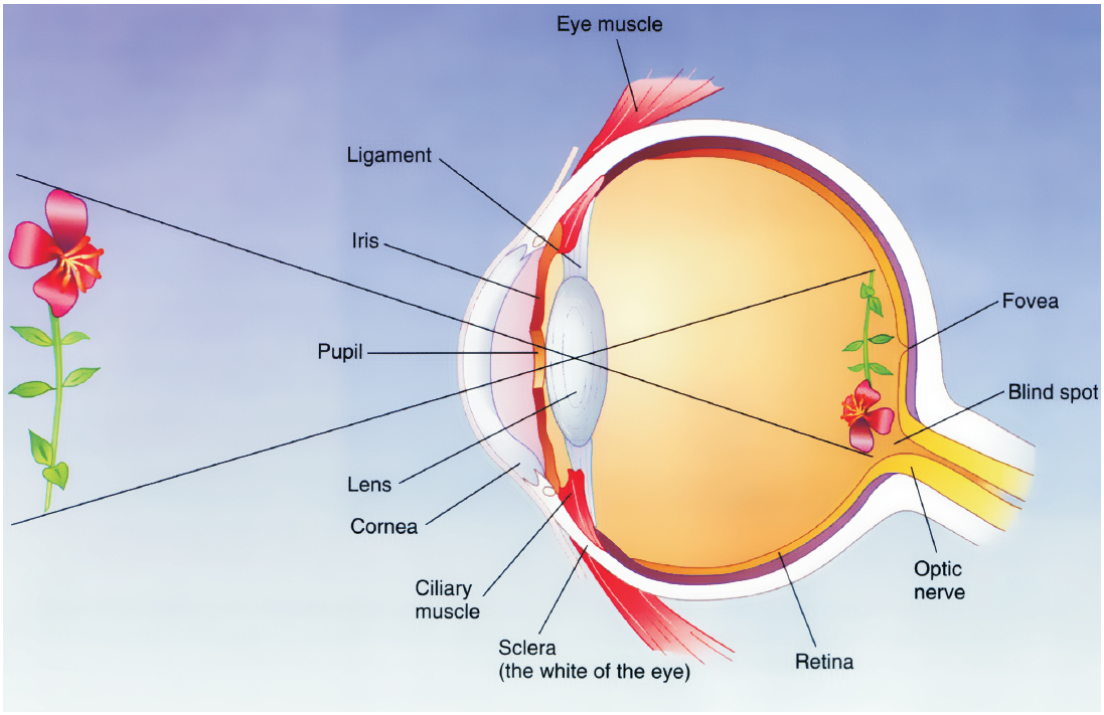

Figure 1.3.: Schematic depiction of the human eye, sagittal view. From: Pinel, 2000

movements. Smooth pursuit eye movements and saccadic eye movements (Leigh & Zee, 2006), the description of both can be found in the next two sections (section 1.2.1 and section 1.2.2). The research about eye movement processing suggested, until some years ago, that there is a strict distinction between networks of brain areas controlling two major kinds of eye movements. This separation seemed valid for a long time, because the brain areas involved in the two kinds of eye movements seem to be separately active when doing some basic neuroscientific research. However, with time, this no longer appeared to be a valid approach (Krauzlis & Stone, 1999), especially not when researching voluntary, attention driven eye movements (Krauzlis, 2005).

1.2.1. Smooth Pursuit Eye movements

Voluntary eye movements of primates can be categorized in two classes of eye movements. One form of eye movements are smooth pursuit eye movements, which allows the eye to

smoothly rotate in pursuit of a moving target falling within the fovea centralis, see figure 1.3. The fovea centralis is the part of the retina that provides the highest resolution of the retinal image. Pursuit eye movements keep the retinal image of a moving target in the area of the fovea centralis. Smooth pursuit eye movements have been investigated on a neurophysiological basis since the second half of the last century, with a vast amount of research information now available (Leigh & Zee, 2006). More elaborated theories about sensorimotor interactions in the central nervous system emerged during the 1980's, driven mainly by lesion studies on the animal brain (Lisberger, Morris, & Tychsen, 1987). Neural pathways and brain areas included in the processing of smooth pursuit eye movements became clearer and first assumptions concerning which areas of the cerebral cortex of mammals should be included were put on a more solid foundation of scientific evidence. In their overview article Lisberger et al. (1987) already mentioned the striate cortex, the middle temporal visual area, the middle superior temporal area and the posterior parietal cortex, as areas of the cerebral cortex that were essential for the study of pursuit eye movements.

1.2.2. Saccadic Eye movements

Another class of eye movements are saccadic eye movements. This class can be observed when a new target appears in the visual field (see figure 1.3). Then a fast eye movement is required to place the image of the target in the fovea centralis. This is because the fovea is the place in the retina of the human eye with the highest density of photo-receptors. Objects that need to be seen with a high resolution are aligned with the fovea. The most obvious example is the description of eye movements during reading. The retinal image of a text has to remain static until the letters fixated in the fovea centralis and neighboring letters are recognized. Then the eye can move on to fixate the next sequence of letters forming words (Rayner, 1998). These kind of 'jumping' movements are called saccadic eye movements. Saccadic eye movements are very fast movements and can

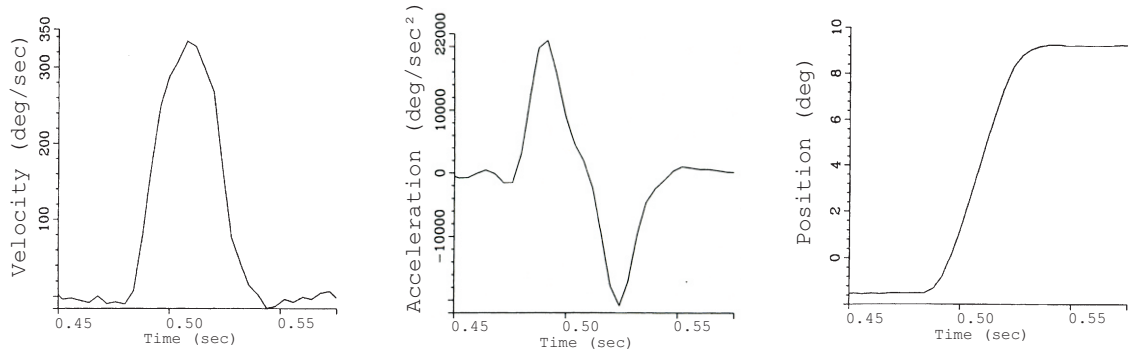

Figure 1.4.: Recording of a rightward 10 saccade of a human subject, showing position velocity and acceleration traces. Data were collected at a 250 Hz sample rate with digital filtering of the velocity (0-100 Hz) and acceleration (0-50 Hz) traces. From: Leigh & Zee, 2006

reach a speed of up to 900°/s and even large saccades can be executed in less than 100ms (Leigh & Zee, 2006). Involuntary saccades made to suddenly appearing flashing objects in the field of view are called reflexive saccades. They are distinguished from voluntary saccades, made while a subject explores an visual scene. Here the subjects guide their eye movements according to the focus of attention. Humans make on average three saccadic eye movements per second when exploring a visual scene (Schiller & Tehovnik, 2005). The neurophysiological basis of saccadic eye movements has also been investigated during the last decades, leading to quite elaborated models of the neurophysiology of saccadic eye movements (Petit & Haxby, 1999; Schiller & Tehovnik, 2005; Leigh & Zee, 2006).

With the emerging new research method of fMRI it was now possible have a closer look on the various activity patterns of the human brain during the processing of saccadic eye movements. At the end of the 1990's the idea became more and more emergent that attentional processes that are involved in the processing of saccadic eye movements probably can be seen in the patterns of activity provided by fMRI recordings (Corbetta et al., 1998).

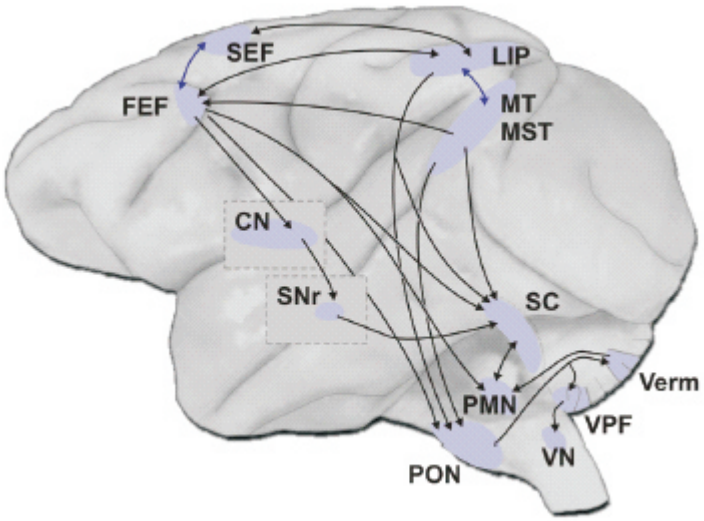

Figure 1.5.: Schematic depiction of the neural pathways for eye movement processing of the macaque monkey in a lateral view. The brain areas for the processing of smooth pursuit and saccadic eye movements are vestibular nuclei VN, ventral paraflocculus in the cerebellum (VPF), oculomotor vermis in the cerebellum (Verm), precerebellar pontine nuclei (PON), premotor nuclei in the brainstem (PMN), superior colliculus SC, SNr, caudate nucleus (CN), middle temporal (MT), middle superior temporal MST, lateral intraparietal area (LIP), frontal eye fields (FEF), supplementary eye fields (SEF). From: Krauzlis, 2005

1.3. The human eye movement system

In the past decades the neuropsychology and neurobiology of the human eye movement system has relied largely on findings that were based on animal models (Leigh & Zee, 2006).For this purpose the macaque monkey served as a good animal model for the human visual system (see figure 1.5 for a schematic depiction).

These findings based on the animal model served well to get an insight how the neural pathways for pursuit and saccadic eye movements are organized. While saccadic eye movements activate other parts of the visual system than smooth pursuit eye movements, so that it was long believed that separate brain areas control these two classes

of eye movements, recent evidence speaks against this strict discrimination (Krauzlis & Stone, 1999). The brain regions mainly for the control of saccadic eye movements were first considered to be lateral intraparietal area (LIP), the frontal eye fields and the supplementary eye fields (SEF). The main regions involved in the processing of smooth pursuit eye movements were considered to be the middle temporal area and the middle superior temporal area (MST), recent evidence points out that subregions in LIP, FEF and SEF are also involved in the processing of smooth pursuit eye movements, so that the classical view of a strict distinction between these processing systems is not longer valid (Krauzlis, 2005).

The work presented here also assumes that the systems for pursuit and saccadic eye movements are partially overlapping and share certain brain regions. This has been shown for the for the frontal eye fields (FEF) of the macaque monkey, which contains subregions that either process pursuit or saccadic eye movements (Tehovnik, Sommer, Chou, Slocum, & Schiller, 2000). There is evidence for assuming that the FEF regions of humans are composed in a similar way (Rosano et al., 2002).

1.3.1. Primary visual cortex, V1

The primary visual cortex is the first stage of cortical processing where signals from the retina are analyzed. The functional equivalent of the primary visual cortex, also known as the striate cortex, is V1 (Lynch & Tian, 2005; Leigh & Zee, 2006). The principal architecture of V1, its organization into direction sensitive columns and ocular dominance columns, in primates has been known since the mid part of the last century (Hubel & Wiesel, 1968, 1974). With emerging neuroimaging techniques the retinotopic organization in humans became clearer (Fox, Miezin, Allman, Essen, & Raichle, 1987), which also led to the revision of the classical Holmes Map by Horton and Hoyt (1991). Recent fMRI studies revealed functional properties of the neuronal pathway from the retina along the optic nerve to the optic chiasm, from where the signal is transmitted

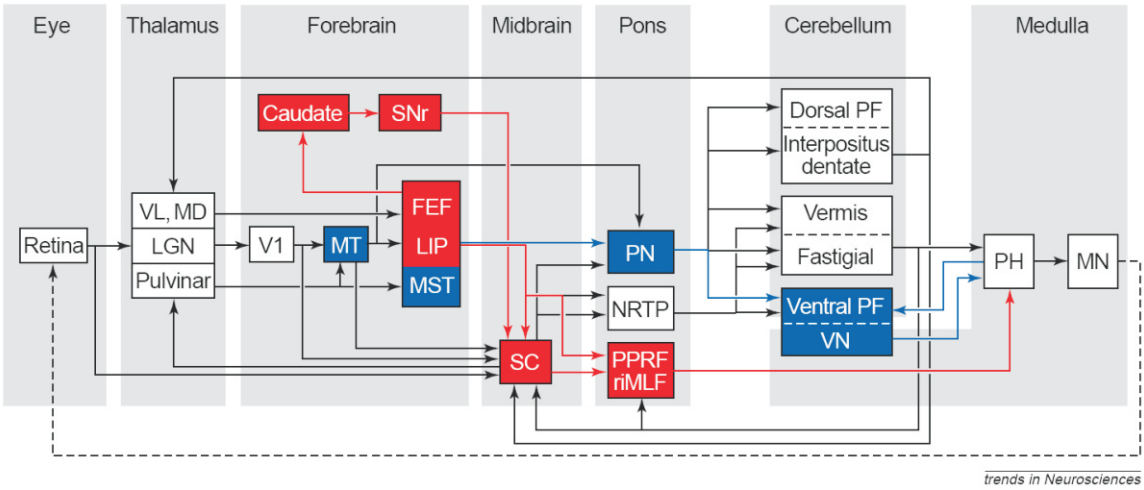

Figure 1.6.: Classical model of the neural pathways in the brain of the macaque monkey for pursuit and saccadic eye movements. The animal model is the best researched and is serving as a model for the human eye movement system. Gray shaded regions are representing brain structures, boxes are representing specific brain regions. The major pathways for pursuit (blue) and saccades (red) are highlighted, according to the traditional distinction between these systems. The solid lines represent the physiological connections between brain regions. The dashed line represents the physical link between the motor neurons (MN, oculomotor nuclei) and the retina. FEF, frontal eye fields; LGN, lateral geniculate nucleus; LIP, lateral intraparietal area; MD, mediodorsal nucleus; MST, middle superior temporal area; MT, middle temporal area; NRTP, nucleus reticularis tegmenti pontis; PF, paraflocculus; PH, nucleus prepositus hypoglossi; PN, basilar pontine nuclei; PPRF, paramedian pontine reticular formation; riMLF, rostral interstitial nucleus of the medial longitudinal fasciculus; SC, superior colliculus; SNr, substantia nigra pars reticulata; V1, primary visual cortex; VL, ventrolateral nucleus; VN, vestibular nuclei. From: Krauzlis & Stone, 1999

further to the lateral geniculate nucleus in the thalamus and to the primary visual cortex.

1.3.2. Human middle temporal area, V5 or hMT+

The middle temporal area is mainly for visual motion processing (Komatsu & Wurtz, 1988a) and plays a central role in the control of smooth pursuit eye movements (Komatsu & Wurtz, 1988b; Newsome, Wurtz, & Komatsu, 1988; Grosbras, Laird, & Paus, 2005; Lynch & Tian, 2005; Leigh & Zee, 2006). Its main purpose is to segregate moving versus non moving parts of the retinal image, as shown by neurocomputational simulations (Grossberg, Mingolla, & Pack, 1999; Furman & Gur, 2003). From previous animal studies it was common to distinguish between the middle temporal area (MT) and the middle superior temporal area (MST). MST corrects for the retinal image motion after it was processed by MT. Object motion is separated from retinal slip caused by eye movements. This is achieved by a functional linkage between MST and areas in the cerebellum that are involved in motor control of the eye muscles. However, due to technical limitations it was long not possible to distinguish in fMRI images of the human brain between MT and MST. So the human analog to MT and MST in the monkey brain was called hMT+ for human middle temporal plus. Only in the recent years, using MRT scanners using higher field strengths, it became possible to distinguish the human analogous to MT and MST (Huk, Dougherty, & Heeger, 2002). However this distinction was not used in the present thesis, because even with high field strengths it was not possible to scan this region in a sufficient resolution.

The role of MT and MST in attention processing has been researched now nearly for one decade. Treue and Maunsell (1999) have shown gain effects of visual attention in a microelectrode study, macaque monkey MT areas showed up to 70% signal gain and up to 100% gain in MST when attention was directed in the receptive field, compared to a locus of attention outside the receptive field of the respective cell populations. Busse, Katzner, and Treue (2008) had studied the effects of endogenous and exogenous

attentional cuing and its effects on the media temporal area in macaque monkeys. Their findings suggest that there are significant attention effects in MT neurons and even endogenous and exogenous cues for attention shifting can be discriminated in the brain of macaque monkeys. Also Womelsdorf, Anton-Erxleben, and Treue (2008) showed effects of spatial attention on the gain modulation of neuronal populations in the middle temporal visual area of macaque monkeys.

1.3.3. Lateral intraparietal area, LIP

The lateral intraparietal area seemed to be involved in preparation of saccades and simple forms of perceptual decision making (Grosbras et al., 2005; Lynch & Tian, 2005; Leigh & Zee, 2006). This has been suggested by the findings of microelectrode studies observing an increased discharge in LIP neurons during the gap period in memory guided saccade tasks (Shadlen & Newsome, 2001).

However the role of LIP in saccade planning remained ambiguous. Reversible inactivation of LIP has no effect on the performance in visually guided saccades and memory guided saccades. On the other hand inactivation had strong effects on contralateral saccades or contralateral targets in visual search tasks, it was speculated that this might be an effect of attentional processing (Wardak, Olivier, & Duhamel, 2002).

More explicit effects of attentional processing could also be found in the lateral intraparietal area of macaque monkeys in other microelectrode studies. It could be shown that LIP neurons are sensitive in their onset of neuronal firing if the locus of attention of the monkey is on an object falling within the receptive field of the measured LIP cells. The onset of firing was significant delayed when the locus of attention was not in the receptive field of the measured cells (Bisley & Goldberg, 2006).

1.3.4. Frontal eye fields, FEF

The frontal eye fields are important for more complex eye movement tasks (Grosbras et al., 2005; Lynch & Tian, 2005; Leigh & Zee, 2006). For simple saccade tasks, where a single target has to be followed, a FEF lesion has little impact (Dias & Segraves, 1999). But when the task gets more complicated and distracter stimuli have to be ignored, lesion of the dorsolateral frontal cortex, where the frontal eye fields are located, have a significant impact on the performance. Such findings suggest that FEF is important for temporal processing and target selection (Schiller & Chou, 2000). Also in the human brain complex tasks seem to be affected, it has been observed that the inhibition of FEF by strong magnetic pulses decreases the performance of human subjects in visual search tasks (Muggleton, Juan, Cowey, & Walsh, 2003).

Also the classical view (see figure 1.6), namely that the FEF areas are not involved in the processing of smooth pursuit eye movements, is not longer valid. It seems that when a task gets complex and more cognitive effort is needed for a smooth pursuit task, then also the frontal eye fields play a important role (Krauzlis, 2004). Stimulation of the subfield for smooth pursuit processing in the frontal eye fields (FEFsem) is able to trigger this class of eye movements and can control the gain of the pursuit response to new visual targets (Tanaka & Lisberger, 2002a, 2002b).

FEF seems also connected with attention phenomena. On the physiological side this is visible when stimulation of FEF neurons, which have receptive fields where a target appears increases V4 responses. Stimulation of FEF neurons with receptive fields that do not correspond with the retinal target area decrease V4 responses (Moore & Armstrong, 2003). In covert attention tasks, microstimulation of FEF regions that corresponded with the retinal field of the target was an effective way to increase the performance of monkeys in such tasks (Moore & Fallah, 2004).

1.3.5. Supplementary eye fields, SEF

The supplementary eye fields are located in the dorsal surface of the medial frontal cortex in non-human primates. However, the exact location in the human brain was not known until Grosbras, Lobel, Moortele, LeBihan, and Berthoz (1999) introduced a localization paradigm for fMRI experiments and found its localization in the upper part of the paracentral sulcus. Together with the frontal (FEF) and parietal eye fields (LIP), SEF is known to be involved in the control of saccades (Grosbras et al., 2005; Lynch & Tian, 2005; Leigh & Zee, 2006).

The supplementary eye fields (SEF) seem to be involved in the control of voluntary saccades and pursuit eye movements especially when the task is more complicated, i.e. when the task is cognitive demanding. For example if macaque monkeys are free to choose one of two identical targets of their choice that will determine the reward they will receive, LIP, FEF and SEF are active but the earliest activity can be measured in SEF. Because this is also during the anticipatory phase Coe, Tomihara, Matsuzawa, and Hikosaka (2002) attribute cognitive anticipation effects to SEF.

Supporting evidence comes from studies where the target of saccades in an experimental task was defined as a complex goal, for example to look to the right or left end of a horizontal bar that served as a target for saccades (Olson & Gettner, 1995). This kind of task was varied by training macaque monkeys to look at the leftmost or rightmost dot in a two dot horizontal array, also leading to early and enhanced SEF activation (Tremblay, Gettner, & Olson, 2002).

There also seems to be a link between cognitive processes like anticipation and pursuit eye movements. When the path of a pursuit target changes and this change had been anticipated by previous training sessions cell populations the supplementary eye fields (SEF) and the dorso lateral prefrontal cortex (DLPFC) of macaque monkeys show change related activity (Heinen & Liu, 1997).

Similar anticipation evoked activity can be observed from electrical stimulation of

SEF. Electrical stimulation can evoke smooth pursuit eye movements. But this effect is the strongest when the onset of a smooth pursuit task is anticipated by the monkey, because the monkey expects a signal to start to track a smooth pursuit target (Missal & Heinen, 2001, 2004).

2. Methods & Models

2.1. General Linear Modeling

A analysis using a General Linear Model, also called GLM analysis, is a statistical analysis to reveal differences in the functional images taken. For this it must be known which experimental condition was present when a certain functional image of the subject was taken. Comparing the images taken when one experimental condition was present against images when another condition was present, makes it possible to determine where activity changes have occurred. Prerequisite for this is that several different images where taken, when one experimental condition was present. The GLM analysis then compares statistically several activity measures of one voxel during one experimental condition was present against the activity measures of the same voxel, when another experimental condition was present. This has to be done statistically because the signal to noise ratio of fMRI imaging is pretty poor. So comparing simply one activity measurement against another would provide erroneous results.

Figure 2.1 shows the time courses for one voxel in each hemisphere. Despite that each time course has been averaged over 50 scans, it can be seen that the time courses for the different tasks are still overlapping. This gets more difficult to distinguish, the more complicated an experimental paradigm gets. So that the GLM model is needed to distinguish between the effects different experimental conditions may elicit in brain areas.

In matrix notation the general linear model breaks down to a simple equation (2.1)

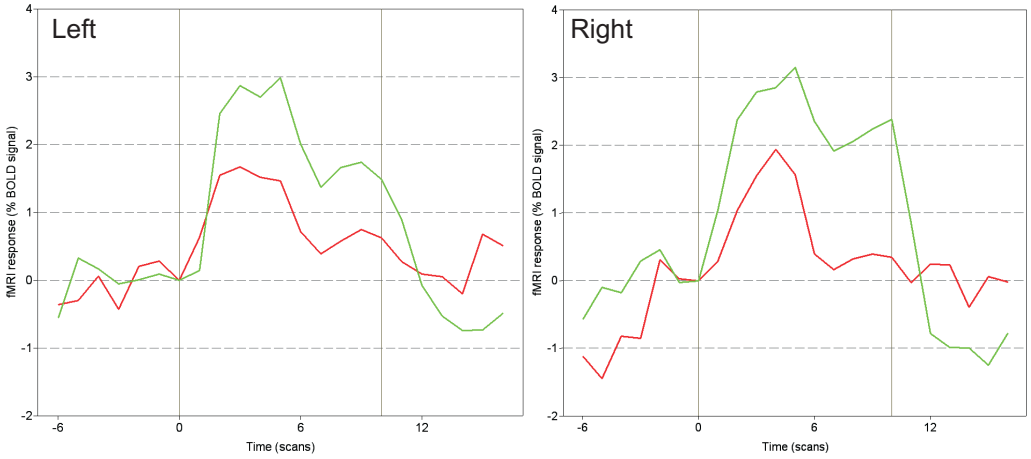

Figure 2.1.: The averaged signal change in a voxel of the lateral intraparietal areas for the left and right hemisphere during a pro- and antisaccade task in a single subject. The signal time course is averaged over 50 scans for each task (prosaccades, red; antisaccades, green) and adjusted to the onset of the target stimuli at the time (scan) zero.

$$Y = X\beta + U \tag{2.1}$$

Where Y are the functional images that were measured during the fMRI experiment. A fMRI image can be thought of a large three dimensional matrix of numbers. This matrix is the assumed result of the matrix constructed by the known experimental conditions X and a measure of the impact of each experimental condition for each image, i.e. β. A β matrix can be explained as a new resulting image that encodes the influences of current experimental conditions (X) for each measured image. However this description is not perfect, because there are many influences in the experiment not known to the researcher, these influences are encoded in the term U.

$$y_{xc,yc,zc,t} = x_{1,t} \cdot \beta_{xc,yc,zc,t,1} + x_{2,t} \cdot \beta_{xc,yc,zc,t,2} + x_{n,t} \cdot \beta_{xc,yc,zc,t,n} + u_{xc,yc,zc,t} \tag{2.2}$$

For a single voxel equation 2.1 can be reformulated in equation 2.2, where xc, yc and zc are the coordinates in space of the voxel. The time in the sequence of images is denoted by t and the different experimental conditions by n. In simple experimental designs the different experimental conditions are simply distinguished by being present or not in a certain point of time, i.e. $x_{n,t} = [0; 1]$

For example in the pro- and antisaccade task mentioned in figure 2.1 equation 2.2 would break down to $y_{xc,yc,zc,t} = 1 \cdot \beta_{xc,yc,zc,t,1} + 0 \cdot \beta_{xc,yc,zc,t,2} + u_{xc,yc,zc,t}$ and simplifies to $y_{xc,yc,zc,t} = 1 \cdot \beta_{xc,yc,zc,t,1} + u_{xc,yc,zc,t}$ when the experimental condition is prosaccades and this condition is encoded in $x_{1,t}$. Assumed that the experimental condition antisaccades is encoded in $x_{2,t}$, this leads to $y_{xc,yc,zc,t} = 0 \cdot \beta_{xc,yc,zc,t,1} + 1 \cdot \beta_{xc,yc,zc,t,2} + u_{xc,yc,zc,t}$ and simplifies to $y_{xc,yc,zc,t} = 1 \cdot \beta_{xc,yc,zc,t,2} + u_{xc,yc,zc,t}$

therefore giving us a complex but solvable equation system to determine the influence of each experimental condition to the measured BOLD response of each voxel.

Statistical measures are necessary because a predicted response seldom matches a measured response as we can see in figure 2.2

2.2. Functional segregation and functional integration

In a conventional fMRI analysis, outlined in the section before (see 2.1) we compare only voxel activity elicited by different factors that are controlled in a common fMRI study. This is called function segregation, making the functional classification of different brain regions possible. This promising approach has been conducted in the history of neuroscience since the method of fMRI was available. We can now provide a pretty good functional map of the human brain on a macroscopic level, for example for the visual system of human eye movements. (for an overview see: Petit & Haxby, 1999; Rosano et al., 2002; Grosbras et al., 2005).

But this helps us little to understand what is going on between the brain regions,

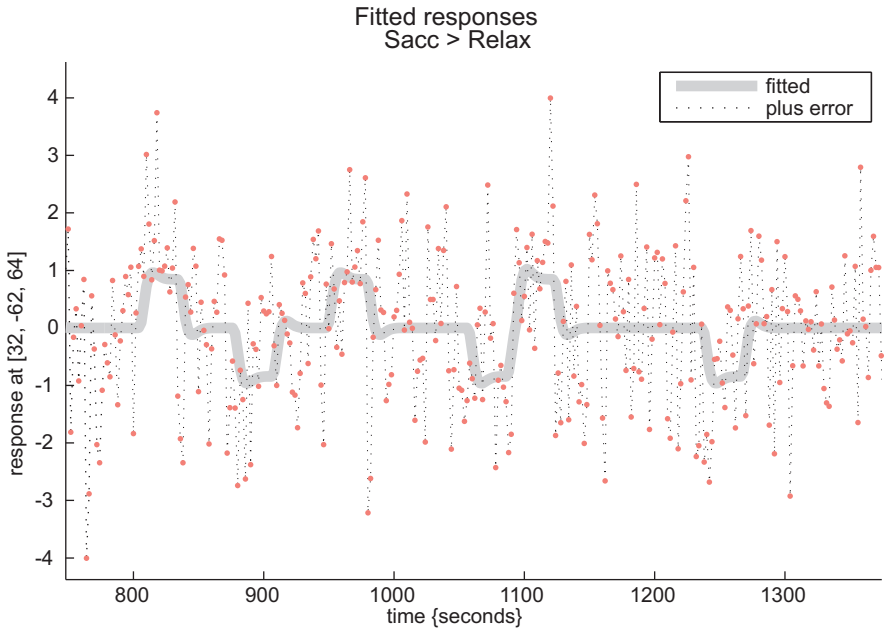

Figure 2.2.: Predicted fitted responses (grey line) of the right lateral intraparietal (LIP) area in a saccade task compared to the measured responses (red dots).

while they are processing specific tasks. Of course this statement is not imperative. With the method of GLM it is possible to make inferences about the interplay between different brain regions. But this method will only provide us a very rough picture and the experimental design has to be very sophisticated to achieve such inferences (For a more expanded discussion see Stephan, 2004). Therefore several methods have been developed, during the past decade, to provide a deeper understanding of the functional dynamics between regions of the human brain. To mention only the most common methods, there are Structural Equation Modeling (SEM, see Horwitz, Tagamets, & McIntosh, 1999; Mechelli, Penny, Price, Gitelman, & Friston, 2002; Caclin & Fonlupt, 2006), which has been compared to the new method of dynamic causal modeling by Penny, Stephan, Mechelli, and Friston (2004b). Psycho Physical Interaction (PPI, see Friston et al., 1997) and Independent Component Analysis (ICA, see McKeown & Sejnowski, 1998; McKeown, Hansen, & Sejnowsk, 2003)

2.3. Dynamic Causal Modeling (DCM)

2.3.1. A primer for DCM

Dynamic Causal Modeling was introduced in the year 2003 by the research team of the function imaging laboratory of the Kings College in London (Friston et al., 2003) . The first implementation was in the SPM2b package of the same laboratory, a software package for the statistical analysis of fMRI images, here the acronym SPM stands for statistical parametric mapping. Dynamic Causal Modeling is the latest invention in a long history of mathematical models to understand the interplay between brain areas better. It was the successor of Psycho Physical Modeling (PPI) , which can be found in earlier implementations of the SPM software package (Friston et al., 1997). There have been other models too to describe the interplay between different brain areas. They are mentioned in brief in the previous section (see 2.2).

One can think of DCM as a theoretical description of an oscillating system, a mechanical analogy is depicted in figure 2.3. As long no external input enters the system the system state is stable. So to say nothing will happen in the interplay between the brain regions. External inputs entering the system are perturbing the system, this is reflected in the rise and fall of activity in the brain regions. As these regions are connected with each other and influencing each others activity, these perturbations are propagated along the modeled connections to other brain regions.

But DCM also takes internal system changes into account. These are factors that will influence the propagation of activity changes according to different operational states the system is. These different operational states are reflected by the internal modulators. An internal modulator can influence either a connection between two brain regions or influence the activity of a brain region itself along time. This influence can be excitatory or inhibitory, excitatory if the rising activity of one brain region leads to an increase in activity of another brain region connected with it. On the other hand we see an

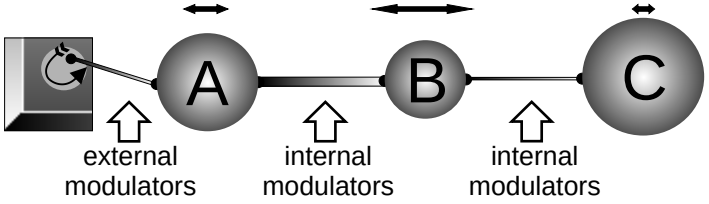

Figure 2.3.: A mechanical analogy to DCM. The engine of the left side depicts the driving stimuli that perturb the system. The spheres are symbols for the brain areas. All elements in this system are connected by rubber bands. The connection (rubber band) between the engine and sphere A is influenced by external modulators. The connections between the other spheres (brain areas) are influenced by internal modulators. In this analogy the modulators change dynamically the thickness and so the flexibility of the rubber bands over time. So that we have simple oscillating system that changes its dynamics over time in dependence of the driving inputs and the modulators. However, inhibitory connections are hard to transport in this analogy and show its limitations.

inhibitory influence if the rise of activity in one brain region will lead to a decrease in activity of the other brain region. This principle works similar if a modulator is influencing a brain region itself. This is modeled by a self connection of the region. We speak then of self excitation or self inhibition.

2.3.2. Mathematical foundations

It is assumed that it is sufficient to describe the neuronal activity of R brain regions in terms of neural state equations. These neural states $z = [z_1, z_2, \cdots, z_R]^T$ are defined by a nonlinear function F, in equation 2.3 describing the neurophysiological influences that activity z in all brain regions R and modulating influences u exert on the system:

$$\dot{z} = F(z, u, \Theta) \tag{2.3}$$

Where Θ contains the model parameters that need to be estimated. The fundamental equation of DCM is a multivariate differential equation, describing the neuronal dynamics:

$$\begin{aligned}\dot{z}_t &\approx Az_t + \sum_{j-1}^{M} u_t(j)B^j z_t + Cu_t \\ &= \left(A + \sum_{j-1}^{M} u_t(j)B^j\right) z_t + Cu_t\end{aligned} \tag{2.4}$$

The temporal dynamics of the main matrices A, B and C can be described more detailed by the equations 2.5.

$$\begin{aligned}A &= \frac{\partial F}{\partial z} = \frac{\partial \dot{z}}{\partial z} \\ B^j &= \frac{\partial^2 F}{\partial z \partial u_j} = \frac{\partial}{\partial u_j}\frac{\partial \dot{z}}{\partial z} \\ C &= \frac{\partial F}{\partial u}\end{aligned} \tag{2.5}$$

In equation 2.4 $\dot{z}$ describes the changes of the neuronal state z of a certain brain region in progress of the time t. This is called a bilinear equation, because $\dot{z}_t$ in linearly dependent on the product of z_t and u_t. z_t is the neuronal state at a given time t, one can think of the electrical activity of the brain area in question as a model for z_t. It is similar to $A(t)$ which describes the neuronal activity in a brain area in terms of spiking rates and which will be introduced in section 2.4.3 as equation 2.34 (page 48). The underlying neuronal state model explains why the standard unit to describe connectivity changes in DCM models is Hz, this comes from the model families that describe the activity in a neuronal population in terms of spikes per second, see figure 2.6 (page 47) for an illustration. u_t describes the influences on the system from the inside and from the outside. Internal influences are for example changes in the attentional level of a subject, processing different stimulus modalities, performing verbal or calculus tasks, in short every thing the researcher hypotheses that has happens inside the brain. External influences are described by the classical concept of the independent variables in experimental psychology, i.e. everything that comes from the sensory receptors of the

body and is controlled by the researcher. In this work internal and external influences are referred as internal or external modulators, respectively. The amount of modulators is contained in M which exert their influences through the index j.

Equation 2.4 contains three fundamental matrices.The A matrix specifies the intrinsic connections of the brain regions, describing how brain regions are connected to each other. Usually the regions connected in the A matrix have to be anatomically connected, i.e. nerve fibers leading directly from one region to another. It is also valid to assume the regions to be indirectly connected, for example the dorsal visual processing stream begins at V1 and continues over V2 to hMT+ (V5). In the models used in this work it is valid to omit the neuronal activity in V2 and model a direct intrinsic connection from V1 to hMT+ in the A matrix. The B^j matrix specifies the influence of M different internal modulators $u_t(j)$ that will perturb the specific system. The C matrix is the description of external modulators u_t entering the system, for example the presence or absence of visual or auditory stimuli. In DCM modeling an internal modulator can also be an external modulator at the same time, for example a moving visual stimulus is a source of external stimulation, but influences internal connections along the dorsal visual processing stream at the same time.

2.3.3. Hemodynamic state equations

Because the foundation of DCM are neuronal state equations, there is still a step needed to make it useful for fMRI data. As Logothetis, Pauls, Augath, Trinath, and Oeltermann (2001) showed the neuronal activity (neuronal state) of a brain region is closely connected to the fMRI BOLD signal. However the transformations used in classical GLM analysis to transform assumed neuronal events into BOLD signals or vice versa are too inaccurate for the precision needed to get a good estimation of the parameters in Θ. It had been shown by Friston, Mechelli, Turner, and Price (2000) that combin-

ing neural state equations of DCM with a sophisticated hemodynamic model gives the accuracy needed. The underlying model is based on the the Balloon Windkessel model (Buxton, Wong, & Frank, 1998; Buxton, Uludağ, Dubowitz, & Liu, 2004) which was expanded by a linear component.

The hemodynamic state equations are unique for every modeled region, in contrast to a GLM stimulus to BOLD response mapping that assumes the same transformation for the whole brain. The neural activity z_i of a region i causes an increase in a vasodilatation signal s_i that ensures enough blood will be provided for the increased metabolic demand of region i. The inflow f_i responds to this signal proportionally, influencing at the same time the blood volume v_i and the content of deoxygenated hemoglobin q_i.

$$\begin{aligned} \dot{s}_i &= z_i - \kappa s_i - \gamma_i(f_i - 1) \\ \dot{f}_i &= s_i \\ \tau_i \dot{v}_i &= f_i - v_i^{\frac{1}{\alpha}} \\ \tau_i \dot{q}_i &= f_i \frac{E(f_i, \rho_i)}{\rho_i} - \frac{v_i^{\frac{1}{\alpha}} q_i}{v_i} \end{aligned} \tag{2.6}$$

The outflow $f_{out}(v) = v^{\frac{1}{\alpha}}$ is related to the volume through Grubb's exponent α as was shown by Grubb, Raichle, Eichling, and Ter-Pogossian (1974). Oxygen is extracted by the enhanced metabolism of the increasingly active neurons, this extraction is a function of flow $E(f, \rho) = 1 - (1 - \rho)^{\frac{1}{f}}$ where ρ is the resting oxygen extraction fraction, i.e. how much oxygen would be extracted when there is assumed no blood flow. A list of the other biophysical parameters is provided by table 2.1, the are taken as priors for the region specific estimation of the relation between neuronal state z and BOLD signal y.

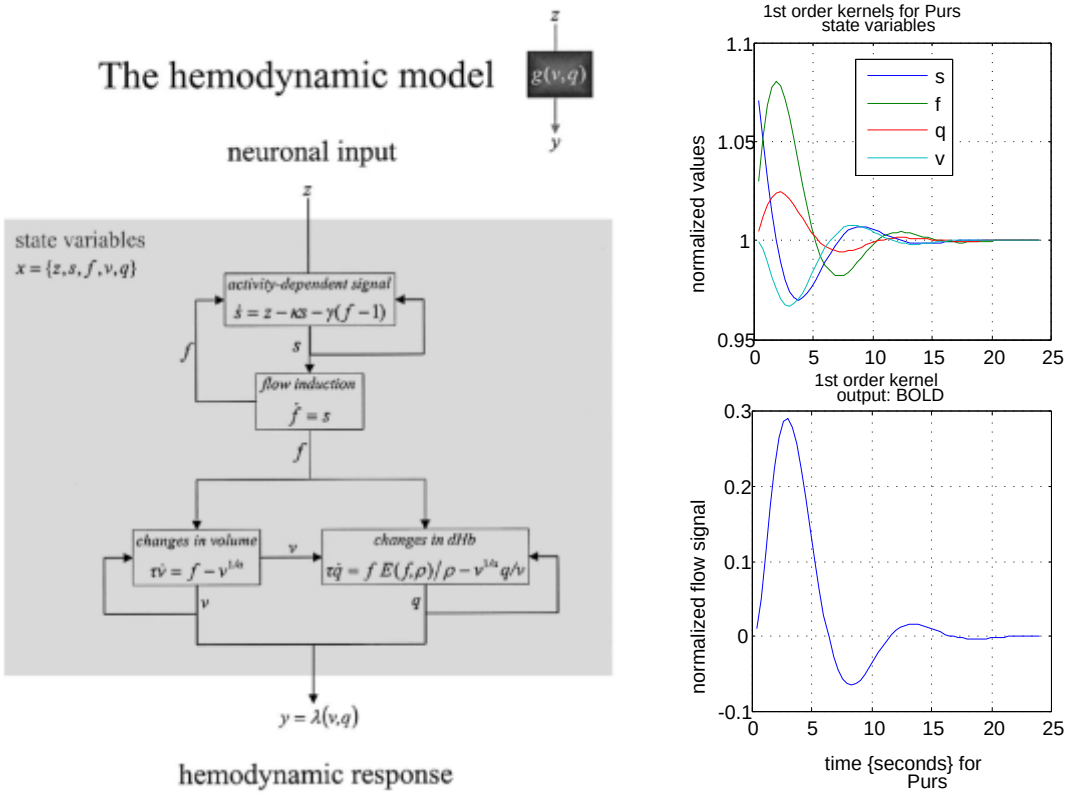

Figure 2.4.: The hemodynamic model of DCM to transfer the neuronal input z into a hemodynamic response $y = \lambda(v, q)$. Neuronal activity induces a vasodilatory and activity dependent signal s that influences the blood flow f. This flow causes a change in the volume of the cerebral blood vessel v and the concentration of deoxygenated hemoglobin q (adapted from: Friston et al., 2003). The right side shows a estimation of the parameters s, f, q and v (top right) that result in a estimated bold response (bottom right) of the area hMT+ in reaction to a stimulation by a smooth pursuit tracking task (unpublished single subject data).

Table 2.1.: A list of the hemodynamic priors for the inference of the BOLD signal y from the neural state z through the transfer function $y = g(q, v)$.

Parameter	Description	Prior mean n_Θ	Prior Variance C_Θ
κ	Rate of signal decay	0.65 s^{-1}	0.015
γ	Rate of flow dependent elimination	0.41 s^{-1}	0.002
τ	Hemodynamic transit time	0.98 s	0.0568
α	Grubb's exponent	0.32	0.0015
ρ	Resting oxygen extraction fraction	0.34	0.0024

$$
\begin{aligned}
y_i = \lambda(q_i, v_i) &= V_0 \left(k(1 - q_i) + k2 \left(1 - \frac{q_i}{v_i} \right) + k_3(1 - v_i) \right) \\
k_1 &= 7\rho_i \\
k_2 &= 2 \\
k_3 &= 2\rho_i - 0.2
\end{aligned}
\tag{2.7}
$$

The BOLD signal itself is modeled as a static non linear function, see equation 2.7, of blood volume and the amount of deoxygenated hemoglobin. Where $V_0 = 0.02$ is the resting blood volume fraction. Now all elements are together to build a model of an oscillating neuronal system that generates BOLD responses and to fit these data with the experimentally measured BOLD time course. It is important to note that the hemodynamic priors Θ^h are part of the general priors Θ that will be important for the understanding of section 2.3.4. For detailed discussion see (Friston et al., 2003).

2.3.4. EM and gradient ascent

The EM or expectation maximization algorithm describes the procedure to optimize the estimation of the B matrix (see equation 2.4) to achieve a better fit of the modeled neuronal response to the neuronal response, given indirectly by the BOLD response measured in the fMRI. This parameter estimation is using Bayesian statistics and is subdivided in two steps, an E step and an M step.

The E step computes the conditional mean $\eta_{\Theta|y}$ which is the expansion point of the gradient ascent. Furthermore the conditional covariance $C_{\Theta|y}$ is computed. The gradient ascent is driven by Fisher scoring (overview in: Wang, 2007) and a Levenberg-Marquardt optimization (detailed in: Levenberg, 1944; Marquardt, 1963). We take a closer look now at the **E-step** and the Fisher scoring. Generally Fisher scoring is identical to the Gauss Newton algorithm, except that the expectation of the Hessian matrix is taken:

$$\Theta^{i+1} = \Theta^i + \left\langle \frac{\partial^2 f}{\partial \Theta^2} \right\rangle^{-1} \frac{\partial f}{\partial \Theta} \tag{2.8}$$

The fisher scoring scheme can be derived by taking partial derivatives of the log posterior with regard to the parameters:

$$f = \log p\left(\Theta|y,\lambda\right) = \log p\left(y|\Theta,\lambda\right) + \log p(\Theta) \tag{2.9}$$

This results in equations equivalent to those derived for posterior mode estimation in non linear cases, using local linearization:

$$\frac{\partial^2}{d\Theta} f\left(\eta_{\Theta|y}\right) = J^T C_e^{-1} r + C_p^{-1}\left(\eta_p - \eta_{\Theta|y}\right) \tag{2.10}$$

$$\left\langle \frac{\partial^2}{d\Theta^2} f\left(\eta_{\Theta|y}\right) \right\rangle = J^T C_e^{-1} J + C_p^{-1} \tag{2.11}$$

equations 2.10 and 2.11 lead to:

$$C_{\Theta|y}^{i+1^{-1}} = \left\langle \frac{\partial^2}{\partial \Theta^2} f\left(\eta_{\Theta|y}^i\right) \right\rangle \tag{2.12}$$

$$\eta_{\Theta|y}^{i+1} = \eta_{\Theta|y}^i + \left\langle \frac{\partial^2}{\partial \Theta^2} f\left(\eta_{\Theta|y}^i\right) \right\rangle^{-1} \frac{\partial}{\partial \Theta} f\left(\eta_{\Theta|y}^i\right) \tag{2.13}$$

After the Fisher scoring the Levenberg-Marquardt regularization follows, it should

provide a good balance between the steepest gradient ascent and the Gauss-Newton ascent:

$$\Theta^{i+1} = \Theta^i + \lambda \frac{\partial f}{\partial \Theta} \tag{2.14}$$

In the steepest gradient ascent (2.14) we get a large step for a large gradient, but with the risk of overshooting a maximum. On the other hand we get small steps for small gradients, with the disadvantage of a slow progress in flat regions of the free energy function.

$$\Theta^{i+1} = \Theta^i + \left(\frac{\partial^2 f}{\partial \Theta^2} \right)^{-1} \frac{\partial f}{\partial \Theta} \tag{2.15}$$

The Gauss-Newton algorithm (2.15) is derived from the 2^{nd} order Taylor expansion. Therefore we get a quadratic assumption of about the local properties of the objective function.

$$\Theta^{i+1} = \Theta^i + \left(\frac{\partial^2 f}{\partial \Theta^2} + \lambda I \right)^{-1} \frac{\partial f}{\partial \Theta} \tag{2.16}$$

The Levenberg algorithm (2.16) dynamically adjusts λ, when λ is small we have a Gauss-Newton approximation (2.15), on the other hand we have a steepest gradient ascent (2.14) for a large λ.

$$\Theta^{i+1} = \Theta^i + \left(\frac{\partial^2 f}{\partial \Theta^2} + \lambda \operatorname{diag}\left(\frac{\partial^2 f}{\partial \Theta^2} \right) \right)^{-1} \frac{\partial f}{\partial \Theta} \tag{2.17}$$

Finally the Levenberg-Marquardt algorithm (2.17) provides an optimal balance for steep and flat ascents of the free energy function. If λ gets large the Levenberg algorithm (2.16) becomes essentially a steepest gradient ascent (2.14) with the risk of overshooting a maximum. The Levenberg-Marquardt algorithm (2.17) corrects this by making use of the curvature of the free energy function even if λ is high. So each com-

ponent of the gradient is scaled according to the curvature.

The **M-step** then estimates the the hyperparameters λ_i, seen in equation 2.18,

$$\lambda^{i+1} = \lambda i + \left\langle \frac{\partial^2 F}{\partial \lambda^2} \right\rangle^{-1} \frac{\partial F}{\partial \lambda} \tag{2.18}$$

for the error covariance components Q_i according to equation 2.19. For the posterior probabilities we have gaussian assumptions.

$$C_e = \sum \lambda_i Q_i \tag{2.19}$$

This M step will be repeated until the criterion $\frac{|\Delta\lambda|}{|\lambda|} < 10^{-5}$ is reached.

Now the E step follows in which a gradient ascent on the log posterior f is performed, where f is defined in equation 2.20

$$\eta^{i+1}_{\Theta|y} = \eta^{i}_{\Theta|y} + \left\langle \frac{\partial^2}{\partial \Theta^2} f\left(\eta^{i}_{\Theta|y}\right) \right\rangle^{-1} \frac{\partial}{\partial \Theta} f\left(\eta^{i}_{\Theta|y}\right) \tag{2.20}$$

here equation 2.20 can also be expressed by

$$\left(C^{i+1}_{\Theta|i}\right)^{-1} = J^T C_e^{-1} J + C_p^{-1} \tag{2.21}$$

where equation 2.21 changes when η is explicitly noted to equation 2.22

$$\eta^{i+1}_{\Theta|y} = \eta^{i}_{\Theta|y} + C^{i+1}_{\Theta|i}\left(J^T C_e^{-1} r + C_p^{-1}\left(\eta_p - \eta^{i}_{\Theta|y}\right)\right) \tag{2.22}$$

This E step is iterated until the criterion $|\Delta\Theta|^2 < 10^{-5}$ is reached.

2.3.5. Model comparison

On the single subject level a model comparison (Penny, Stephan, Mechelli, & Friston, 2004a) is calculated to determine which of the models explain the fMRI data best. The results of these model comparisons are used as the basis for a group model comparison using the Group Bayes Factor (GBF) and the Positive Evidence Ratio (PER) to determine the winning model for each hemisphere on a group level (Stephan, Marshall, Penny, Friston, & Fink, 2007). These indicators are based on the Akaike information criterion (AIC) and Bayes information criterion (BIC) that are the results of every DCM model comparison on a single subject level, see Penny et al. (2004a) for details. BIC tends to prefer simple models whereas AIC tends to prefer more complex models. So both criteria do not necessarily agree and this should also be taken into account on the group level. A selection of any single model is only made if AIC and BIC concur. The calculation of both criteria results in a Bayes factor for both. When comparing model m_i and model m_j the Bayes factor is defined as:

$$BF_{ij} = \frac{P(y|m_i)}{P(y|m_j)} \tag{2.23}$$

Then the Group Bayes Factor (GBF) is computed in a way assuming that the model comparisons of different individuals are statistically independent, here k is the index across subjects:

$$GBF_{ij} = \prod_k BF_{ij}^k \tag{2.24}$$

For every subject we calculate first pairwise model comparisons between all models (equation 2.23). Then the GBF is computed over all subjects as in equation 2.24.

Additionally the Positive Evidence Ratio (PER) is calculated, because the GBF comparison result can be sensitive to extreme outliers (Stephan, Weiskopf, Drysdale, Robinson, & Friston, 2007). It is an established convention to speak of 'positive evidence' in

a comparison, when the Bayes factor is BF>3 (Raftery, 1995). Each model is compared against all other models across all subjects. When AIC and BIC concur and the minimum Bayes factor is BF>3, then this increases the value of the PER comparison by one, providing a result like (a,b), where a denotes the number of subjects for whose data the model won according to the criteria above and b denotes the number of subjects for whose data the other model won. For example table 3.3 (page 67) shows the PER results for the study in chapter 3.

2.3.6. Model averaging

According to Garrido, Kilner, Kiebel, Stephan, and Friston (2007) it is easy to combine the conditional densities from several subjects to calculate the conditional density for the group. The conditional probability of the parameters y_j given data from all subjects is:

$$p(\theta|y_1, K, y_n) \propto p(y_1, K, y_n|\theta)p(\theta) \tag{2.25}$$

Then we assume that the conditional densities for each subject have a Gaussian form and are given by

$$p(\theta_j|y_j) = N(\mu_j, \Sigma_j) \tag{2.26}$$

With the mean μ and the precision $\Lambda = \Sigma^{-1}$, the conditional density of a parameter at the group level can be calculated from the individual mean μ_j and the precision matrices:

$$\begin{aligned} \Lambda_j &= \Sigma_j^{-1} \\ \Lambda &= \sum_{j=1}^{n} \Lambda_j \\ \mu &= \Lambda^{-1} \sum_{j=1}^{n} \Lambda_j \mu_j \end{aligned} \tag{2.27}$$

This leads to a representative averaged model across all subjects

2.4. Neural Mass Modeling

To describe the spiking behavior of large cell assemblies in mathematical models can be beneficial to get deeper insight in the mechanisms that are causing the changes of brain activity. Hopefully it will be possible with such models one day to explain various phenomena that have been observed by neuroscientific research in the last years in means of a mathematical foundations. Much like physics started centuries ago to describe phenomena of the inanimate world with the help of mathematical models.

Because this is a own field of research and the underlying theories are very complex a complete explanation would excess the scope of the present work, which mainly aims at the discussion of fMRI data analyzed with dynamic causal modeling. In the scope of the present work only the most important aspects of neural mass modeling and the connection to brain areas and to dynamic causal modeling will be outlined. An extensive review article, describing the evolution from single cell models to mathematical models of whole cortex areas was published by (Deco et al., 2008). A general introduction into the field of computational neuroscience was written by Trappenberg (2002).

2.4.1. Hodgkin & Huxley

All started when Hebb (1949, 2002) formulated a basic learning rule that described neuronal learning the first time and is still valid, however in an adapted form. He stated that the connection strength between two neurons get stronger when they fire together at the same time, which led to the famous proverb 'what fires together that wires together'. However at this time neurophysiological measurements were at the beginning and the theory could not experimentally verified.

This changed some years later when Hodgkin and Huxley (1952) measured the electrical signals in the axons of giant squid neurons (republished: Huxley, 2002). Together

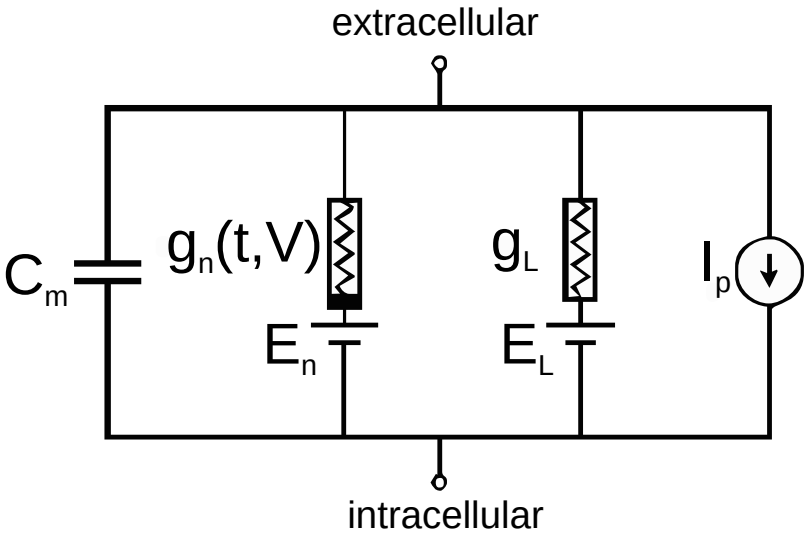

Figure 2.5.: A schematic depiction of the Hodgkin Huxley model. The biophysical characters of a neuron cell membrane are modeled by the representation of the bilipid layer as a capacitor (C_m), the voltage gated and leak ion channels are represented by a nonlinear (g_n) and a linear component (g_L). Electrochemical gradients that are driving the flow of ions are represented by batteries (E_n, E_L). Ion pumps and exchangers are modeled by current sources (I_p). Adapted from: Behrang Amini (1.5.2006), http://commons.wikimedia.org/wiki/File:Hodgkin-Huxley.jpg

with Sir John Carew Eccles they received the nobel prize in 1963 'for their discoveries concerning the ionic mechanisms involved in excitation and inhibition in the peripheral and central portions of the nerve cell membrane'.

Figure 2.5 shows a schematic depiction of the Hodgkin Huxley model, where the time derivative ($\dot{V}_m$) of the membrane potential is proportional to the sum of currents in the circuit, see equation 2.28.

$$\dot{V}_m = -\frac{1}{C_m}\left(\sum_i I_i\right) \tag{2.28}$$

Now the currents flowing through the ion channels (I_i) are represented by equation 2.29.

$$I_i(V_m, t) = (V_m - E_i)g_i \tag{2.29}$$

here E_i is the reversal potential of of the i-th ion channel. The reversal potential or Nernst potential of an ion is the membrane potential at which the net flow of ions deceases and no ion specific current is measurable any more. The channel conductance in voltage gated ion channels is a function of time and voltage ($g_n(t, V)$), while in leaky channels the ion flow and therefore the current is constant (g_L). The dynamics of voltage gated channels can now be described by the equations 2.30.

$$\begin{aligned} g_n(V_m, t) &= \bar{g}_n \varphi^\alpha \chi^\beta \\ \dot{\varphi}(V_m, t) &= \frac{1}{\tau_\varphi}(\varphi_\infty - \varphi) \\ \dot{\chi}(V_m, t) &= \frac{1}{\tau_\chi}(\chi_\infty - \chi) \end{aligned} \tag{2.30}$$

Where τ and χ are the gating variables for activation or inactivation, representing the maximum conductance that is possible at a given time and voltage. α and β are constants. τ_φ and τ_χ are the time constants for activation and inactivation. φ_∞ and χ_∞ are the steady state values for activation and inactivation.

To find the balance between a simplified model and a complex model of a neuron that explains the observed data sufficiently but is simple enough to be computable is a problem for itself and has been discussed by Herz et al. (2006).

2.4.2. Leaky integrate and fire neurons

When observing the behavior of neuronal cells it is evident that they are not communicating by mere changes in the current of the axon. The change of current can be seen as a process underlying the spiking behavior of neuronal cells. In nervous systems neuronal cells are exchanging signals with each other in the form of spikes, that are short and

uniform bursts of electrical activity emitted by a neuron along its axon, other neurons are picking up these spikes through their dendrites. Early last century it became evident that the integration of spikes from other neurons happened relatively slow but once a threshold was passed that a neuron would fire spikes, in fact the process generating spikes was fast and uniform (Hill, 1936). If focus is put now on the spike generation, caused by spiking activity from other neurons, it became possible to omit the detailed dynamics of different ion channels and to make a model of a neuron that integrates spikes from other neurons and generates spikes itself (Stein, 1967; Knight, 1972). The term leaky was introduced because these neuronal models return slowly to a resting state when no input from other neurons is present, simulating the constant diffusion of ions through the cellular membrane.

$$I(t) - \frac{V_m(t)}{R_m} = C_m \frac{dV_m(t)}{dt} \tag{2.31}$$

Equation 2.31 is now one of the possible ways to describe the input $I(t)$ at a given time when a neuron integrates the spikes of other neurons. The membrane of the neuron has the properties of a resistor R_m which decreases the potential of the neuron over time if not the firing threshold $I_{th} = \frac{V_{th}}{R_m}$ is reached.

$$f(I) = \begin{cases} 0 & I \leq I_{th} \\ \left(t_{ref} - R_m C_m \log\left(1 - \frac{V_{th}}{I R_m}\right)\right)^{-1} & I > I_{th} \end{cases} \tag{2.32}$$

The shape or amplitude of the neuronal spikes is omitted in these class of models. Therefore equation 2.32 describes the spiking rate $f(I)$ only in terms of spikes per second or Hz. t_{ref} implements a refractory period, that prevents the neuron from spiking during that period.

A detailed discussion of leaky integrate and fire models can be found in Burkitt (2006a, 2006b). At this point of the discussion the idea to be communicated is that the behavior

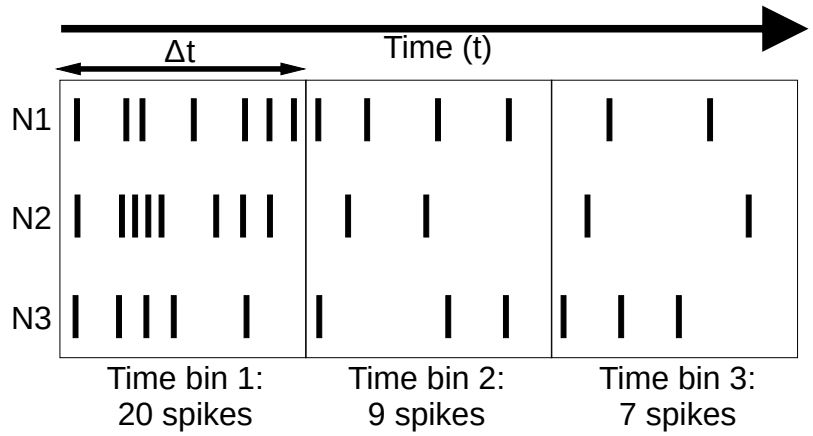

Figure 2.6.: Schematic depiction of a small population of three spiking neurons (N1, N2, N3). Along the time axis the resulting activity of this group of neurons can be described in spikes per time bin. Usually a moving time window Δt is used to describe the spiking rate at a given point in time t.

of single neurons in dependence of other neurons can also be modeled just in terms of spiking rates that are given in Hz.

2.4.3. Modeling a neuronal population

The next step in simplifying modeling assumptions is now to move from the mathematical description of the behavior of a single neuron to that of a large number of neurons. Since many neurons in large cell assemblies behave in a uniform way such a simplification is appropriate. For example it has been shown that neurons in the primary visual cortex are organized in columns and each column processes inputs in a uniform way (Hubel & Wiesel, 1959, 1968).

Figure 2.6 shows how such a simplification is done in principle. The firing rate $v(t, \Delta t)$ of a population of neurons with the size N can be described as the number of spikes generated by this pool of neurons in a certain time window Δt. Now the average activation of a neuron in the population at a given time $A(t)$ can be expressed by equation 2.33.

$$A(t) = \lim_{\Delta t \to 0} \frac{v(t, \Delta t)}{N} \tag{2.33}$$

The basis of many of these population fire models is the model of the leaky integrate and fire neuron (section 2.4.2). Such models can be used to to study various psychological phenomena that are topics of neuroscientific research such as perceptual decision making (Wong & Wang, 2006), attention (Corchs & Deco, 2002; Deco & Rolls, 2005b; Buehlmann & Deco, 2008), working memory (Brunel, 2003), processing of visual motion in MST (Grossberg et al., 1999; Pack, Grossberg, & Mingolla, 2001).

Under the prerequisite of a large homogeneous population of spiking neurons, all neurons in the pool share the same membrane time constant, the same mean numbers and synaptic efficiencies of and receive the same input current it can be shown mathematically, that a pool of neurons can be replaced by the description of the activity $A(t)$ of a single unit. A first approximation of the population dynamics was done by Wilson and Cowan (1972) and can be found in equation 2.34.

$$\tau \frac{dA(t)}{dt} = -A(t) + g\left(\int_0^\infty \epsilon(s)A(t-s) + \tilde{\epsilon}(s)I^{ext}(t-s)ds\right) \tag{2.34}$$

Neurons are coupled with a delay kernel ϵ. They receive input from other populations or an external source that is filtered by a kernel $\tilde{\epsilon}$. The transfer function of the population is $g(\cdots)$. The time constant τ has to be chosen arbitrarily because it is only known in the case of a typical membrane time constant τ_m but is unknown for the population level. Populations of integrate and fire neurons can react quasi instantaneously to rapid changes in the input, thus making the function $A(t)$ constrained to a limited field of measurable activity of neuronal populations (Muir, 1979; Buice & Cowan, 2007). So consequently the Wilson Cowan model has been adapted and expanded (Gerstner, 2000; Buice & Cowan, 2007).

When such a model of a assembly of neurons gets an input from another assembly

we can speak of a network of cell populations. Here it is important to understand the concept of mean field. Such a mass model has the simplified assumption that every neuron gets a similar input, which is called the mean field (Trappenberg, 2002).

2.4.4. Connection to fMRI and DCM

Since one decade now the idea persists that models and data of the research fields of computational neuroscience, neuroimaging and cognitive modeling could be exchanged, thus leading to more accurate theories and explanation of data (Horwitz et al., 1999; B. Horwitz & Tagamets, 1999; B. Horwitz, Friston, & Taylor, 2000). Neuroimaging studies have produced a vast amount of data so far, the interpretation of the findings is difficult without a elaborated theoretical framework. So far most of imaging results are still interpreted in the way of making a cortical map of cognitive functions. This taxonomical approach provides valuable insight in the relationship between psychological phenomena and anatomy of the cortex. Stephan (2004) pointed out that this approach is not sufficient to understand the operational principles of a complex dynamic system like the brain, he suggests to put neuroimaging data in the framework of general systems theory. A first step was the research of functional relationships between brain areas, so called functional integration (see section 2.2). Computational neuroscience itself fulfills the demands of general systems theory, thus being an ideal methodological bridge to integrate the approaches of neuroimaging and general systems theory. First research to combine the disciplines of neuroimaging and computational neuroscience seems promising. Tagamets and Horwitz (2000) have tried to combine functional brain imaging data and large scale neural models to get a plausible model of the working memory.

Chapter 5 (page 91) introduces a study where dynamic causal modeling was used to verify assumptions for a possible extension of the neural mass model of Wong and Wang (2006). It was investigated if also the intensity of a stimulus and not only the level of

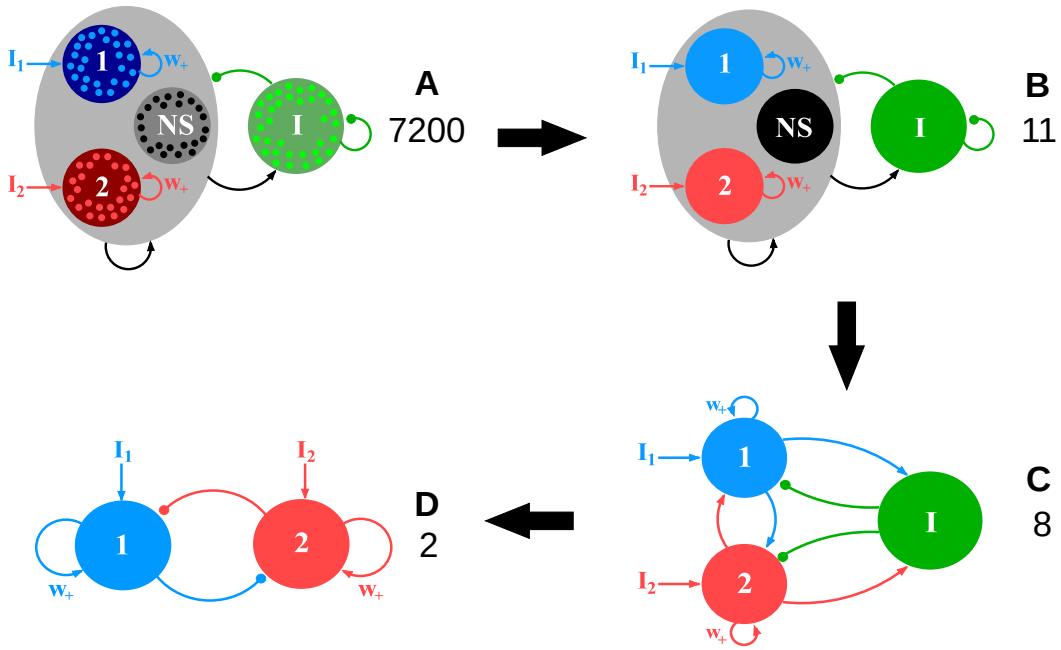

Figure 2.7.: Schematic depiction of the simplification process from a complicated neuronal decision making model with many leaky integrate and fire neurons (**A**) to a mass model just modeling the average spiking rate of two cell populations (**D**). NS and I denote the non selective (black) and inhibitory (green) pools of cells. Arrows indicate excitatory connections; circles indicate inhibitory connections. Enhanced excitatory connections within each neuronal pool are indicated by w_+. I_1 and I_2 are inputs to each population of selective neurons (red & blue). *The simplification process:* First, the mean field approach reduces a model with 7200 variables (**A**) to four neuronal units with 11 dynamical variables (**B**). Second, simplifying the input output relation of the neurons: 1. The input output relation of a leaky integrate and fire model is modeled in a transfer function. 2. Linearize the fire and integrate curves. 3. Assuming constant activity of NS neurons, thus leading to a model with 8 variables (**C**). Third, in the last step it is assumed that all fast variables of the system reach steady state much earlier than the system develops a significant activity in the means of average firing rates $A_{pop}(t)$ of cell populations, leading to a simple model of neuronal decision making with just two dynamical variables (**D**). Adapted from: Wong & Wang, 2006

coherence of this stimulus has an influence for perceptual decision making in the lateral intraparietal area (LIP). LIP receives its inputs from MST (or hMT+ in this study) and was modeled as two pools of neuron populations in a neural mass model (see figure 2.7). This study helped to answer the above assumptions.

Dynamic causal modeling like presented in this work was using a single state model to describe the neuronal activity of cell populations, i.e. assuming one cell population to be responsible for activity changes in a certain brain region. Wong and Wang (2006) used a two competing cell populations, which is a two state model. Marreiros, Kiebel, and Friston (2008) could show that it is possible to expand the mathematical foundation of DCM to assume a two state model, i.e. assuming two competing cell populations in a brain region. However this approach was not used in the presented work because it was not yet implemented in SPM5.

In another study Lee, Friston, and Horwitz (2006) have used a large scale neurocomputational simulation about visual delayed match to sample tasks (Tagamets & Horwitz, 1998) to validate model comparison routines applied dynamic causal modeling. It could be proofed that the DCM method correctly identified the structure of the network, that was generating synthetic fMRI data, by selecting a DCM model that had a similar architecture like the underlying neurocomputational simulation. Also the magnitude of effects generated by the simulation was very similar to the magnitude of effects estimated by the DCM model estimation process

The sigmoid activation function that is used to describe the population activity of large neural cell assemblies is linking mean population depolarization to expected firing rate. Marreiros, Daunizeau, Kiebel, and Friston (2008) use this in terms of variance or dispersion of neuronal states to link it with EEG based DCM models. Real EEG data was used to show that population variance, in the depolarization of neurons from

somatosensory sources generating sensory evoked potentials (SEP), can be quite substantial. Using DCM the SEP parameter density was estimated controlling the shape of the sigmoid function used to describe the input output relations in mean field models ($A(t)$). This allowed it to quantify the population variance in relation to the evolution of mean activity of neural mass models. The quantitative results of this analysis suggests that only a small proportion of neurons are actually firing at any time, even during the peak of evoked responses.

So it seems that the combination of neurocomputational models, cognitive models and neuroimaging methods for exploring the functional integration of the brain can lead to promising new theories to understand the brain on a general systems level like it was demanded by Stephan (2004).

Part II.

Experiments

3. Attention shifting in early visual areas

To explore the effects of covert and overt attention to visual stimuli a simple experimental paradigm was developed including moving targets for pursuit and saccadic eye movements. With the method of Dynamic Causal Modeling (DCM) the interactions of certain brain areas involved in eye movement processing were explored in detail.

The neural control of eye movements in non-human primates has been studied over the last several decades (see Leigh & Zee, 2006 for a review). Recent functional magnetic resonance imaging (fMRI) studies have made it possible to validate some of these findings for the human brain (see Lynch & Tian, 2005 for a review). The brain areas involved, as well as their respective connectivity, has been thoroughly investigated in the brain of the macaque monkey, which commonly serves as a model for the human visual system. Using the technique of fMRI, several studies have revealed that the areas involved in the neural control of pursuit and saccade eye movements are comparable to that found in macaques (Petit & Haxby, 1999; Kimmig et al., 2001; Müri, 2005). The models we explored here are based on well established facts about the early stages of visual processing and oculomotor control in primates (Lisberger et al., 1987; Krauzlis & Stone, 1999; Krauzlis, 2005; Lynch & Tian, 2005; Leigh & Zee, 2006). Here we focus on the following structures in the dorsal visual cortex: the primary visual area in the striate cortex (V1), middle temporal (MT), middle temporal (hMT+), and lateral intraparietal area (LIP). We apply general systems theory to analyze functional MRI time series (Stephan, 2004).

Models from computational neuroscience so far have described the behavior of the visual system in primates (Rolls & Deco, 2002). For example, interactions between the primary visual cortex (V1), the middle-temporal (MT) and the middle-superior-temporal (MST) during smooth pursuit eye movements of macaque monkeys have been modeled (Furman & Gur, 2003). Our approach here is to describe the effective connectivity between interacting regions involved in the control of voluntary eye movements. The method of Dynamic Causal Modeling (Friston et al., 2003) can be applied to fMRI time-series data to determine the effective connectivity between several brain regions. We assume that different external perturbations (tracking a saccadic or pursuit target) along with internal states (overt/covert attention to the moving target) affect the interplay between these brain regions. This interplay is reflected in the time course of the BOLD responses in the fMRI data set. DCM is a tool to quantify these modulations in activity due to different conditions on the basis of the measured BOLD time course for each region. In the present study, subjects were instructed to track a smoothly moving pursuit stimulus or a ballistic saccadic target either overtly or covertly by shifting attention to a target without moving their eyes. We explore the effects of covert attention during the early stages of visual processing. Previous studies on attention effects on the visual system can be revealed by an analysis of the connectivity between involved brain regions with fMRI data (Büchel & Friston, 1997). We were particularly interested in the effects on connectivity during covert and overt tracking of pursuit and saccade targets. In particular we asked whether these attention effects can best explained by feed-forward or by feedback processing in terms of modulation effects in the modeled connections. Therefore we generated 15 models and determined empirically which model can explain the data best.

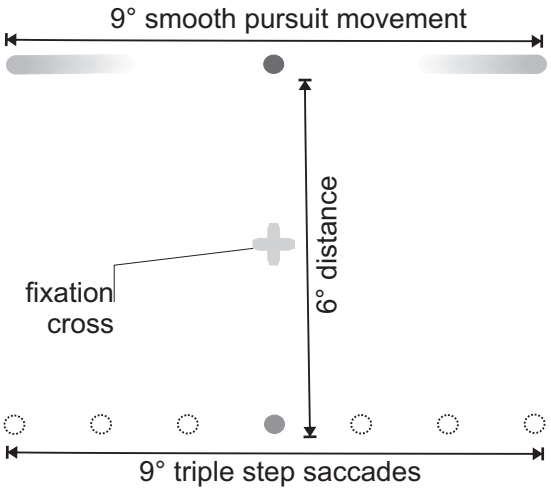

Figure 3.1.: A schematically depiction of the visual stimuli used in the experimental setup. Two dots and a yellow fixation cross were visible. The upper green dot served as a smooth pursuit target, it performed a sinusoidal movement with a period of 0.28 Hz and an amplitude of 9. The lower turquoise dot was the target for triple step saccades, also with an amplitude of 9. Its movement was synchronized with the movement of the pursuit target. The distance of the dots was 6 in the visual field. This stimulation was used for the conditions PT, ST, PC and SC. In the rest condition (R) only the yellow fixation cross was visible. From: Acs & Greenlee, 2008

3.1. Materials & Methods

3.1.1. Subjects

We examined eight healthy subjects with no known neurological or psychological disorders. Five males and three females in the age range between 20 and 35 years (mean = 26.5 years), all subjects were right handed.

3.1.2. Stimuli

The visual stimuli consisted of a yellow fixation cross in the center of the visual field and two horizontally moving dots located above and below the fixation cross (Figure 3.1).

These stimuli were computer generated, using Presentation (Neurobehavioral Systems,

Albany, CA). The dot movement followed a sinusoidal function with a frequency of 0.28 Hz; the amplitude resulted in a 9° movement in the visual field. The upper dot was green and it served as the pursuit target. The lower dot was turquoise in color and it served as the saccadic target. Subjects had to perform triple-step saccades in each direction, with the saccade target shifting synchronously to the movement of the pursuit target. To control for alertness, the moving targets occasionally changed their color (probability of 0.05% per frame with 75Hz refresh rate) briefly (200 ms). Subjects had to indicate this color change by a button press with the right index finger. During the reaction time task the color of both dots changed to a red circle with a black center. The experiment consisted of five main conditions: **1)** Pursuit (PT) in which the subject was instructed to track the pursuit target; **2)** Saccades (ST), in which the subject was asked to follow the saccadic target; **3)** Covert attention to pursuit target (PC), in which the subject kept his or her gaze on the fixation cross but paid attention to the pursuit target; **4)** Covert attention to saccade target (SC): Same as condition PC, but now the subject attended to the saccadic target. Rest (R): Only the fixation cross was visible, the subject had to rest with open eyes and to keep his or her fixation on the cross. The fixation cross served also as an indicator for the task. A red bar in the upper flank of the cross indicated to the subject to perform the pursuit task. If the bar was visible at the lower flank of the cross, this indicated to the subject to track the saccadic target. A red dot in the center of the fixation cross indicated to the subject to keep his or her gaze fixed at the central cross. Each condition was preceded by a written instruction to indicate to the subject what to do next. The instruction was displayed on the projection screen for six seconds.

3.1.3. In Scanner Eye Tracking

Horizontal eye movements were acquired by a MR compatible limbus-reflection-based eye tracker by Cambridge Research Systems (Kimmig, Greenlee, Huethe, & Mergner,

1999). An onboard sampling rate of 500 Hz was used. The scanner triggers were digitized to provide the correct assignment of the eye tracking data to each block. Eye tracking was used for monitoring purposes only in order to control whether the subject followed the instructions correctly.

3.1.4. fMRI data acquisition

We used a 3T Siemens Allegra^{TM} MRT Scanner for acquiring the functional and structural images. The EPI sequence had the following parameters: TR=2s, 1160 volumes, 3×3×3 mm voxel size, 90 flip angle, 34 slices per volume, interleaved slice order. This allowed us to acquire images of the entire cerebral cortex. We used a block design, employing five different conditions (PT, ST, PC, SC, R), with 15 scans per block resulting in duration of 30s per block. Each block was preceded by a 6-second presentation of the instructions for the current block. Total run time was 38 min for the acquisition of the functional imaging data. The order of the blocks PT, ST, PC and SC was permutated by the method of the Latin square, after 4 blocks with targets present the Rest (R) block followed. For a better localization of volumes of interest a structural scan (T1-weighted MP-RAGE sequence, Siemens Medical Solutions) was acquired at the end of the session in each subject.

3.1.5. GLM Analysis

SPM5 was used for the fMRI data analysis (Functional Imaging Laboratory, London). Pre-processing involved realignment, slice timing correction, normalization and smoothing. Slice timing correction was adjusted to the first slice, which was the middle slice in time according to the interleaved acquisition. A normalization of the EPI mean image to EPI template provided the parameters for normalizing the EPI scans. The realigned images were smoothed using a 6 mm FWHM smoothing kernel. In the GLM analysis the regressors denoting the 4 main conditions were modeled (pursuit-tracking, PT; saccadic-

tracking, ST; pursuit-covert, PC; saccade-covert, SC). Additionally the condition Rest (R), the presentation of the instructions, and the response events (i.e., button presses) were included. Head movements formed six more regressors, three describing the rotation and three describing the translation of the subject's head during the functional scan. The Volumes of Interest (VOI) were selected manually for each subject. For this purpose the T-contrast of the main tracking conditions (PT, ST) against the rest conditions guided this selection. The localization of the peak activity for each region was always performed with the T-contrast that seemed most suitable for the specific region, for example the Saccades > Rest contrast to locate the LIP regions. This location was then transferred to the F-contrast map of the relevant DCM conditions and was adjusted slightly to match the peak there; Table 3.1 shows the MNI coordinates of the volume of interest centers used for the time course extraction.

The volumes of interest had a radius of 6 mm and these were adjusted for the relevant conditions for the DCM model (PT, ST, PC, SC and R). We used a threshold of $p<0.001$ uncorrected. The region in V1 selected for the DCM analysis corresponded with V1 regions representing the area around the fovea centralis in the striate cortex (Horton & Hoyt, 1991), which is in the posterior part of the striate cortex. V1 was pooled for the right and left hemisphere, because a hemispheric specific assignment of the functional voxels was not unequivocal with our resolution of 3×3×3 mm and a smoothing factor of 6 mm. Further regions of interest were the middle temporal area (hMT+) and the lateral intraparietal area (LIP) in both hemispheres. We assumed that the human area MT+ is composed of human homologous of the areas MT and MST known from the macaque brain. This is supported by fMRI studies of the human brain, showing that hMT+ is composed of two subareas that behave like macaque MT and MST (Dukelow et al., 2001; Huk et al., 2002). Using a voxel size of 3×3×3 mm made it difficult to separate the MT from the MST area. As a consequence the MT and MST areas were merged in a single volume of interest, called MT/MST (also referred to as hMT+) for

Table 3.1.: Locations of the regions of interest for each subject. The MNI coordinates for each region describe the center of the sphere with a radius of 6mm that was used for the volume of interest extraction process of SPM5. Size indicates the number of voxels included for the extraction process. The volumes of interest were adjusted to the F-contrast of the main conditions and the rest condition, using a significance threshold of $p<0.0001$. V1 was the same VOI for both hemispheres. From: Acs & Greenlee, 2008

V1	X	Y	Z	Voxels	Z-score	X	Y	Z	Voxels	Z-score
S1	2	-94	6	123	Inf					
S2	2	-80	4	123	Inf					
S3	2	-92	-6	122	Inf					
S4	0	-86	8	123	Inf					
S5	6	-78	10	123	Inf					
S6	6	-96	8	123	Inf					
S7	0	-96	12	121	Inf					
S8	-4	-88	-6	116	Inf					
Group*	-2	-84	-6		4.90					

	Left					Right				
hMT+	X	Y	Z	Voxels	Z-score	X	Y	Z	Voxels	Z-score
S1	-42	-74	12	116	7.80	44	-68	10	117	Inf
S2	-50	-72	10	114	7.65	44	-66	14	83	5.99
S3	-58	-66	6	85	Inf	52	-56	0	123	Inf
S4	-42	-72	-8	122	Inf	48	-66	0	123	Inf
S5	-50	-72	2	120	Inf	52	-72	8	110	Inf
S6	-48	-72	4	123	Inf	52	-70	-4	121	Inf
S7	-52	-72	2	95	6.43	58	-68	2	47	5.71
S8	-46	-80	-8	101	Inf	50	-78	-8	91	Inf
Group	-46	-68	12		3.61	50	-70	4		3.96

LIP	X	Y	Z	Voxels	Z-score	X	Y	Z	Voxels	Z-score
S1	-20	-62	64	104	Inf	20	-62	66	106	Inf
S2	-26	-60	60	121	Inf	24	-66	64	106	Inf
S3	-20	-58	62	88	6.59	30	-62	64	94	Inf
S4	-30	-56	56	114	7.05	30	-54	54	114	Inf
S5	-24	-68	58	116	Inf	24	-72	60	82	Inf
S6	-28	-58	64	116	Inf	24	-64	62	118	Inf
S7	-26	-58	64	79	6.79	20	-58	62	49	4.89
S8	-22	-72	62	75	Inf	26	-64	64	110	7.63
Group	-22	-62	60		4.26	28	-58	68		4.44

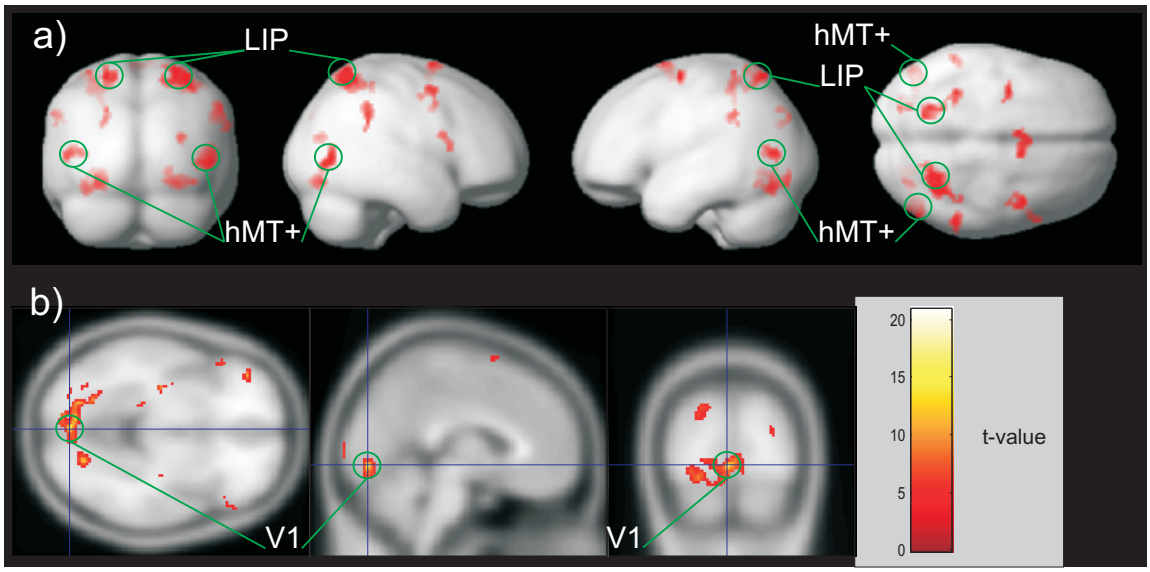

Figure 3.2.: Results of the random effects group analysis for the regions used in this study. a) depicts the regions hMT+ and LIP, the rendering of the analysis results was done using a threshold of p>0.001. The contrast used here was comparing the covert attention conditions against the resting condition (PC,SC > R). b) shows the location of the V1 area used in this study, a threshold of p>0.001 was used for these results too. But here all four conditions were taken into account to get a clear localization of the most active V1 region. (PT,ST,PC,SC > R) From: Acs & Greenlee, 2008

each hemisphere.

Furthermore a group random effects analysis was calculated, to assure that the selected coordinates at the single subject level matched the coordinates determined by the group analysis (Figure 3.2 and Table 3.1) The t-contrast of the tracking conditions against the resting condition was used to localize the peak of activation of the brain areas included in this study. The MNI coordinates of the peak were transferred to the F-contrast map of the conditions relevant for the DCM analysis (PT, ST, PC, SC, R; p<0.001). The coordinates of the peak were used to find the most significant voxel nearby in the F-contrast map. This voxel served as the center of the time course extraction for each volume of interest. A spherical shape with a radius of 6 mm was used to extract the time series of the cluster by the 'eigenvariate' extraction tool from SPM5. The volume

of interest extraction was adjusted to the main conditions PT, ST, PC, SC and R.

3.1.6. DCM Modeling

Our connectivity analysis was guided by the model of Krauzlis (2005) and Lynch and Tian (2005) concerning the processing pathways for voluntary pursuit and saccadic eye movements. The regions V1, hMT+ and LIP were assumed to be interconnected in a serial order with intrinsic connections in both feed-forward and feedback directions between the areas. Two inputs stimulated V1; one input represented the physical stimulus, which was the same for the conditions PT, ST, PC and SC. The other input represented the rest condition (R), which stimulated V1. In this condition, only the fixation cross was presented on the screen. Accordingly, these two inputs represented the external perturbations for V1 (DCM.C matrix). For the conditions PT, ST, PC and SC four different regressors modeled the internal modulation of the system. These regressors represent the effects due to the different ways the subjects had to attend to the visual stimulus. These effects were represented as changes in the connectivity between the regions used in the models (DCM.B matrix). Fifteen models for both hemispheres were specified. The influence of the Pursuit and Saccadic conditions was kept constant (PT, ST) over all models. Only the connections modulated by the attention conditions (PC, SC) differed between the models to determine where an attention effect would most likely occur and to determine if this is best explained by feed forward or feed back processes. Figure 3.3 shows an overview of all models.

3.1.7. Averaged model

To generate a model that is representative for the winning model from the individual subject models we used the DCM averaging routine provided by SPM5. The principles of model averaging are described in section 2.3.6 (page 42), these principles are used by the SPM5 model averaging routine to average the parameters of the single subject

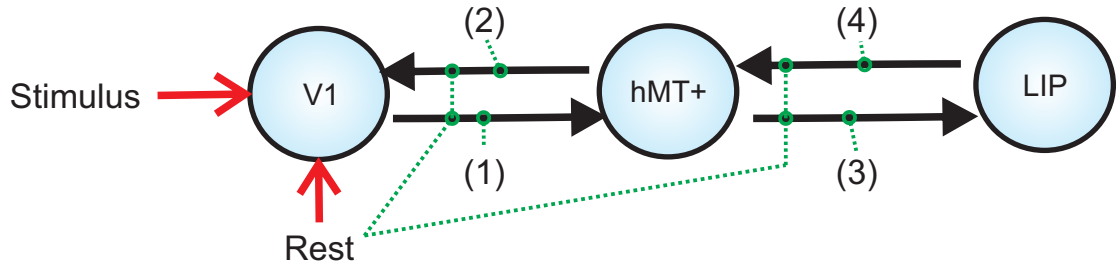

Connection		T1	T2	T3	T4	T5	T6	T7	T8	T9	T10	T11	T12	T13	T14	T15
V1 to	PT	X	X	X	X	X	X	X	X	X	X	X	X	X	X	X
hMT+	ST	X	X	X	X	X	X	X	X	X	X	X	X	X	X	X
(1)	PC	X	X	-	-	-	X	X	-	X	-	X	-	X	X	-
	SC	X	X	-	-	-	X	X	-	X	-	X	-	X	X	-
hMT+ to	PT	X	-	X	X	X	X	X	X	X	X	X	X	X	X	X
V1	ST	X	-	X	X	X	X	X	X	X	X	X	X	X	X	X
(2)	PC	X	-	-	-	X	X	-	X	X	-	-	X	X	-	X
	SC	X	-	-	-	X	X	-	X	X	-	-	X	X	-	X
hMT+ to	PT	X	X	X	X	X	X	X	X	X	X	X	X	X	X	X
LIP	ST	X	X	X	X	X	X	X	X	X	X	X	X	X	X	X
(3)	PC	X	X	X	X	-	-	-	-	X	X	X	-	-	-	-
	SC	X	X	X	X	-	-	-	-	X	X	X	-	-	-	-
LIP to	PT	X	-	X	X	X	X	X	X	X	X	X	X	X	X	X
hMT+	ST	X	-	X	X	X	X	X	X	X	X	X	X	X	X	X
(4)	PC	X	-	X	-	X	-	-	-	X	X	-	X	-	-	-
	SC	X	-	X	-	X	-	-	-	X	X	-	X	-	-	-

Figure 3.3.: Schematic depiction of all models. X depicts a connection modulated by a main condition (PT, ST, PC and/or SC). The intrinsic connections were the same in all models (solid arrows). Stimulus and Rest were the external modulators (open arrows) perturbing the system. The models differed only in which connection was affected by the modulators (dotted lines) PT, ST, PC and SC representing the four main experimental conditions. The table below depicts which connection was affected by the modulators for each model. Models T1 and T6 had a different C matrix, compared to the other models, the main conditions were treated as external modulators as well and drove directly the V1, hMT+ & LIP areas (T1); or only the active tracking conditions (PT, SC) drove V1 and hMT+ areas directly. All conditions were assumed to drive LIP directly (T6). In all other models the C matrix for PT, ST, PC SC contained zeroes. From: Acs & Greenlee, 2008

Table 3.2.: The averaged results of model T14 for the left and the right hemisphere, $P(|connection| > 0.00)$. The upper number represents the connectivity estimation, respectively the modulatory effects for the five different conditions modeled. The lower number represents the Bayesian FFX posterior probability. The sign → refers to the connection between two areas. From: Acs & Greenlee, 2008

Model T14 left	Intrinsic	Tracking Pursuit	Tracking Saccades	Covert Pursuit	Covert Saccades	Rest
V1 -> hMT+	-0.20 1.00	-0.47 1.00	-0.49 1.00	0.15 1.00	0.09 1.00	-0.25 1.00
hMT+ -> V1	0.52 1.00	0.24 1.00	0.41 1.00	---	---	-0.03 0.71
hMT+ -> LIP	0.41 1.00	0.12 1.00	0.13 1.00	---	---	-0.09 0.90
LIP -> hMT+	0.57 1.00	0.67 1.00	0.17 1.00	---	---	-0.24 1.00
Model T14 right	Intrinsic	Tracking Pursuit	Tracking Saccades	Covert Pursuit	Covert Saccades	Rest
V1 -> hMT+	-0.34 1.00	-0.31 1.00	-0.34 1.00	0.07 0.94	0.08 0.98	-0.06 0.96
hMT+ -> V1	0.33 1.00	0.33 1.00	0.58 1.00	---	---	0.07 0.83
hMT+ -> LIP	0.46 1.00	0.07 0.96	0.09 1.00	---	---	0.02 0.61
LIP -> hMT+	0.86 1.00	0.78 1.00	0.26 1.00	---	---	-0.09 0.89

models. Thus leading to a averaged model.

3.2. Results

3.2.1. Model comparison

A total of 105 comparisons were performed for each hemisphere according to their Akaike's Information Criterion (AIC) and Bayes Information Criterion (BIC) values and the resulting Bayes Factor of each comparison (see Penny et al., 2004a) on the

single subject level. The AIC and BIC values and AIC and BIC Bayes factor matrices where then fed in a group analysis to determine the Positive Evidence Ratio (PER, see 3.3) and the Group Bayes Factor (GBF, see Tables 3.4 and 3.5) according to (Stephan, Marshall, et al., 2007).

There was one winning model for both hemispheres (T14). Two other comparisons at the group level were performed, comparing models T14 and T15 for the left hemisphere and T10, T12, T14 for the right hemisphere, because these were the most likely candidates according to the entire model analysis. These selective group comparisons showed also that T14 was the winning model. Model T14 assumes a modulation in the bottom up connection between V1 and hMT+. In contrast model T15 models the influence of attention in the top down connection from hMT+ to V1. Model T10 modeled an influence of attention in the connections between hMT+ and LIP. Model T12 modeled and influence of attention only in the feed back connections between LIP and hMT+, and between hMT+ and V1. However the best model was model T14, which assumes an influence of covert attention only in the feed forward connection from V1 to hMT+

3.2.2. Attentional modulation

A group model of T14 across all eight subjects was created, by using the DCM model averaging routine of the SPM5 package. In both hemispheres an inversion of the connectivity compared to active tracking tasks can be observed. In model T14 left the inhibitory effect of the active tracking task for the connection from V1 to hMT+ turns into an excitatory effect for the covert attention tasks (Table 3.2). There was a high confidence for a modulatory effect for a threshold of 0.4 Hz. (Bayesian Fixed Effects: Left Hemisphere: P(contrast > 0.40) = 100%, mean = 1.4195, variance = 0.0183; Right Hemisphere: P(contrast > 0.40) = 100%, mean = 1.0876, variance = 0.0189; see figure 3.4)

In model T14 right the same effect can be found, for the connection from V1 to

Table 3.3.: Positive Evidence Ratio (PER) for each possible model comparison, the models of interest can be found in the columns and are compared per row against the other models. The numbers in the brackets denote how often the model of interest (left number) won against the other model (right number). Two criteria had to be met; first the AIC and BIC values of each comparison had to concur, second the evidence in terms of the minimal Bayes factor (AIC or BIC) had to provide good evidence (BF $\geq$ 3). The winning model was T14, however model T15 performed close to T14 in the right hemisphere. From: Acs & Greenlee, 2008

PER Left

Model	T1	T2	T3	T4	T5	T6	T7	T8	T9	T10	T11	T12	T13	T14	T15
T1	(0,0)	(2,5)	(6,2)	(7,1)	(7,1)	(5,2)	(6,1)	(8,0)	(4,3)	(5,1)	(6,0)	(5,1)	(5,1)	(6,0)	(5,1)
T2	(5,2)	(0,0)	(6,0)	(7,0)	(6,1)	(5,2)	(7,0)	(8,0)	(5,3)	(7,1)	(8,0)	(7,1)	(6,1)	(8,0)	(7,1)
T3	(2,6)	(0,6)	(0,0)	(3,3)	(5,1)	(2,5)	(3,1)	(7,1)	(4,4)	(5,2)	(6,0)	(4,3)	(4,3)	(6,0)	(4,1)
T4	(1,7)	(0,7)	(3,3)	(0,0)	(3,3)	(2,4)	(6,1)	(6,2)	(2,6)	(4,4)	(5,3)	(4,4)	(3,5)	(5,2)	(4,4)
T5	(1,7)	(1,6)	(1,5)	(3,3)	(0,0)	(0,5)	(3,0)	(7,0)	(4,4)	(5,3)	(6,1)	(4,3)	(4,3)	(6,1)	(4,3)
T6	(2,5)	(2,5)	(5,2)	(4,2)	(5,0)	(0,0)	(5,0)	(8,0)	(4,4)	(5,2)	(7,1)	(5,2)	(5,2)	(7,1)	(5,2)
T7	(1,6)	(0,7)	(1,3)	(1,6)	(0,3)	(0,5)	(0,0)	(5,2)	(2,6)	(3,4)	(4,2)	(3,5)	(3,5)	(4,2)	(3,3)
T8	(0,8)	(0,8)	(1,7)	(2,6)	(0,7)	(0,8)	(2,5)	(0,0)	(2,5)	(4,3)	(6,1)	(4,3)	(3,4)	(6,1)	(4,3)
T9	(3,4)	(3,5)	(4,4)	(6,2)	(4,4)	(4,4)	(6,2)	(5,2)	(0,0)	(5,0)	(7,0)	(6,0)	(6,0)	(7,0)	(6,0)
T10	(1,5)	(1,7)	(2,5)	(4,4)	(3,5)	(2,5)	(4,3)	(3,4)	(0,5)	(0,0)	(4,1)	(3,3)	(2,3)	(5,0)	(3,1)
T11	(0,6)	(0,8)	(0,6)	(3,5)	(1,6)	(1,7)	(2,4)	(1,6)	(0,7)	(1,4)	(0,0)	(2,5)	(2,4)	(3,0)	(3,4)
T12	(1,5)	(1,7)	(3,4)	(4,4)	(3,4)	(2,5)	(5,3)	(3,4)	(0,6)	(3,3)	(5,2)	(0,0)	(0,3)	(5,1)	(5,0)
T13	(1,5)	(1,6)	(3,4)	(5,3)	(3,4)	(2,5)	(5,3)	(4,3)	(0,6)	(3,2)	(4,2)	(3,0)	(0,0)	(5,0)	(6,0)
T14	(0,6)	(0,8)	(0,6)	(2,5)	(1,6)	(1,7)	(2,4)	(1,6)	(0,7)	(0,5)	(0,3)	(1,5)	(0,5)	(0,0)	(3,5)
T15	(1,5)	(1,7)	(1,4)	(4,4)	(3,4)	(2,5)	(3,3)	(3,4)	(0,6)	(1,3)	(4,3)	(0,5)	(0,6)	(5,3)	(0,0)

PER Right

Model	T1	T2	T3	T4	T5	T6	T7	T8	T9	T10	T11	T12	T13	T14	T15
T1	(0,0)	(1,5)	(4,3)	(6,1)	(4,3)	(7,1)	(5,2)	(7,1)	(4,3)	(6,1)	(5,1)	(5,0)	(5,2)	(5,1)	(5,1)
T2	(5,1)	(0,0)	(5,3)	(7,1)	(5,3)	(7,1)	(6,2)	(7,1)	(6,2)	(7,1)	(7,1)	(7,1)	(7,1)	(7,1)	(7,1)
T3	(3,4)	(3,5)	(0,0)	(6,2)	(5,1)	(5,2)	(4,2)	(6,1)	(3,4)	(4,2)	(4,1)	(5,1)	(4,2)	(4,1)	(4,2)
T4	(1,6)	(1,7)	(2,6)	(0,0)	(5,2)	(4,2)	(6,2)	(5,2)	(2,5)	(4,1)	(3,1)	(4,1)	(4,2)	(3,1)	(3,2)
T5	(3,4)	(3,5)	(1,5)	(2,5)	(0,0)	(3,3)	(2,2)	(5,0)	(2,4)	(4,2)	(3,2)	(3,1)	(4,2)	(3,2)	(2,2)
T6	(1,7)	(1,7)	(2,5)	(2,4)	(3,3)	(0,0)	(3,2)	(4,1)	(2,3)	(4,2)	(3,2)	(3,2)	(3,2)	(4,2)	(3,2)
T7	(2,5)	(2,6)	(2,4)	(2,6)	(2,2)	(2,3)	(0,0)	(5,2)	(2,4)	(4,3)	(3,3)	(3,1)	(4,3)	(3,2)	(4,1)
T8	(1,7)	(1,7)	(1,6)	(2,5)	(0,5)	(1,4)	(2,5)	(0,0)	(1,6)	(3,3)	(2,3)	(2,2)	(2,3)	(2,2)	(2,2)
T9	(3,4)	(2,6)	(4,3)	(5,2)	(4,2)	(3,2)	(4,2)	(6,1)	(0,0)	(5,2)	(6,0)	(6,1)	(7,0)	(7,0)	(6,1)
T10	(1,6)	(1,7)	(2,4)	(1,4)	(2,4)	(2,4)	(3,4)	(3,3)	(2,5)	(0,0)	(4,4)	(3,3)	(4,4)	(4,2)	(4,3)
T11	(1,5)	(1,7)	(1,4)	(1,3)	(2,3)	(2,3)	(3,3)	(3,2)	(0,6)	(4,4)	(0,0)	(5,2)	(3,1)	(4,0)	(5,1)
T12	(0,5)	(1,7)	(1,5)	(1,4)	(1,3)	(2,3)	(1,3)	(2,2)	(1,6)	(3,3)	(2,5)	(0,0)	(3,5)	(2,2)	(5,1)
T13	(2,5)	(1,7)	(2,4)	(2,4)	(2,4)	(2,3)	(3,4)	(3,2)	(0,7)	(4,4)	(1,3)	(5,3)	(0,0)	(3,0)	(5,1)
T14	(1,5)	(1,7)	(1,4)	(1,3)	(2,3)	(2,4)	(2,3)	(2,2)	(0,7)	(2,4)	(0,4)	(2,2)	(0,3)	(0,0)	(5,1)
T15	(1,5)	(1,7)	(2,4)	(2,3)	(2,2)	(2,3)	(1,4)	(2,2)	(1,6)	(3,4)	(1,5)	(1,5)	(1,5)	(1,5)	(0,0)

Table 3.4.: Group Bayes Factors for the 15 models of the left hemisphere. Multiple model comparisons provides the GBF evidence for the group. The models in the rows are compared against the models in the columns. Inf denotes a infinite value, the number was too big to be represented by the computer. The winning model (T14) is highlighted. From: Acs & Greenlee, 2008

Model	1	2	3	4	5	6	7	8	9	10	11	12	13	14	15
1	-	Inf	Inf	Inf	Inf	Inf	Inf	8.72E-163	Inf	Inf	3.24E-204	Inf	Inf	2.27E-222	Inf
2	3.86E-160	-	1.59E-90	5.52E-308	3.57E-105	Inf	9.55E-265	4.32E-254	Inf	Inf	1.10E-264	Inf	Inf	2.84E-277	Inf
3	Inf	Inf	-	3.79E-217	Inf	Inf	2.61E-189	5.34E-114	Inf	Inf	2.96E-155	Inf	Inf	1.40E-172	Inf
4	Inf	Inf	2.64E+216	-	Inf	Inf	6.89E+27	4.17E-08	Inf	Inf	2.31E-49	Inf	Inf	1.09E-66	Inf
5	2.89E+89	Inf	2.92E+19	5.23E-208	-	Inf	2.12E-170	1.23E-17	Inf	Inf	9.60E-50	Inf	Inf	6.43E-65	Inf
6	1.87E+56	Inf	3.18E+82	9.76E-133	1.65E+64	-	3.03E-91	5.10E-26	Inf	Inf	6.21E-53	Inf	Inf	4.80E-65	Inf
7	Inf	Inf	1.04E+171	3.94E-46	Inf	Inf	-	8.86E+10	Inf	Inf	4.90E-31	Inf	Inf	2.32E-48	Inf
8	Inf	Inf	Inf	Inf	Inf	Inf	Inf	-	Inf	Inf	2.64E-51	Inf	Inf	1.31E-71	Inf
9	3.56E+56	Inf	Inf	Inf	Inf	Inf	Inf	2.29E-16	-	4.72E-35	6.04E-34	1.03E-49	8.21E-36	6.47E-47	1.64E-66
10	Inf	Inf	Inf	Inf	Inf	Inf	Inf	52.656	Inf	-	6.14E-05	6.91E-11	Inf	7.69E-23	1.22E-33
11	Inf	Inf	Inf	Inf	Inf	Inf	Inf	2.78E+15	Inf	Inf	-	Inf	Inf	4.94E-21	Inf
12	Inf	Inf	Inf	Inf	Inf	Inf	Inf	7.61E+11	Inf	1.45E+10	8.88E+05	-	Inf	1.11E-12	1.77E-23
13	2.09E+82	Inf	Inf	Inf	Inf	Inf	Inf	2.98E-09	Inf	6.57E-05	1.99E-10	1.93E-20	-	3.52E-26	2.70E-40
14	Inf	Inf	Inf	Inf	Inf	Inf	Inf	1.53E+18	Inf	Inf	548.4	Inf	Inf	-	Inf
15	Inf	Inf	Inf	Inf	Inf	Inf	Inf	1.58E+16	Inf	2.21E+15	1.84E+10	1.53E+05	Inf	5.41E+07	-

Table 3.5.: Group Bayes Factors for the 15 models of the right hemisphere. Multiple model comparisons provide the GBF evidence for the group. The models in the rows are compared against the models in the columns. Inf denotes a infinite value, the number was too big to be represented by the computer. The winning model (T14) is highlighted. From: Acs & Greenlee, 2008

Model	1	2	3	4	5	6	7	8	9	10	11	12	13	14	15
1	-	Inf	Inf	1.30E-110	Inf	Inf	Inf	Inf	Inf	Inf	1.86E-183	2.00E-209	4.99E-168	1.08E-200	3.85E-144
2	6.88E-107	-	Inf	5.87E-139	Inf	Inf	Inf	Inf	Inf	Inf	0	2.14E-187	0	0	2.93E-119
3	2.34E-07	Inf	-	2.44E-17	7.29E-58	8356.7	Inf	7.71E-19	6.86E+64	Inf	1.02E+23	3.56E-77	1.61E+40	1.23E+11	2.92E-06
4	1.54E+57	Inf	Inf	-	Inf	Inf	Inf	Inf	Inf	Inf	1.06E-25	1.54E-99	2.85E-10	6.15E-43	2.97E-34
5	3.21E+50	Inf	Inf	3.35E+40	-	4.01E-293	Inf	7.03E-19	6.25E+64	Inf	9.33E+22	4.88E-20	1.47E+40	1.12E+11	4.01E+51
6	Inf	Inf	Inf	Inf	Inf	-	Inf	4.07E-76	6.08E-22	Inf	2.01E-74	7.14E+243	5.78E-58	2.35E-91	Inf
7	4.62E+99	Inf	Inf	1.23E+06	Inf	1.2656	-	17822	1.30E+54	Inf	4185.1	9.98E-21	3.44E+20	5.73E-12	2.75E-37
8	Inf	Inf	Inf	Inf	Inf	6.65E+57	Inf	-	1.49E+54	Inf	0.042497	Inf	1.22E+15	4.98E-19	Inf
9	Inf	Inf	Inf	Inf	Inf	4457.3	Inf	6.70E-55	-	Inf	2.85E-56	Inf	8.19E-40	3.34E-73	Inf
10	Inf	Inf	Inf	Inf	Inf	Inf	Inf	Inf	Inf	-	6.31E+46	Inf	2.77E+61	3.27E+30	Inf
11	Inf	Inf	Inf	Inf	Inf	Inf	Inf	Inf	Inf	Inf	-	Inf	9.39E+14	4.95E-20	Inf
12	1.98E+103	Inf	Inf	1.29E+46	Inf	Inf	Inf	Inf	Inf	Inf	8.73E+22	-	2.34E+38	5.05E+05	1.92E+65
13	Inf	Inf	Inf	Inf	Inf	Inf	Inf	Inf	Inf	Inf	1.07E-15	Inf	-	5.27E-35	Inf
14	Inf	Inf	Inf	Inf	Inf	Inf	Inf	Inf	Inf	Inf	54.748	Inf	5.14E+16	-	Inf
15	2.79E+20	Inf	Inf	1.82E-37	Inf	Inf	Inf	Inf	Inf	Inf	6.99E+26	1.41E-83	1.87E+42	9.50E+24	-

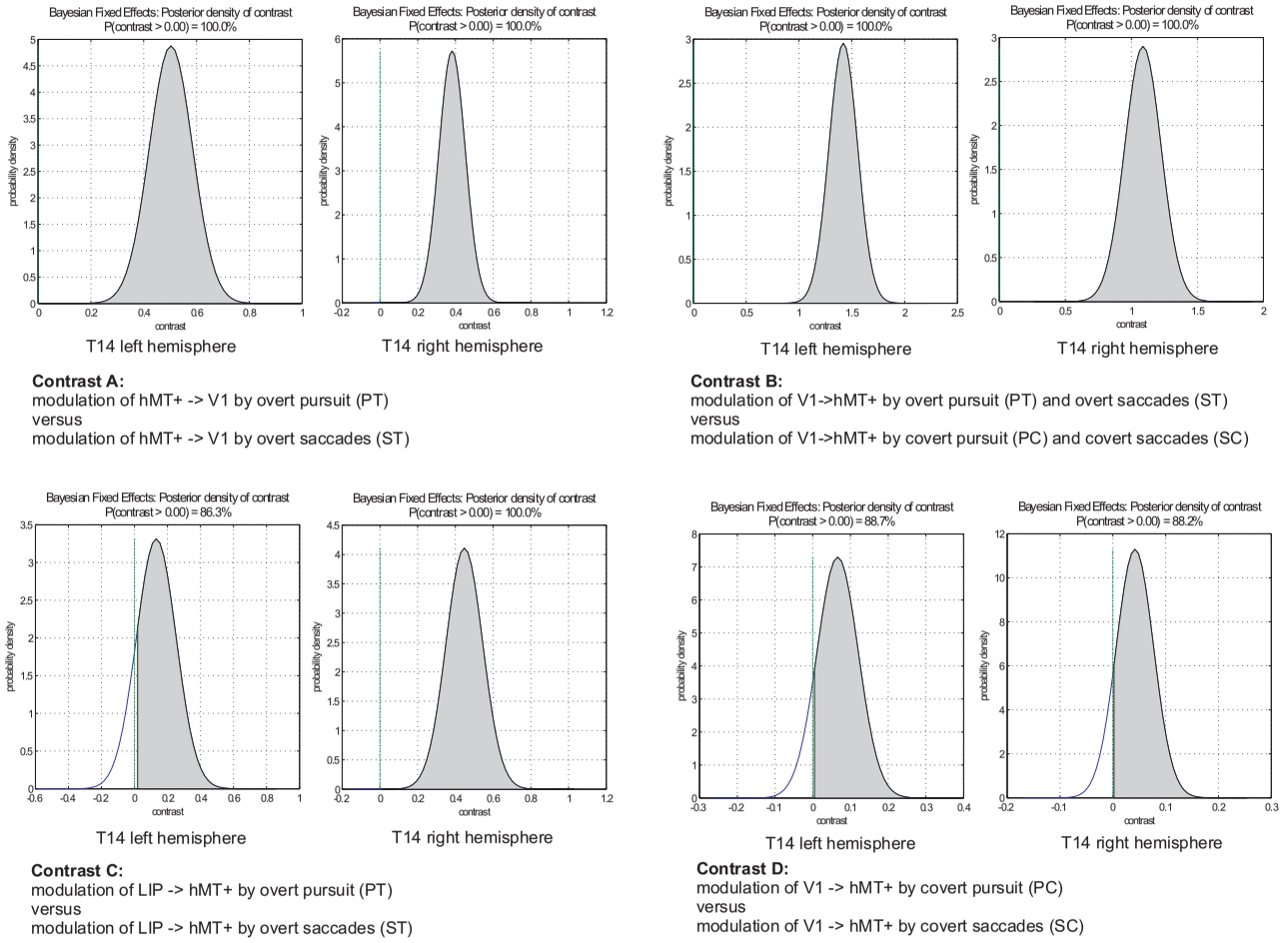

Figure 3.4.: Probabilities of differences between modulatory effects of the conditions pursuit and saccades in model T14. **Contrast A:** For the connection from hMT+ to V1 we can be confident about a difference in modulation caused by actively tracking a pursuit target comparing it to the modulation caused by actively tracking a saccadic target. **Contrast B:** For the connection from V1 to hMT+ we can be confident about a difference in modulation caused by actively tracking both, pursuit and saccadic targets, compared to covertly tracking both types of targets. **Contrast C:** A difference between the left and the right hemisphere can be found in the LIP to hMT+ connection. We can only be sure about a difference caused by actively tracking pursuit targets compared to actively tracking saccadic targets for the right hemisphere. The confidence threshold is >90%. **Contrast D:** Comparing modulations caused by covertly attending to pursuit targets with covertly attending to saccadic targets show posterior densities near to the confidence threshold of 90%. From: Acs & Greenlee, 2008

hMT+. There was no difference over the confidence threshold of 90% observable when comparing the effects of the covert pursuit tasks with the covert saccade tasks in both models. (Bayesian Fixed Effects: Left Hemisphere: P(contrast > 0.00) = 88.7%, mean = 0.0661, variance = 0.0239; Right Hemisphere P(contrast > 0.00) = 88.2%, mean = 0.0419, variance = 0.0012; see figure 3.4). Pursuit and saccade tracking As expected we found major differences in the interplay between V1, hMT+ and LIP for the different types of tracking tasks. Tracking of a saccadic target modulates the hMT+ to V1 connection more than pursuit tasks do, in both hemispheres (Bayesian Fixed Effects: Left Hemisphere: P(contrast > 0.20) = 100%, mean = 0.5031, variance = 0.0067; Right Hemisphere P(contrast > 0.20) = 99.6%, mean = 0.3821, variance = 0.0049; see figure 3.4). The LIP to hMT+ connection showed also major effects comparing pursuit and saccade tracking tasks, however the fixed effects analysis for the left hemisphere failed to pass the confidence threshold of 90%. (Bayesian Fixed Effects: Left Hemisphere: P(contrast > 0.00) = 86.3%, mean = 0.1319, variance = 0.0145; Right Hemisphere P(contrast > 0.40) = 99.8%, mean = 0.7236, variance = 0.0126; see figure 3.4).

3.3. Discussion

The aim of the present study was to explore the interplay between cortical areas in the human visual cortex that are involved in the processing of pursuit and saccadic eye movements, as well as those underlying the control of covert attention to moving targets. During active tracking tasks the top down connections from hMT+ to V1 and LIP to hMT+ were mainly affected. The connectivity from LIP to hMT+ seems to be more pronounced during the processing of smooth pursuit eye movements. This finding is in agreement with the finding concerning the role of LIP in the processing of saccadic eye movements (Lynch & Tian, 2005). However, little is known about the role of LIP in the processing of smooth pursuit eye movements (Krauzlis, 2005). The effect in the hMT+ to the V1 connection was more pronounced during saccadic eye movement processing

compared to the processing of pursuit eye movements, which seems to indicate that there is a top down effect from higher visual processing areas to V1. This may be related to the saccadic suppression effect in V1 observed with fMRI by Vallines and Greenlee (2006). An unexpected finding was that the model won that favored a pronounced influence of attention modulation on the connection from V1 to hMT+. Due to the major role of LIP in processing of voluntary eye movements (Lynch & Tian, 2005), we would have expected that models which assume an effect of attention on the connection between hMT+ and LIP would have won. These models were all outperformed by the one that modeled only an attention effect in the connection from V1 to hMT+. Bisley and Goldberg (2003) suggest that the locus of attention evokes differences in activity of the LIP. Krauzlis (2005) argued that LIP plays a role in the preparation of a saccadic inhibition, which would be present in our covert attention condition. However, the models assuming an attention effect between LIP and hMT+ (T1-T5, T9-T12) were all outperformed by model T14, which assumed only an attention effect on the bottom up connection from V1 to hMT+. Other fMRI studies have already suggested that V1 not only processes retinal signals in a bottom-up fashion but also receives inhibitory input from other cortical areas during saccades (Vallines & Greenlee, 2006). Our results suggest that the connections between V1 and hMT+ are sensitive to covert versus overt attention. Büchel and Friston (1997) already showed a similar behavior with the method of structural equation modeling, related to attention versus no attention toward a moving dot field. We did not model separately the human analogues of MT and MST shown to be important in the control of pursuit eye movements (Dukelow et al., 2001; Huk et al., 2002). For technical reasons we pooled voxels into a common area hMT+ in the tested models. We believe, however, that this is only a minor shortcoming, because the routine (in spm_regions.m), that extracts the signal time course representative for one region derives the first eigenvariate of the voxel time courses in that region of interest. This represents a time course that explains most of the variance over all voxel time

series of that region. Attention can be defined as an emergent property of the interplay between cortical areas. Our findings indicate that task-defined manipulations in covert or overt attention also affect this interplay. Numerical simulations with the methods of computational neuroscience support this argumentation, through studies that simulate networks of brain areas (Deco & Rolls, 2005a, 2005b; Hamker, 2005). Corbetta et al. (1998) suggested that attention and eye movement processes are functionally related. Furthermore Krauzlis (2005) showed that areas involved in voluntary eye movements, either pursuit or saccadic eye movements, are functionally interrelated. Our findings described these functional relations in the human visual system with the methods of a connectivity analysis.

4. Connectivity analysis of attention shifting

The major downsides of using the DCM approach is that there has to be solid empirical evidence or at least well supported theories of how brain areas are connected in certain tasks. For the early stages of visual processing this was not a major obstacle, because of the vast research basis of the recent decades. This became a serious problem when the connectivity modulation of attention shifting in higher brain areas became the focus of interest. Some evidence was found so far that the frontal eye fields and a cluster in the superior frontal sulcus / middle frontal gyrus are involved in covert shifts of attention or attentional processing in general (Corbetta et al., 1998; Astafiev et al., 2003; Erickson, Ho, Colcombe, & Kramer, 2005; Grosbras et al., 2005). Also the role of the lateral intraparietal area (LIP) for attention processing is undisputed (Shadlen & Newsome, 2001; Roitman & Shadlen, 2002; Bisley & Goldberg, 2003; Schiller & Tehovnik, 2005). However it was not clear how higher brain areas are interconnected during overt attentional processing of pursuit and saccadic eye movements. In terms of dynamic causal modeling, there were no plausible models which could serve as a starting point for the modeling process. This problem was solved in a pragmatic way, every mathematically possible model was modeled and the empirical data of 4096 models were compared against each other with a sophisticated model comparison approach to determine the most plausible model for this purpose. Section 2.3.5 (page 41) explains the theory of extensive model comparisons in detail.

4.1. Materials & Methods

For this study the measured data of the study in chapter 3 (page 55) was re-analyzed. A new pre-processing of the fMRI data and a new extraction of regions of interest was conducted to extract the time series of the areas hMT+, LIP, FEF and SEF. Based on this a new modeling process was started.

4.1.1. Subjects

We examined eight healthy subjects with no known neurological or psychological disorders. Five males and three females in the age range between 20 and 35 years, all subjects were right handed. However only seven subjects, two female and five male, remained in the analysis. In one subjects not all of the needed brain areas could be localized on the single subject level. This localization is crucial for the time course extraction of a certain brain area for the subsequent DCM analysis.

4.1.2. GLM Analysis

The underlying GLM analysis was slightly different that the one used in chapter 3 (page 59). Pre-processing involved again realignment. The slice timing correction was omitted this time because in the meantime the DCM implementation in SPM5 was changed in the way to incorporate slice timing corrections especially for DCM analysis (Kiebel, Klöppel, Weiskopf, & Friston, 2007). The normalization of the EPI mean image to EPI template provided the parameters for normalizing the EPI scans. The realigned images were smoothed using a 6 mm FWHM smoothing kernel. In the GLM analysis the regressors denoting the 4 main conditions were modeled (pursuit-tracking, PT; saccadic-tracking, ST; pursuit-covert, PC; saccade-covert, SC). Additionally the condition Rest (R), the presentation of the instructions, and the response events (i.e., button presses) were included. Head movements formed six more regressors, three describing the rotation and three describing the translation of the subject's head during the functional scan.

The first 163 scans were discarded (first 80 seconds of the experiment). The Volumes of Interest (VOI) were selected manually for each subject. For this purpose the T-contrast of the main tracking conditions (PT, ST) against the rest conditions guided this selection. The localization of the peak activity for each region was always performed with the T-contrast that seemed most suitable for the specific region, for example the Saccades > Rest contrast to locate the LIP regions. This location was then transferred to the F-contrast map of the relevant DCM conditions and was adjusted slightly to match the peak there. The MNI coordinates of the regions stayed the same and can be seen in table 3.1 (page 61)

4.1.3. DCM Models

Based on the findings in chapter 3 and in Acs and Greenlee (2008), it was assumed that the best model for explaining the neural interaction between V1 and hMT+ was model T14 (see figure 3.3, page 64). Model T14 assumes bi-directional connections between the areas V1, hMT+ and LIP. All of these connections are affected by the direct tracking tasks (PT, ST) but only the bottom up connection from V1 to hMT+ is modulated by the covert attention conditions (PC, SC). In recent models of pursuit and saccadic eye movements the connections between the areas FEF, SEF and LIP are assumed to be bi-directional (Krauzlis, 2004, 2005; Lynch & Tian, 2005). Consequently it was assumed that the active tracking conditions (PT, ST) affected every connection. This assumption was mainly useful to reduce the number of models to investigate. The question to solve now was how attentional processing is implemented in even higher brain areas (FEF, SEF and LIP) when there was even little known about the interplay between these areas for attentional tasks. This problem was challenged by taking the model, known as T14, and expanding it to a larger family of models which involve the brain areas FEF and SEF. Given are six possible connections between the areas LIP, FEF and SEF, at every connection the two relevant internal modulators for covert attentional processing (PC

Table 4.1.: 4,096 possible permutations of the B matrix result from the combinations visible below. The influence of PC and SC on the connections LIP $\rightleftarrows$ FEF, FEF $\rightleftarrows$ SEF and SEF $\rightleftarrows$ LIP was unknown. So all possible models had to be explored. Thus the influence of a modulator on a connection had to be either present or absent, leading to binary combinations. Two possibilities for $2 \cdot 6$ possible influences leading to $2^{2 \cdot 6} = 4096$ possible B matrices. According to results of a previous study the influence of PC and SC to the hMT+ $\rightleftarrows$ LIP connections could be assumed zero (Acs & Greenlee, 2008). The self connections in the main diagonal were also assumed to be zero. Non existent intrinsic connections are denoted by a $\emptyset$.

to/from	**hMT+**	**LIP**	**FEF**	**SEF**
hMT+	0	0	$\emptyset$	$\emptyset$
LIP	0	0	PC/SC	PC/SC
FEF	$\emptyset$	PC/SC	0	PC/SC
SEF	$\emptyset$	PC/SC	PC/SC	0

and SC) could possibly modulate the connection.

Adopting some combinations this leads to $2^{12} = 4096$ possible models. So 4096 model estimations were computed for each of the seven subjects and for each hemisphere. This led to $4096 \cdot 7 \cdot 2 = 57,344$ model estimations that had to be computed; see table 4.1 for details. Due to the excessive computational amount needed for this the model estimation was performed by a specially developed model comparison algorithm that was around 100 times faster than the model estimation by the standard SPM5 package, called Fast DCM[1]. The model estimation for all 57,344 models took six months on a eight core 2.6GHz Xeon 5300$^{\text{TM}}$ CPU server system[2].

4.1.4. Model comparisons

For each hemisphere and each subject the models were first compared on a single subject level to get the Bayes Factors and the estimations for the PER ratios. This led

[1] Fast DCM is available at: *http://fast-dcm.sourceforge.net/*

[2] Hereby I thank the head of the Computer Centre at the University of Regensburg, Dr. Martin Wimmer, for his kind support, which allowed the utilization of this server system for several months.

to $4,096 \cdot 4,096 - 4,096 = 16,773,120$ comparisons. Because of the large numbers of comparisons the comparisons on both, the single subject and the group level, had been implemented by MATLAB^{TM} scripts. According to the explanations in section 2.3.5 (page 41) the large AIC and BIC matrices for each subjects led to the Group Bayes Factor (GBF) and Positive Evidence Ratio (PER) matrices for the group level.

The model selection process had to be divided in three stages, first the GBF and PER values were computed leading to rather large 4096 $\cdot$4096 matrices. There was no specific winning model for either the left or the right hemisphere. This is because the GBF value of certain models gets so large that it cannot be longer represented in the 64 Bit coding scheme of MATLAB^{TM} and is then stored as an infinite value (Inf). In a second comparison step then the 15 highest performing models for each hemisphere were selected according to their PER values, because the GBF values were infinite anyways. Because the model comparison is a relative comparison approach, comparisons of the 15 best models led to more interpretable results. This is because the model comparison is a relative procedure, it tells whether certain models are better than other ones but does not provide an absolute judgement how good a specific model is against all possible models. In a final step it was then necessary to run another model comparison, comparing two models for the left hemisphere and three models of the right hemisphere.

4.2. Results

4.2.1. Model comparisons

It was necessary to implement a two-step model comparison approach due to the large number of models used. In a first step the 4096 models were reduced to 15 models, this was done by picking out the 15 models with the best Group Bayes Factors. The Positive Evidence Ratio could not contribute too much insight because the highest possible PER

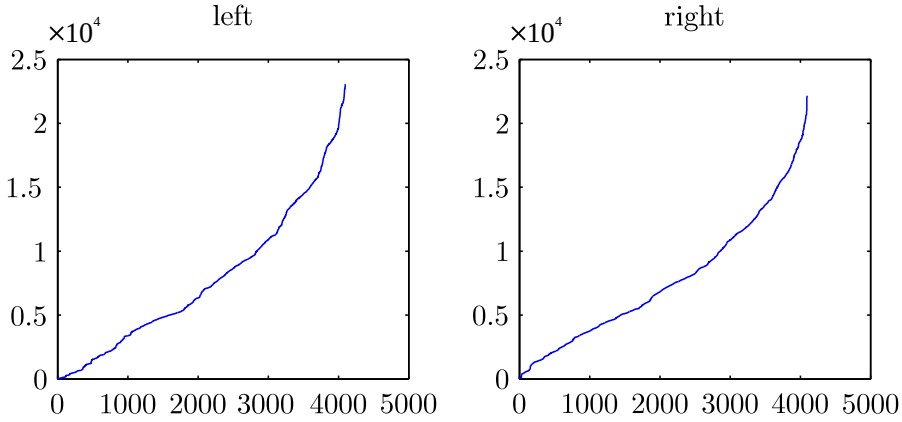

Figure 4.1.: Sum of GBF for each hemisphere. Sorted for 4096 models from the worst to the best performing model according to the Group Bayes Factor.

value in a seven subjects group comparison is seven. It was not practical to group 4096 models in only seven categories. So the GBF serves here the best. As we can see in figure 4.1 the sum of the GBF values for each model evolved in an exponential manner sorting from the worst to the best model. The elbow criteria, known from multivariate statistics, was used here to set a cutoff point at 15 models.

Comparing 15 remaining models

With at total of 30 models, 15 for each hemisphere, now a more sophisticated model comparison approach could be performed. The 30 remaining models (see figure 4.2) were fed into a MATLAB^{TM} script that calculated the GBF and PER values and generated models averaged over all subjects for a later inspection.

The comparisons for the right hemisphere generated two possible winners according to the Group Bayes Factor results, that were models 3572 and 4087 (see figure 4.3). The Positive Evidence Ratio was in favor for model 4096 (see figure 4.5).

For the left hemisphere the Group Bayes Factor results favored models 4024 and 2048 (see figure 4.4). Here the Positive Evidence Ratio results concurred partly with the Group Bayes Factor results by being in favor of model 2048 (see figure 4.6).

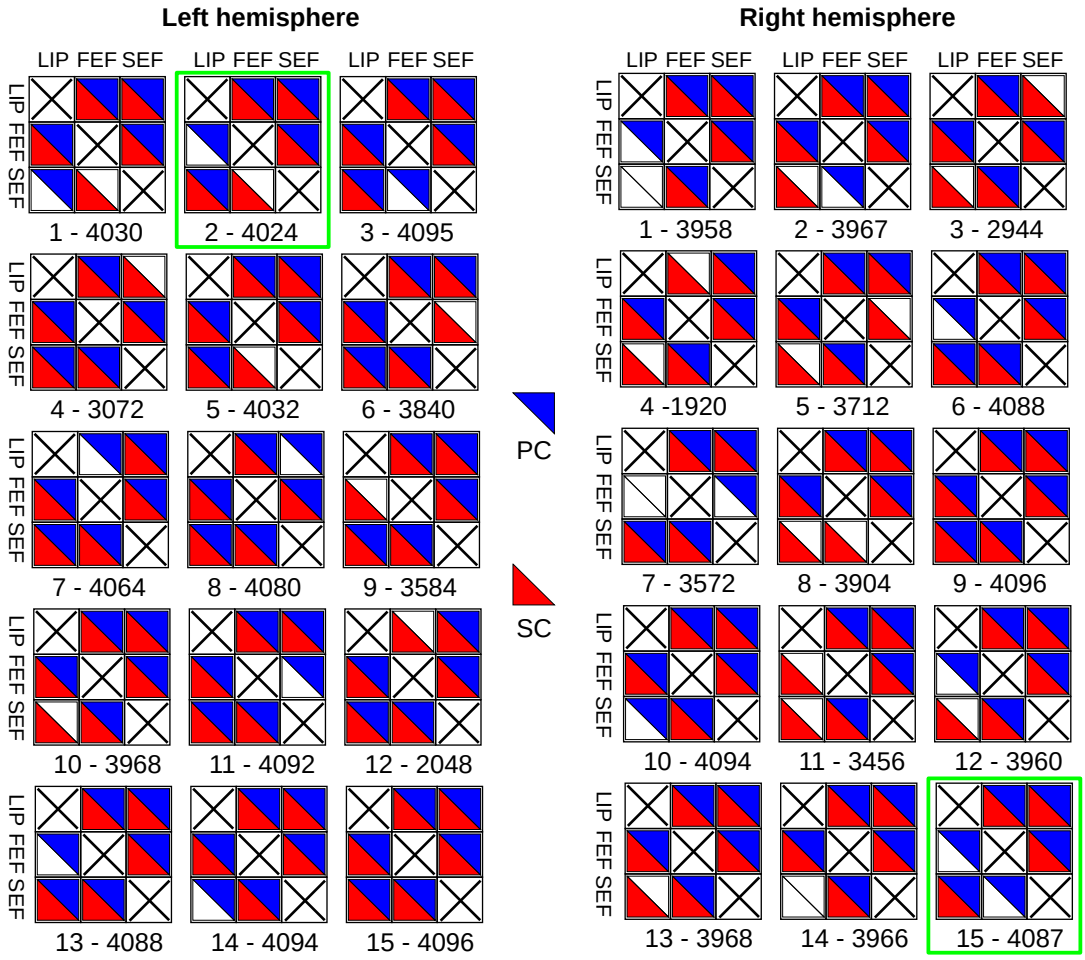

Figure 4.2.: 15 models survived the model comparison of 4096 models. 15 comparisons were now performed, the corresponding model number can be found below the diagram. The fields are red from left to right LIP, FEF and SEF. Top down is the same order. Each area in a column is connected to the corresponding area in a row. Modulation by covert pursuit (PC) modulators is indicated by a blue triangle in the upper right corner. Modulation by covert saccades (SC) by a red triangle in the lower left corner. The models are sorted according to their GBF of the 4096 model comparison. 1 is lowest, 15 is highest. The green boxes indicate the winning models of this study (see also: section 4.2.2 and figure 4.7).

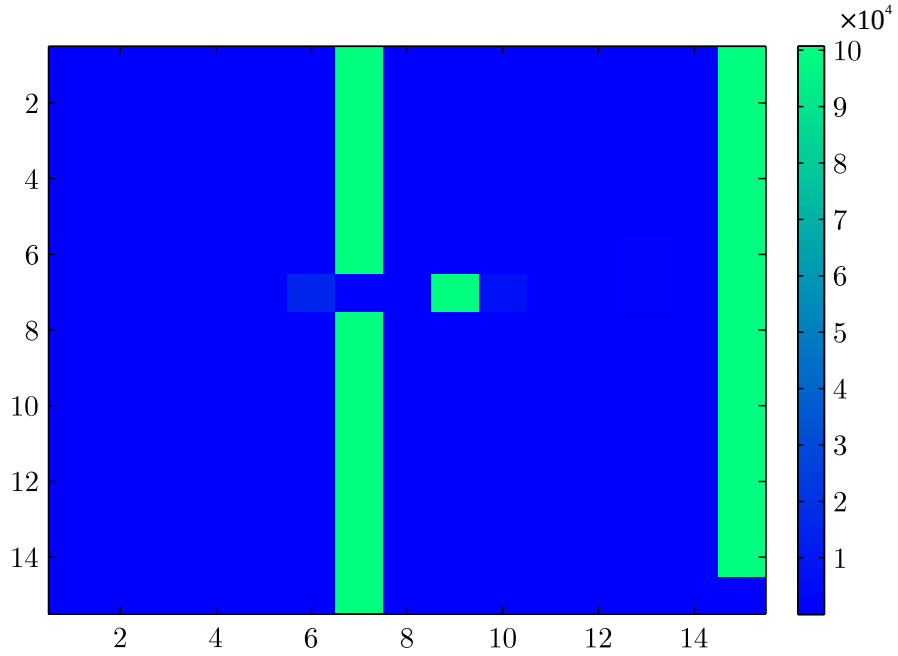

Figure 4.3.: GBF for the right hemisphere of 15 models. The comparison chart has to be read column wise. Here the 7'th (3572) and 15'th (4087) models in the comparison performed well against the other models.

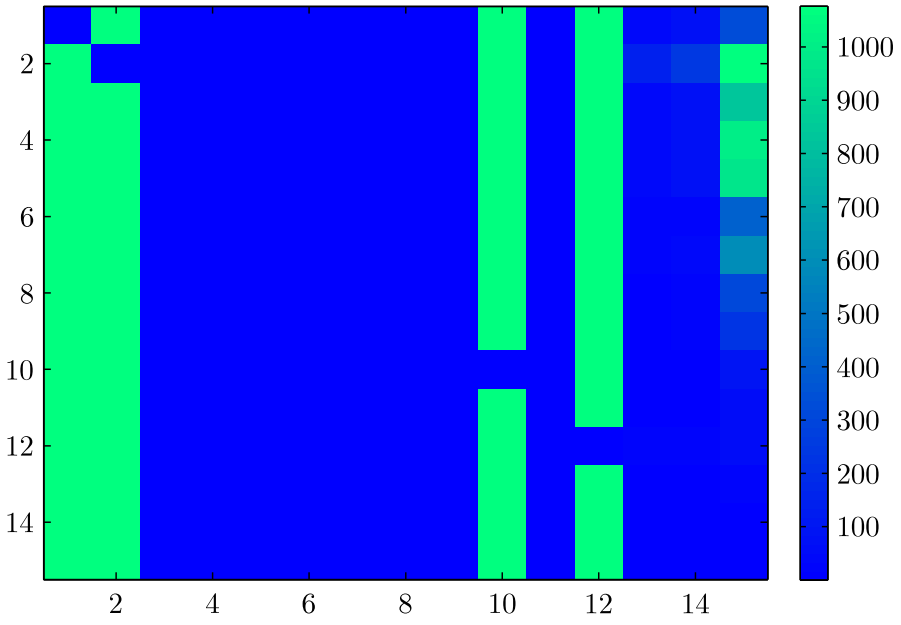

Figure 4.4.: GBF for the left hemisphere of 15 models. The 2'nd (4024) and the 12'th (2048) model scored highest in this comparison. The 1'st (4030) and 10'th (3968) model look good, however their numerical values were lower than the other two ones.

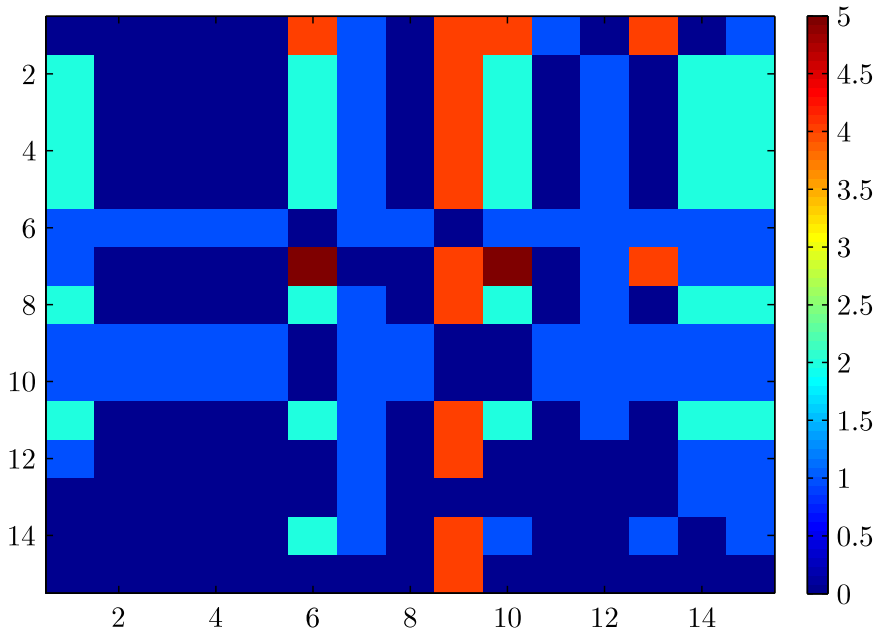

Figure 4.5.: PER for the right hemisphere of 15 models. The model in the 9'th comparison (4096) scores highest. The positive evidence ratio is four in most rows. Thus meaning that model 4096 won in four subjects with good evidence against the other model in the row.

To get more evidence which models consistently won a second model comparison was run, comparing models 3572, 4087 and 4096 for the right hemisphere and models 4024 and 2048 for the left hemisphere.

The remaining five models

Despite the fact that only 15 models entered the above analysis, it could still not be concluded which model was the winning model, this is because of the GBF comparisons (see figures 4.3 and 4.4). To get the Bayes Factor of a comparison the conditional probabilities of two models (i,j) are compared to get a numerical estimation for BF_{ij} (see equation 2.23, page 41). If a very good model is compared against a rather poor model the numerical value of BF_{ij} can get quite high. To make things worse GBF_{ij} is the product of BF_{ij} over all subjects (see equation 2.24, page 41). So if there is a very good

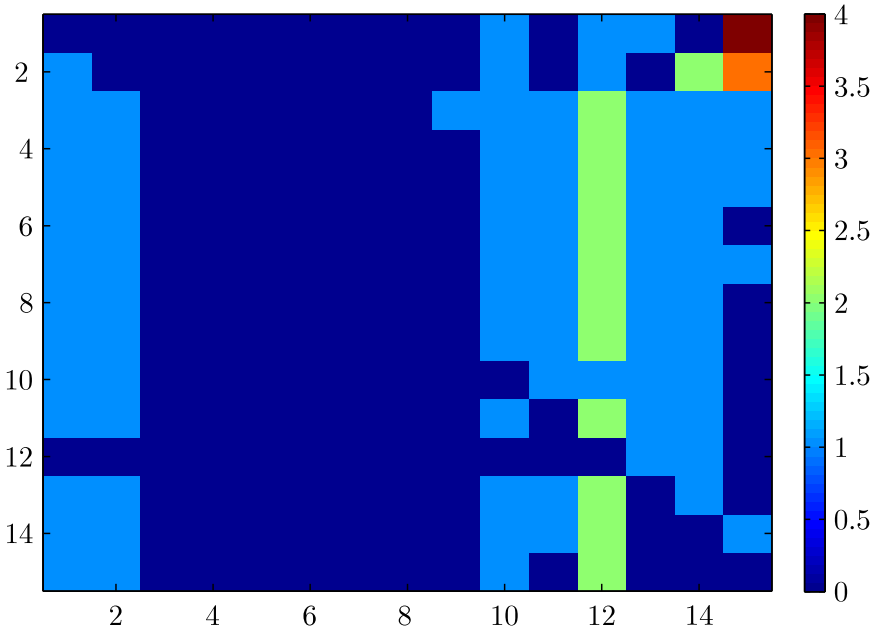

Figure 4.6.: PER for the left hemisphere of 15 models. The model in the 12'th (2048) comparison had here the highest positive evidence ration, winning most of times in three subjects against the other models in the corresponding row.

model competing against relative poor models, very high numerical values of GBF_{ij} are reached very fast. This happened here. The GBF_{ij} values went so high that they could not be discriminated numerically from each other because they left the range of the double precision (64 Bit) number space. This could be seen by several MATLAB^{TM} matrices that had 'Inf' values in their cells. 'Inf' means here infinite number. The solution is now to only take good models and compare them against each other in the hope that GBF_{ij} will stay in reasonable boundaries. This is what was done here by picking 15 models of 4096 and then compare the remaining three models for the right hemisphere and the remaining two models for the left hemisphere against each other.

Table 4.2 shows the group comparison results for comparing two models for the left hemisphere and three models for the right hemisphere. Looking at the right hemisphere the comparison results are clear, model 4087 won according to the GBF and PER es-

Table 4.2.: Model comparisons for the five remaining models, separated by hemisphere. 'Inf' indicates that the GBF value got too big for numerical representation by the computer.

left			**right**			
GBF	**4024**	**2048**	**GBF**	**3572**	**4096**	**4087**
4024	1	Inf	**3572**	1	Inf	100734
2048	Inf	1	**4096**	Inf	1	599
			4087	Inf	Inf	1

PER	**4024**	**2048**	**PER**	**3572**	**4096**	**4087**
4024	1	0	**3572**	0	1	4
2048	0	0	**4096**	0	0	4
			4087	1	1	0

timations. For the left hemisphere the comparison results are ambiguous. The GBF values are infinite for both models, this means that both models must be very similar in terms of model fitting to a given fMRI time series. The PER indicates that model 4024 won in one subject with a Bayes Factor greater than 3.

It became necessary to compare the two models for the left hemisphere on a single subject level, the results can be seen in table 4.3. In most of the comparisons model 4024 performed better, however not every time passing the criterion of positive evidence in sense of Bayesian model comparisons (Raftery, 1995). In subject S2 the Bayes Information Criterion and Akaike's Information Criterion did not concur, which is quite common when models are very similar. In two subjects (S1, S4) a comparison was not possible because at least one model needed for the comparison could not be estimated.

So for the left hemisphere the winner is model 4024, at the same time pointing out that model 2048 is nearly indistinguishable. As mentioned above the winner for the right hemisphere is model 4087.

Table 4.3.: Comparing the models for the left hemisphere on a subject by subject basis. 1 denotes that the model won because AIC and BIC concurred. 0 means a model lost. If one of the models was not available, due to errors during the estimation process, this is indicated by 'na'. In subject S2 the BIC and AIC comparisons did not concurred, model 2048 won in AIC and model 4024 won in BIC.

	4024	**2048**
S1	na	na
S2	BIC	AIC
S3	1	0
S4	na	na
S5	1	0
S6	1	0
S7	1	0

4.2.2. The winning models

Figure 4.7 shows the winning models for each hemisphere. The models differ only in the point that the left hemispheric connection from FEF to SEF seems to be modulated by covert attention tasks to the saccade target (SC) but not by covert attention to the pursuit target. Here it is to mention that model 2048 (left hemisphere), which performed nearly as good, modulates this connection by covert attention to both targets (PC & SC). The right hemispheric connection from FEF to SEF is modulated by covert attention to the pursuit target (PC) but not to the saccade target.

Table 4.4 shows the estimated effective connectivity values and their probabilities for the winning models.

4.3. Discussion

The lateralization of attentional processing was also shown by Erickson et al. (2005) in a fMRI study about a Flanker task using Structural Equation Modeling. In this study only the coefficients of the right hemisphere were significantly distinguishable

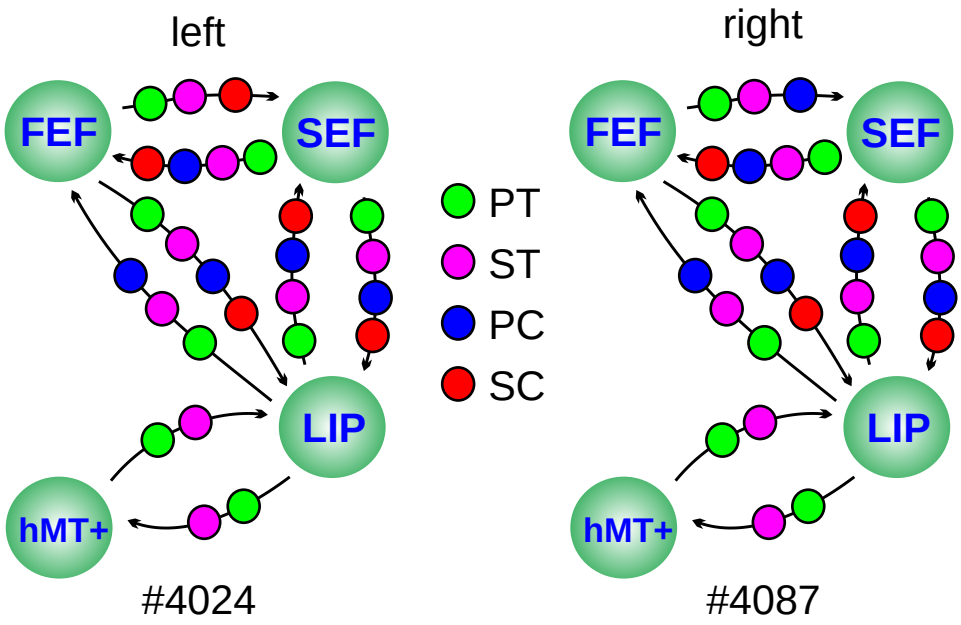

Figure 4.7.: The winning models for each hemisphere. The models 4024 (left) and 4087 (right) differ in only one point. For the connection from FEF to SEF the left hemisphere seems to be sensitive for covert attention to the saccadic target (SC), where the same connection on the right hemisphere seems to be sensitive for covert attention to the pursuit target (PC). Every connection is affected by the active tracking conditions for the pursuit (PT) and the saccade (ST) target by default.

Table 4.4.: Averaged connectivity estimates for the winning models of the left and right hemisphere. The numbers in the brackets indicate the Bayesian posterior probability value of the estimated modulatory effects.

Left, #4024	*PT*	*ST*	*PC*	*SC*	*IN*
hMT+ to LIP	0.0800 (0.90)	0.0048 (0.96)	—	—	0.3012 (1.00)
LIP to hMT+	0.1141 (0.93)	0.1053 (0.53)	—	—	0.0702 (0.83)
LIP to FEF	-0.0485 (0.76)	0.2407 (1.00)	-0.0248 (0.62)	—	0.1602 (0.99)
FEF to LIP	-0.0016 (0.51)	0.2105 (0.99)	0.0009 (0.50)	-0.0046 (0.52)	0.1876 (0.99)
LIP to SEF	-0.1357 (0.97)	0.1964 (1.00)	-0.0557 (0.74)	0.0909 (0.86)	0.1369 (0.98)
SEF to LIP	-0.0202 (0.60)	0.1865 (0.98)	-0.0023 (0.51)	-0.0020 (0.51)	0.1484 (0.96)
FEF to SEF	0.0357 (0.66)	0.1964 (0.99)	—	-0.0046 (0.63)	0.2577 (1.00)
SEF to FEF	0.0226 (0.60)	0.2010 (0.99)	0.0035 (0.51)	0.0559 (0.74)	0.2678 (1.00)

Right, #4087	*PT*	*ST*	*PC*	*SC*	*IN*
hMT+ to LIP	0.0246 (0.66)	0.0603 (0.84)	—	—	0.3723 (1.00)
LIP to hMT+	0.0870 (0.85)	0.0622 (0.80)	—	—	0.0380 (0.69)
LIP to FEF	-0.1309 (0.95)	0.1501 (0.98)	-0.0116 (0.56)	—	0.1772 (0.99)
FEF to LIP	-0.0147 (0.56)	0.1704 (0.98)	-0.0079 (0.53)	0.1297 (0.96)	0.2504 (1.00)
LIP to SEF	-0.1405 (0.96)	0.0964 (0.91)	-0.0370 (0.67)	0.2072 (1.00)	0.1202 (1.00)
SEF to LIP	-0.0203 (0.59)	0.1505 (0.97)	-0.0056 (0.52)	0.1461 (0.94)	0.2467 (0.96)
FEF to SEF	0.0182 (0.58)	0.1734 (0.98)	-0.0173 (0.58)	—	0.3169 (1.00)
SEF to FEF	0.0425 (0.68)	0.1621 (0.97)	-0.0058 (0.52)	0.1444 (0.95)	0.3246 (1.00)

from the baseline condition. Though the study was essentially about congruent and incongruent visual stimuli, it is one of the few studies investigating attentional effects on the connectivity of brain regions.

Also Büchel and Friston (1997) considered in another structural equation study about movement processing in visual areas only the right hemisphere. Though their reasons were more pragmatic; the activation in the dorsolateral prefrontal cortex in the left hemispheres of the subjects in this attention related tasks was not significant. But this can also be taken as an indicator that the right hemisphere is dominant when it comes to attentional processing of visual stimuli.

Hasegawa, Peterson, and Goldberg (2004) have shown that inhibition of saccades during no-go tasks causes more spiking activity in the frontal eye fields of macaque monkeys. Also in this study FEF has been a source of strong connectivity modulations in the efferent connections driven by covert attention to saccade targets.

The functional areas FEF, SEF and LIP play also an active role in other visual attention tasks. In a fMRI group study Polk, Drake, Jonides, Smith, and Smith (2008) have shown this attentional shifting effects in a Stroop task. The attention shifting of the human subjects was here performed in the dimensions color and word. In one class of conditions the subjects had to attend the color of a word in other conditions the main objective was to recognize the semantic content of a color word.

In summary, the findings of this exploratory analysis indicate that DCM can be used to explore for possible effective connectivity in regions known to be involved in the control of pursuit and saccadic tracking. Differences in overt and convert tracking became evident in the patterns of connectivity between higher cortical regions.

5. Neural Mass modeling and connectivity analysis

In this empirical study the methods of connectivity analysis were used to provide predictions for more accurate models of neural mass modeling. Our aim was to show that the scientific disciplines of experimental and computational neuroscience which use these methods can mutually benefit from each other. DCM is a advanced method of neuroimaging, neural mass modeling is a method of computational neuroscience. This chapter shows how DCM was used to explore an assumption of a neural mass model about the interactions of brain areas involved in motion processing and eye movement control.

The interaction of the brain areas hMT+ and LIP was investigated in a visual decision task involving random-dot motion. The subjects saw a set of spheres moving towards them in three dimensional space. Some spheres shared a similar motion vector, so their movement appeared coherently in contrast to the other spheres that were moving according to random motion vectors.

5.1. Materials & Methods

5.1.1. Stimuli

The stimuli consisted of random positioned spheres with a high contrast, which were constructed in a virtual three dimensional space, providing monocular depth cues. Spheres

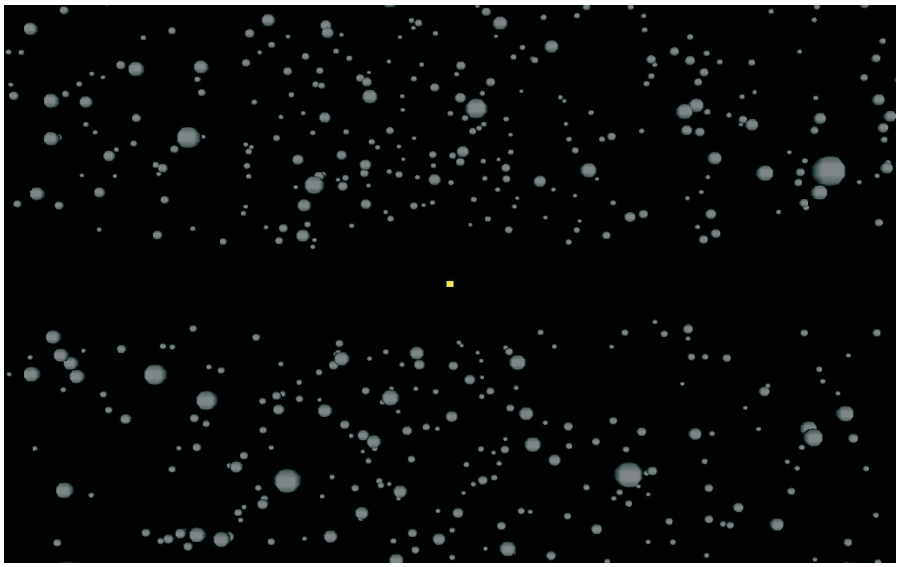

Figure 5.1.: The stimuli consisting of 3D spheres which approach the observer. The yellow fixation dot should be watched all the time during a trial. The black area had a vertical expansion of 3.2° visual angle and should prevent that the eyes of the subjects follow involuntarily a moving object.

seemingly to appeared in the distance and moved toward the observer. The spheres appeared in random positions in the upper half or the lower half of the screen and a certain fraction of them shared the same direction vector, to create the impression of coherently moving objects. This fraction was varied per experimental condition, either 10%, 30% or 50% of all visible spheres moved coherently, i.e. they shared the same movement vector. To inhibit involuntary eye movements of the subjects an horizontal area of 3.2° in the visual field was present, where no new spheres were created. The number of visible spheres was kept constant during a trial, every sphere that disappeared out of the field of view was replaced after 33ms by a new sphere, randomly positioned in the visible virtual space. In the center of the screen a colored fixation point was visible permanently, the color of the point served as an indicator for the subjects when the maximum time to give the feedback was nearly reached (3000ms), each trial had a duration of 4000ms(Figure 5.1). The stimuli were implemented with the Presentation^{TM} software package (v11.3, Neurobehavioral Systems Inc, Albany, Canada). The stimulation was presented with a 17" TFT monitor with an average frame rate of 30Hz.

5.1.2. fMRI data acquisition

A 3T Siemens Allegra MRT Scanner for acquiring the functional and structural images was used. The EPI sequence had the following parameters: TR=2s, 544 volumes, 3×3×3 mm voxel size, 90° flip angle, 34 slices per volume, bottom up slice order. This allowed us to acquire images of the entire cerebral cortex. A pseudo random block design was used implementing a jittered ISI interval. Each coherence level (10%, 30% and 50%) was combined with the various amount of visible spheres (100, 200, 500) to nine balanced conditions. A tenth condition was introduced, it served as a baseline condition by only having the fixation target visible on the screen and no spheres. Each block had a total of fourteen scans during which a each subject had to process eight decision tasks. The total time was about thirty minutes for the acquisition of the functional imaging data,

depending on the randomized ISI.

Table 5.1 shows the location of the regions that were used for the extraction process, resulting in a voxel-time-series of a region which was used to model the hemodynamic response of a certain region of a DCM model.

5.1.3. Behavioral Data

The subjects responded their judgement of the movement direction of the coherently moving spheres (left or right) by pressing one of two buttons in a scanner compatible LUMItouch^{TM} device (Photon Control Inc., Burnaby, BC, Canada). All subjects were right handed so the right middle finger was used to indicate a perceived movement to the right, respectively the left index finger was used to indicate a perceived movement of the coherently moving spheres to the left.

5.2. Results

5.2.1. Behavioral results

Table 5.2 shows the amount of correct responses for each condition. The subjects showed a general tendency to solve the task better the higher the coherence level was. However the influence of the number of visible spheres seems to be minimal. Subject BF had a remarkable low performance at 10% and 250 spheres with 31.25%. This might mean that she got the instructions wrong at the beginning of the experiment.

The percentage of correct responses concur with a previous behavioral study that was performed in our lab on 40 subjects (Figure 5.2). There the differences between the different levels of coherence were statistically significant ($F=246.5$, $p<0.01$), however a significant effect could not be shown for the influence of the number of visible spheres ($F=0.119$, $p=0.888$).

The total decision times (table 5.3 left) dropped accordingly to the level of coherence.

Table 5.1.: Locations of the regions of interest for the four subjects. The MNI coordinates for each region describe the center of the sphere with a radius of 6mm that was used for the volume of interest extraction process of SPM5. Size indicates the number of voxels included for the extraction process. The volumes of interest were adjusted to the T-contrast that contrasted the main conditions against the rest condition, using a significance threshold of $p<0.001$. The subject LS had no detectable LIP activation in the left hemisphere.

	hMT+ (left)						*hMT+ (right)*				
subject	**x**	**y**	**z**	**Voxels**	**Z-score**	**subject**	**x**	**y**	**z**	**Voxels**	**Z-score**
BF	-44	-70	4	112	5.27	BF	46	-68	6	46	4.35
FD	-46	-78	14	88	7.73	FD	44	-74	8	96	5.72
LS	-38	-70	4	91	6.03	LS	50	-74	8	68	4.99
LA	-52	-62	6	104	5.91	LA	54	-66	2	63	5.12

	LIP (left)						*LIP (right)*				
subject	**x**	**y**	**z**	**Voxels**	**Z-score**	**subject**	**x**	**y**	**z**	**Voxels**	**Z-score**
BF	-28	-64	64	36	4.45	BF	26	-68	66	4	3.44
FD	-24	-66	50	46	3.84	FD	26	-72	48	77	4.67
LS	-	-	-	-	-	LS	38	-58	60	40	4.06
LA	-26	-68	54	114	7.23	LA	18	-70	62	93	5.20

Table 5.2.: Behavioral Data of four subjects. Percent correct judgements of the direction of the coherent moving spheres.

% Correct (BF)

Coh. Level	*10%*	*30%*	*50%*
100 Spheres	40.00%	41.18%	60.00%
250 Spheres	31.25%	57.89%	53.33%
500 Spheres	58.82%	58.82%	70.00%

% Correct (FD)

Coh. Level	*10%*	*30%*	*50%*
100 Spheres	30.00%	50.00%	50.00%
250 Spheres	45.00%	50.00%	65.00%
500 Spheres	60.00%	60.00%	60.00%

% Correct (LS)

Coh. Level	*10%*	*30%*	*50%*
100 Spheres	80.00%	65.00%	95.00%
250 Spheres	50.00%	75.00%	100.00%
500 Spheres	75.00%	85.00%	100.00%

% Correct (LA)

Coh. Level	*10%*	*30%*	*50%*
100 Spheres	50.00%	65.00%	80.00%
250 Spheres	65.00%	60.00%	95.00%
500 Spheres	70.00%	70.00%	85.00%

% Correct (Total)

Coh. Level	*10%*	*30%*	*50%*
100 Spheres	50.00%	55.29%	71.25%
250 Spheres	47.81%	60.72%	78.33%
500 Spheres	65.96%	68.46%	78.75%

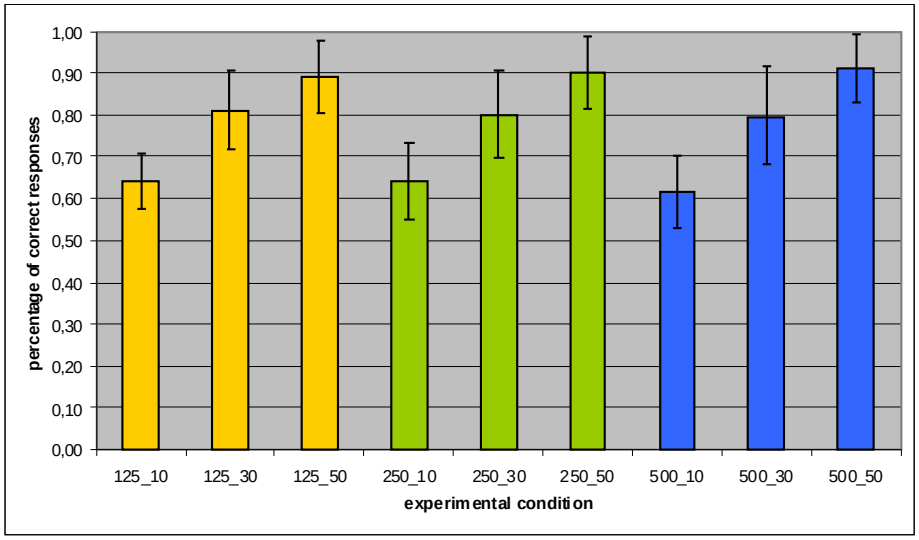

Figure 5.2.: Results of a previously conducted behavioral study outside the fMRI laboratory on 40 subjects. The number left of the '_' sign indicates the number of spheres and the number right of it indicates the coherence level. The error bars show the standard deviation. There were significant effects for the influence of the level of coherence but no significant effects for the number of spheres. Yellow columns show the results for 125 spheres, green columns for 250 spheres and blue columns for 500 spheres respectively.

The higher the coherence level was, the less time was needed by the subjects to judge the direction of the coherent movement. This tendency is even clearer when only the trials are taken into account where no warning after 3000ms was given, i.e. where the subjects signalled their decision within less than 3000ms (table 5.3 right). These findings are accordingly to the previously made behavioral study.

Table 5.4 compares the results of correct trials against incorrect trials. A tendency can be seen that incorrect trials, on the right half, had a longer decision time than the correct trials visible on the left half. However the statistical significance of this finding can not be judged with four subjects. The 40 subjects behavioral study showed no significant effects comparing correct against incorrect trials.

5.2.2. DCM model comparison

The areas hMT+ and LIP could influence each other in three possible ways. First the brain areas could influence each other in a reciprocal manner, this model was called model BI for a bi-directional influence. Second hMT+ area only influenced the LIP area without a major contribution from LIP back to hMT+, this was called the BU model, for bottom-up processing. The there was the possibility that hMT+ is influenced by LIP and no major influence is processed the way back. However that this model would contradict the majority of findings about visual processing in primates it was included to have a collection of all possible models in the study. This model was called TD, for top-down processing. A fourth model would be possible, that is that there is no connection at all between the areas hMT+ and LIP. But this would not only contradict the findings of the recent decades about visual processing in primates, such a model would also be not comparable to the other three models. So the value of modeling such a 'null model' would be null, therefore it was omitted.

Having only four subjects and a strong background of empirical evidence no sophisticated model comparison approach was applied here. It was sufficient just to perform

Table 5.3.: Decision times in milliseconds, left half: total decision times, right half: decision times of trials without the 3000ms warning

Decision Times (BF)

Coh. Level	*10%*	*30%*	*50%*	*10%*	*30%*	*50%*
100 Spheres	2,485	2,650	2,342	2,249	2,039	1,896
250 Spheres	2,696	2,606	2,086	2,298	2,362	1,578
500 Spheres	2,584	2,658	2,646	2,176	2,034	2,071

Decision Times (FD)

Coh. Level	*10%*	*30%*	*50%*	*10%*	*30%*	*50%*
100 Spheres	2,539	2,499	2,642	1,806	1,960	2,091
250 Spheres	2,278	2,342	1,790	1,815	1,513	1,514
500 Spheres	2,321	2,861	2,132	2,131	2,183	1,788

Decision Times (LS)

Coh. Level	*10%*	*30%*	*50%*	*10%*	*30%*	*50%*
100 Spheres	2,260	1,903	1,492	1,980	1,903	1,492
250 Spheres	2,383	1,747	1,721	2,154	1,487	1,652
500 Spheres	2,543	1,707	1,506	2,227	1,544	1,307

Decision Times (LA)

Coh. Level	*10%*	*30%*	*50%*	*10%*	*30%*	*50%*
100 Spheres	2,361	2,160	1,877	2,168	2,019	1,877
250 Spheres	2,188	2,344	2,118	2,188	2,208	2,003
500 Spheres	2,136	2,418	2,295	2,077	2,360	2,189

Decision Times (Total)

Coh. Level	*10%*	*30%*	*50%*	*10%*	*30%*	*50%*
100 Spheres	2,411	2,303	2,088	2,051	1,980	1,839
250 Spheres	2,386	2,260	1,929	2,114	1,892	1,687
500 Spheres	2,396	2,411	2,145	2,153	2,030	1,839

Table 5.4.: Decision times in milliseconds (ms), left half: for correct trials, right half: for incorrect trials. Note that the subject LS had no incorrect trials at 50% coherence level with 250 and 500 spheres.

Decision Times (BF)

Coh. Level	*10%*	*30%*	*50%*	*10%*	*30%*	*50%*
100 Spheres	2,775	2,746	2,206	2,291	2,583	2,547
250 Spheres	2,877	2,524	2,483	2,613	2,718	1,631
500 Spheres	2,735	2,764	2,385	2,368	2,507	3,254

Decision Times (FD)

Coh. Level	*10%*	*30%*	*50%*	*10%*	*30%*	*50%*
100 Spheres	2,184	2,477	2,557	2,691	2,521	2,726
250 Spheres	2,174	2,614	1,848	2,363	2,071	1,681
500 Spheres	2,216	2,590	2,020	2,479	3,267	2,299

Decision Times (LS)

Coh. Level	*10%*	*30%*	*50%*	*10%*	*30%*	*50%*
100 Spheres	2,204	1,893	1,473	2,483	1,921	1,853
250 Spheres	2,151	1,647	1,721	2,615	2,045	–
500 Spheres	2,501	1,620	1,506	2,670	2,198	–

Decision Times (LA)

Coh. Level	*10%*	*30%*	*50%*	*10%*	*30%*	*50%*
100 Spheres	2,410	1,990	1,869	2,311	2,475	1,912
250 Spheres	2,058	2,280	2,078	2,430	2,441	2,872
500 Spheres	2,083	2,366	2,248	2,261	2,539	2,562

Decision Times (Total)

Coh. Level	*10%*	*30%*	*50%*	*10%*	*30%*	*50%*
100 Spheres	2,393	2,276	2,026	2,444	2,375	2,259
250 Spheres	2,315	2,266	2,033	2,505	2,319	2,061
500 Spheres	2,384	2,335	2,040	2,444	2,627	2,705

Table 5.5.: Model comparison results for four subjects. The posterior probabilities for AIC and BIC are given for each subject and each hemisphere. Models winning either comparison are marked by their posterior probability values appearing in boldface.

$p(y\|m)$ ***right***	*AIC BI*	*AIC BU*	*AIC TD*	*BIC BI*	*BIC BU*	*BIC TD*
BF	0.000	**0.841**	0.159	0.000	**0.841**	0.159
FD	0.000	**0.918**	0.082	0.000	**0.918**	0.082
LS	**1.000**	0.000	0.000	0.000	**1.000**	0.000
LA	0.001	**0.999**	0.001	0.000	**0.999**	0.001

$p(y\|m)$ ***left***	*AIC BI*	*AIC BU*	*AIC TD*	*BIC BI*	*BIC BU*	*BIC TD*
BF	0.000	0.000	**1.000**	0.000	0.000	**1.000**
FD	0.000	**1.000**	0.000	0.000	**1.000**	0.000
LS	-	-	-	-	-	-
LA	0.000	**1.000**	0.000	0.000	**1.000**	0.000

model comparisons on a single subject level and to compare the posterior probability values for Akaike's Information Criterion (AIC) and Bayes Information Criterion (BIC). According to table 5.5 the most plausible model on a empirical basis of past findings was also the favored model by the two information criteria. So model BU, which models a unidirectional influence of hMT+ to LIP was selected as the model which explains the fMRI data of this experiment the best.

5.2.3. Connectivity changes

The connectivity changes for the left and right hemisphere had a similar profile. Table 5.6 shows the connectivity changes in means of the unit Hz, which is highly artificial in this context. The strongest effect can be found in the 30% and 250 spheres conditions for both hemispheres, which is 0.24Hz for the right hemisphere and 0.23Hz for the left hemisphere. Compared to the modulatory effects of the other experimental conditions this is a strong effect. There is also a rather strong connectivity change for the 50% and 100 spheres condition, but this can be only found for the left hemisphere.

Table 5.6.: Averaged connectivity changes of four subjects depending on the level of coherence and the number of visible spheres. Connectivity changes are given in the unit Hertz (Hz). The numbers in the brackets are the Bayesian posterior probability estimates.

Connectivity from hMT to LIP (left hemisphere)

coherence	*10%*	*30%*	*50%*
100 Spheres	-0.01 (0.53)	-0.07 (0.67)	-0.03 (0.59)
250 Spheres	0.08 (0.72)	0.24 (0.95)	-0.05 (0.64)
500 Spheres	0.01 (0.52)	0.07 (0.70)	-0.05 (0.64)

Connectivity from hMT to LIP (right hemisphere)

coherence	*10%*	*30%*	*50%*
100 Spheres	0.10 (0.85)	0.11 (0.85)	-0.23 (0.99)
250 Spheres	-0.02 (0.60)	0.23 (0.98)	0.06 (0.72)
500 Spheres	-0.08 (0.80)	-0.04 (0.65)	-0.12 (0.88)

5.3. Discussion

The previous behavioral study, that included 40 subjects, discovered no significant effects caused by the number of visible spheres but a clear effect caused by the coherence level. This is in accordance with previous findings in similar experimental paradigms (Roitman & Shadlen, 2002).

LIP plays a crucial role in visual decision making, this has been shown already in several previous experimental studies (Shadlen & Newsome, 2001; Roitman & Shadlen, 2002; Bisley & Goldberg, 2003). It has not been clear how the input to LIP from hMT+ was processed in dependance of various stimuli attributes, some neurocomputational models simply assumed a linear influence of the coherence level of the stimuli to LIP, i.e. assuming that the input from hMT+ to LIP gets linearly stronger with a higher level of coherence (Wong & Wang, 2006). Other models include even a very complex processing of stimuli properties to model the desired outcome in behavioral data (Deco & Rolls, 2005b). In case of an assumed influence of the intensity of the stimuli, i.e. the number of

visible spheres here the behavioral data suggests no influence. The connectivity data are ambiguous and suggest a strong effect only for medium degrees of intensity. The impact of the coherence level is proportional to the reaction time data and the performance data. However this proportional relation seems not to be valid to assume for the interplay between the brain areas hMT+ and LIP. The findings suggest that neurocomputational models need to be more sophisticated if they want to take data of connectivity analysis into account instead of relying on neurophysiological measurements of just one brain area and hypothesize about the neuronal effect of the stimuli on the basis of behavioral data. This study shows clear that behavioral results and results of a connectivity analysis can differ greatly. Despite that hMT+ is a part of early dorsal visual processing areas the presented data suggests that its influence on LIP could be better explained by non-linear models.

Future neurocomputational models could benefit from findings of connectivity studies and neurocomputational models can guide the experimental neuroscientist in which models should be tested.

Part III.

Conclusions

6. Discussion

6.1. Attention

The present thesis suggests strongly that the source of conscious processing of visual covert attention tasks can be located in the interplay between higher visual processing areas.

The predominance of the right hemisphere in attentional tasks has been documented from other stimulus modalities as well, for example for flanker tasks Erickson et al. (2005) that present non moving visual targets.

The presented findings suggest that only tasks that are more demanding, in the terms of systems theory (Stephan, 2004), affect higher brain regions. Less demanding tasks, like simply following a visual target with gaze can be described easily by a simple feed-back system.

A computational model for biased competition has been introduced by Deco and Rolls (2005b) which proposed that feed-back connections between cortical areas need to be about 2.5 times weaker than feed-forward connections. They have shown that competing pools of neurons, combined with a top-down biasing effect can be the base of the cognitive process that we call attention. Buehlmann and Deco (2008) compare rate versus synchronization modulation in the interplay of V1 and V4 in biased attention processing. They conclude that rate modulation is always present, in terms of fMRI this means that when the bias of attention shifts it can be seen in the BOLD response of a brain region because different mean field spiking rates lead to different BOLD responses

(Logothetis et al., 2001). The results presented in chapter 3 (page 55) indicated that the connection between V1 and hMT+ (V5) is affected by attentional shifts, demonstrating that also in the dorsal processing stream such effects may arise.

As it has been showed in chapter 3 endogenous attentional effects can be found in the connection from V1 to hMT+. Busse et al. (2008) have shown by microelectrode studies in the macaque middle temporal area that attentional effects can be measured already in this early stage of visual processing. If V1 is now the major driving source of these effects or if influences of other brain areas have to be taken into account cannot be answered on the base of the findings available. One possible candidate is the area V4, which is part of the ventral processing stream, effects of covert attention in this area are well documented in the animal model (Connor, Preddie, Gallant, & Essen, 1997; McAdams & Maunsell, 1999; Reynolds, Chelazzi, & Desimone, 1999; Reynolds, Pasternak, & Desimone, 2000). Even peri-saccadic activity of V4 in attentional experiments is evident (Motter, 1993). Moore, Armstrong, and Fallah (2003) could show for the ventral processing stream that effects of covert attention appear to emerge in the frontal eye fields (FEF). This was shown by microstimulation of FEF that enhanced corresponding receptive fields in V4 in covert attention tasks. However a possible interaction in terms of effective connectivity needs still to be explored. The findings suggest that the lateral intraparietal area LIP is not a driving source for effects in hMT+. But it is plausible that a enhancement in V1 hMT+ connectivity is the only driving force for these effects mentioned by Busse et al. (2008). Womelsdorf et al. (2008) state that 'selective attention is the top-down mechanism to allocate neuronal processing resources to the most relevant subset of the information provided by an organism's sensors'. They showed it to be a measurable effect in the media temporal (MT) area of macaque monkeys. The magnitude of the shift of the spatial tuning functions of MT was positively correlated with the narrowing of spatial tuning around the attentional focus. So a connection from a higher brain region triggering covert attention related V1 activity, therefore modulating the V1 to

hMT+ connection is plausible.

Roelfsema, Lamme, and Spekreijse (1998) could show attentional enhancement in V1 for tasks mainly affecting the ventral processing stream, i.e. object recognition. Neural mechanisms of covert attentional processing, where visuomotor responses are inhibited, like in the covert attention task of chapters 3 & 4 are poorly understood so far.

6.2. Outlook

In a recent review article assumptions about the basic organizational principle of the neocortex were supported that may also explain phenomena as attention, working memory, sensory perception and motor integration (Haider & McCormick, 2009). These phenomena have long been supported by neurocomputational models that use oscillatory coupling between cell populations to bind them to a functional ensemble (Malsburg & Schneider, 1986; Crook, Ermentrout, & Bower, 1998; Corchs & Deco, 2002; Deco & Rolls, 2005a; Buehlmann & Deco, 2008). Oscillatory coupling has been first observed in the striate cortex (V1) of cats to synchronize columns to functional ensembles and therefore seemed a plausible organizational principle (Gray, Knig, Engel, & Singer, 1989; Gray, Engel, Knig, & Singer, 1992). But the transients of the neocortical dynamics discussed in this article are very fast, compared to the time resolution that is possible in fMRI experiments, optimistic assumptions point to events that are apart several hundreds milliseconds that are still detectable (Friston et al., 2000). While the effects discussed by Haider and McCormick happen in a time span of a few dozen milliseconds up to hundreds of milliseconds (Fujisawa, Amarasingham, Harrison, & Buzski, 2008; Haider & McCormick, 2009). Non-invasive connectivity studies in humans of these phenomena became possible since DCM for EEG was theoretically explored (David & Friston, 2003; David et al., 2006; Kiebel, David, & Friston, 2006; Kiebel, Garrido, & Friston, 2007) and was implemented in the SPM5 software package. So first experimental publications about this method became available (Garrido, Kilner, Kiebel, & Friston, 2007; Garrido,

Kilner, Kiebel, Stephan, & Friston, 2007) and since the introduction of the SPM8 software package a computational framework with a sufficient user interface is available.

The general demand for a more systems-theoretical approach to understand the mechanisms of the brain (Stephan, 2004) has been recently specified and embedded in more specialized framework of interpretation and theory generation by David (2007). The latter author suggests a synthesis of the theory of autopoietic systems, which is embedded in general-systems-theory, with the method of dynamic causal modeling to get a framework to understand several neuropsychological phenomena better. The human brain is viewed in the theory of autopoietic systems as a self organizing system which changes its topological and functional properties in dependence of environmental inputs. David points out that this theory is similar to DCM theory and can be implemented by slightly altering the theoretical framework of DCM, i.e. by utilizing the parameters Θ in the way that they are determined by neural states z. Reciprocally the parameters contained in Θ specify the neural states z (see equation 2.3, page 32). These alterations to the DCM formalism would be minor as showed by David (2007). A case documentation of a pre-surgical treatment by amygdala stimulation of an epilepsy patient that was suffering from temporal lobe epilepsy is reported. The DCM analysis of these data led to a better understanding of the oscillatory phenomena during an epileptic episode. This approach enabled David to test different functional hypotheses (i.e., DCM models) for a given data set. In particular David proposes a simple modification of the standard formulations of DCM that includes autonomous processes. The idea is to use model comparison approaches of DCM for system identification in neuroimaging to test the face validity of the autopoietic theory applied to neural subsystems.

6.3. A brief chronology of this work

This work began five years ago with a first glance into the paper where the method of dynamic causal modeling, in short called DCM, was introduced (Friston et al., 2003). At this time it was possible to make first experiments using the SPM2b software package, which contained a very early and slow implementation of the DCM algorithm. First experiments about pursuit and saccade eye movements showed very early that the 1.5T Siemens Sonata^{TM} scanner had a sub-optimal signal-to-noise ratio to build models that involved also higher processing areas like the frontal eye fields (FEF) and the supplementary eye fields (SEF). But it was enough to start off with first simple models to research the connectivity of early visual processing areas, like the primary visual cortex (V1) and the human middle temporal area (hMT+), which produce strong signals correlated with the experimental conditions. About one year later the 3T Siemens Allegra^{TM} scanner was accessible that provided a far better signal-to-noise ratio, making it possible to create DCM models that incorporate higher processing areas and weak effects like attention shifting. Investigating paradigms and models that were introduced in chapter 3 at that time became possible in Regensburg.

Model comparison on a group level had been a problem until the first article describing the process on a group level was available (Stephan, Marshall, et al., 2007). Before it was necessary to make as good as possible inferences from the single subject based comparisons (Penny et al., 2004a), which have been described only a short time after the original DCM publication. Examples can be found in chapter 5 (page 98), where a sophisticated group analysis was not necessary because already the comparisons at a single subject level pointed in a clear direction. In early publications different comparison approaches have been used to get a clear insight into which model to choose out of a pool of subjects and models (e.g.: Mechelli, Price, Noppeney, & Friston, 2003) or the papers were restricted to discuss single subject observations (e.g.: Stephan, Penny, Marshall, Fink, & Friston, 2005). With foundations for robust group comparison techniques it

was possible to compare large number of models in a group study, as has been shown in chapter 4.

During the Decisions in Motion STREP Project, that was funded by the European Commission 6'th framework programme (reference #: 027198), connections between the areas of neuroimaging and computational neuroscience could be explored and resulted in the experiment of random-dot motion perception and perceptual decision making that was introduced in chapter 5.

References

Acs, F., & Greenlee, M. W. (2008, Jun). Connectivity modulation of early visual processing areas during covert and overt tracking tasks. *Neuroimage*, *41*(2), 380–388. Available from http://dx.doi.org/10.1016/j.neuroimage.2008.02.007

Astafiev, S. V., Shulman, G. L., Stanley, C. M., Snyder, A. Z., Essen, D. C. V., & Corbetta, M. (2003, Jun). Functional organization of human intraparietal and frontal cortex for attending, looking, and pointing. *J Neurosci*, *23*(11), 4689–4699.

Bisley, J. W., & Goldberg, M. E. (2003, Jan). Neuronal activity in the lateral intraparietal area and spatial attention. *Science*, *299*(5603), 81–86. Available from http://dx.doi.org/10.1126/science.1077395

Bisley, J. W., & Goldberg, M. E. (2006, Mar). Neural correlates of attention and distractibility in the lateral intraparietal area. *J Neurophysiol*, *95*(3), 1696–1717. Available from http://dx.doi.org/10.1152/jn.00848.2005

Brunel, N. (2003, Nov). Dynamics and plasticity of stimulus-selective persistent activity in cortical network models. *Cereb Cortex*, *13*(11), 1151–1161.

Büchel, C., & Friston, K. J. (1997, Dec). Modulation of connectivity in visual pathways by attention: cortical interactions evaluated with structural equation modelling and fmri. *Cereb Cortex*, *7*(8), 768–778.

Buehlmann, A., & Deco, G. (2008, Jul). The neuronal basis of attention: rate versus synchronization modulation. *J Neurosci*, *28*(30), 7679–7686. Available from

http://dx.doi.org/10.1523/JNEUROSCI.5640-07.2008

Buice, M. A., & Cowan, J. D. (2007, May). Field-theoretic approach to fluctuation effects in neural networks. *Phys Rev E Stat Nonlin Soft Matter Phys*, *75*(5 Pt 1), 051919.

Burkitt, A. N. (2006a, Jul). A review of the integrate-and-fire neuron model: I. homogeneous synaptic input. *Biol Cybern*, *95*(1), 1–19. Available from http://dx.doi.org/10.1007/s00422-006-0068-6

Burkitt, A. N. (2006b, Aug). A review of the integrate-and-fire neuron model: Ii. inhomogeneous synaptic input and network properties. *Biol Cybern*, *95*(2), 97–112. Available from http://dx.doi.org/10.1007/s00422-006-0082-8

Busse, L., Katzner, S., & Treue, S. (2008, Oct). Temporal dynamics of neuronal modulation during exogenous and endogenous shifts of visual attention in macaque area mt. *Proc Natl Acad Sci U S A*, *105*(42), 16380–16385. Available from http://dx.doi.org/10.1073/pnas.0707369105

Buxton, R. B., Uludağ, K., Dubowitz, D. J., & Liu, T. T. (2004). Modeling the hemodynamic response to brain activation. *Neuroimage*, *23 Suppl 1*, S220–S233. Available from http://dx.doi.org/10.1016/j.neuroimage.2004.07.013

Buxton, R. B., Wong, E. C., & Frank, L. R. (1998, Jun). Dynamics of blood flow and oxygenation changes during brain activation: the balloon model. *Magn Reson Med*, *39*(6), 855–864.

Caclin, A., & Fonlupt, P. (2006, Nov). Effect of initial fmri data modeling on the connectivity reported between brain areas. *Neuroimage*, *33*(2), 515–521. Available from http://dx.doi.org/10.1016/j.neuroimage.2006.07.019

Coe, B., Tomihara, K., Matsuzawa, M., & Hikosaka, O. (2002, Jun). Visual and anticipatory bias in three cortical eye fields of the monkey during an adaptive decision-making task. *J Neurosci*, *22*(12), 5081–5090.

Connor, C. E., Preddie, D. C., Gallant, J. L., & Essen, D. C. V. (1997, May). Spatial

attention effects in macaque area v4. *J Neurosci*, *17*(9), 3201–3214.

Corbetta, M., Akbudak, E., Conturo, T. E., Snyder, A. Z., Ollinger, J. M., Drury, H. A., et al. (1998, Oct). A common network of functional areas for attention and eye movements. *Neuron*, *21*(4), 761–773.

Corchs, S., & Deco, G. (2002, Apr). Large-scale neural model for visual attention: integration of experimental single-cell and fmri data. *Cereb Cortex*, *12*(4), 339–348.

Crook, S. M., Ermentrout, G. B., & Bower, J. M. (1998, May). Spike frequency adaptation affects the synchronization properties of networks of cortical oscillations. *Neural Comput*, *10*(4), 837–854.

David, O. (2007). Dynamic causal models and autopoietic systems. *Biol Res*, *40*(4), 487–502. Available from `http://dx.doi.org//S0716-97602007000500010`

David, O., & Friston, K. J. (2003, Nov). A neural mass model for meg/eeg: coupling and neuronal dynamics. *Neuroimage*, *20*(3), 1743–1755.

David, O., Kiebel, S. J., Harrison, L. M., Mattout, J., Kilner, J. M., & Friston, K. J. (2006, May). Dynamic causal modeling of evoked responses in eeg and meg. *Neuroimage*, *30*(4), 1255–1272. Available from `http://dx.doi.org/10.1016/j.neuroimage.2005.10.045`

Deco, G., Jirsa, V. K., Robinson, P. A., Breakspear, M., & Friston, K. (2008). The dynamic brain: from spiking neurons to neural masses and cortical fields. *PLoS Comput Biol*, *4*(8), e1000092. Available from `http://dx.doi.org/10.1371/journal.pcbi.1000092`

Deco, G., & Rolls, E. T. (2005a, Jul). Attention, short-term memory, and action selection: a unifying theory. *Prog Neurobiol*, *76*(4), 236–256. Available from `http://dx.doi.org/10.1016/j.pneurobio.2005.08.004`

Deco, G., & Rolls, E. T. (2005b, Jul). Neurodynamics of biased competition and cooperation for attention: a model with spiking neurons. *J Neurophysiol*, *94*(1),

295–313. Available from http://dx.doi.org/10.1152/jn.01095.2004

Dias, E. C., & Segraves, M. A. (1999, May). Muscimol-induced inactivation of monkey frontal eye field: effects on visually and memory-guided saccades. *J Neurophysiol*, *81*(5), 2191–2214.

Dukelow, S. P., DeSouza, J. F., Culham, J. C., Berg, A. V. van den, Menon, R. S., & Vilis, T. (2001, Oct). Distinguishing subregions of the human mt+ complex using visual fields and pursuit eye movements. *J Neurophysiol*, *86*(4), 1991–2000.

Erickson, K. I., Ho, M.-H. R., Colcombe, S. J., & Kramer, A. F. (2005, Mar). A structural equation modeling analysis of attentional control: an event-related fmri study. *Brain Res Cogn Brain Res*, *22*(3), 349–357. Available from http://dx.doi.org/10.1016/j.cogbrainres.2004.09.004

Fox, P. T., Miezin, F. M., Allman, J. M., Essen, D. C. V., & Raichle, M. E. (1987, Mar). Retinotopic organization of human visual cortex mapped with positron-emission tomography. *J Neurosci*, *7*(3), 913–922.

Friston, K. J., Buechel, C., Fink, G. R., Morris, J., Rolls, E., & Dolan, R. J. (1997, Oct). Psychophysiological and modulatory interactions in neuroimaging. *Neuroimage*, *6*(3), 218–229. Available from http://dx.doi.org/10.1006/nimg.1997.0291

Friston, K. J., Harrison, L., & Penny, W. (2003, Aug). Dynamic causal modelling. *Neuroimage*, *19*(4), 1273–1302.

Friston, K. J., Mechelli, A., Turner, R., & Price, C. J. (2000, Oct). Nonlinear responses in fmri: the balloon model, volterra kernels, and other hemodynamics. *Neuroimage*, *12*(4), 466–477. Available from http://dx.doi.org/10.1006/nimg.2000.0630

Fujisawa, S., Amarasingham, A., Harrison, M. T., & Buzski, G. (2008, Jul). Behavior-dependent short-term assembly dynamics in the medial prefrontal cortex. *Nat Neurosci*, *11*(7), 823–833. Available from http://dx.doi.org/10.1038/nn.2134

Furman, M., & Gur, M. (2003, Sep). Self-organizing neural network model of motion processing in the visual cortex during smooth pursuit. *Vision Res*, *43*(20), 2155–

2171.

Garrido, M. I., Kilner, J. M., Kiebel, S. J., & Friston, K. J. (2007, Dec). Evoked brain responses are generated by feedback loops. *Proc Natl Acad Sci U S A*, *104*(52), 20961–20966. Available from http://dx.doi.org/10.1073/pnas.0706274105

Garrido, M. I., Kilner, J. M., Kiebel, S. J., Stephan, K. E., & Friston, K. J. (2007, Jul). Dynamic causal modelling of evoked potentials: a reproducibility study. *Neuroimage*, *36*(3), 571–580. Available from http://dx.doi.org/10.1016/j.neuroimage.2007.03.014

Gerstner, W. (2000, Jan). Population dynamics of spiking neurons: fast transients, asynchronous states, and locking. *Neural Comput*, *12*(1), 43–89.

Gray, C. M., Engel, A. K., Knig, P., & Singer, W. (1992, Apr). Synchronization of oscillatory neuronal responses in cat striate cortex: temporal properties. *Vis Neurosci*, *8*(4), 337–347.

Gray, C. M., Knig, P., Engel, A. K., & Singer, W. (1989, Mar). Oscillatory responses in cat visual cortex exhibit inter-columnar synchronization which reflects global stimulus properties. *Nature*, *338*(6213), 334–337. Available from http://dx.doi.org/10.1038/338334a0

Grosbras, M.-H., Laird, A. R., & Paus, T. (2005, May). Cortical regions involved in eye movements, shifts of attention, and gaze perception. *Hum Brain Mapp*, *25*(1), 140–154. Available from http://dx.doi.org/10.1002/hbm.20145

Grosbras, M. H., Lobel, E., Moortele, P. F. V. de, LeBihan, D., & Berthoz, A. (1999). An anatomical landmark for the supplementary eye fields in human revealed with functional magnetic resonance imaging. *Cereb Cortex*, *9*(7), 705–711.

Grossberg, S., Mingolla, E., & Pack, C. (1999, Dec). A neural model of motion processing and visual navigation by cortical area mst. *Cereb Cortex*, *9*(8), 878–895.

Grubb, R. L., Raichle, M. E., Eichling, J. O., & Ter-Pogossian, M. M. (1974). The effects of changes in paco2 on cerebral blood volume, blood flow, and vascular

mean transit time. *Stroke*, *5*(5), 630–639.

Haider, B., & McCormick, D. A. (2009, Apr). Rapid neocortical dynamics: cellular and network mechanisms. *Neuron*, *62*(2), 171–189. Available from http://dx.doi.org/10.1016/j.neuron.2009.04.008

Hamker, F. H. (2005, Apr). The reentry hypothesis: the putative interaction of the frontal eye field, ventrolateral prefrontal cortex, and areas v4, it for attention and eye movement. *Cereb Cortex*, *15*(4), 431–447. Available from http://dx.doi.org/10.1093/cercor/bhh146

Hasegawa, R. P., Peterson, B. W., & Goldberg, M. E. (2004, Aug). Prefrontal neurons coding suppression of specific saccades. *Neuron*, *43*(3), 415–425. Available from http://dx.doi.org/10.1016/j.neuron.2004.07.013

Hebb, D. O. (1949). *The organization of behavior: A neuropsychological theory.* John Wiley & Sons Inc.

Hebb, D. O. (2002). *The organization of behavior: A neuropsychological theory* (P. M. Richard Brown, Ed.). Lawrence Erlbaum Assoc Inc., Mahwah, NJ, USA.

Heinen, S. J., & Liu, M. (1997). Single-neuron activity in the dorsomedial frontal cortex during smooth-pursuit eye movements to predictable target motion. *Vis Neurosci*, *14*(5), 853–865.

Herz, A. V. M., Gollisch, T., Machens, C. K., & Jaeger, D. (2006, Oct). Modeling single-neuron dynamics and computations: a balance of detail and abstraction. *Science*, *314*(5796), 80–85. Available from http://dx.doi.org/10.1126/science.1127240

Hill, A. (1936). Excitation and accommodation in nerve. *Proceedings of the Royal Society of London*, *119*, 305-355.

Hodgkin, A. L., & Huxley, A. F. (1952, Aug). A quantitative description of membrane current and its application to conduction and excitation in nerve. *J Physiol*, *117*(4), 500–544.

Horton, J. C., & Hoyt, W. F. (1991, Jun). The representation of the visual field in human striate cortex. a revision of the classic holmes map. *Arch Ophthalmol*, *109*(6), 816–824.

Horwitz, Tagamets, & McIntosh. (1999, Mar). Neural modeling, functional brain imaging, and cognition. *Trends Cogn Sci*, *3*(3), 91–98.

Horwitz, B., Friston, K. J., & Taylor, J. G. (2000). Neural modeling and functional brain imaging: an overview. *Neural Netw*, *13*(8-9), 829–846.

Horwitz, B., & Tagamets, M. A. (1999). Predicting human functional maps with neural net modeling. *Hum Brain Mapp*, *8*(2-3), 137–142.

Hubel, D. H., & Wiesel, T. N. (1959, Oct). Receptive fields of single neurones in the cat's striate cortex. *J Physiol*, *148*, 574–591.

Hubel, D. H., & Wiesel, T. N. (1968, Mar). Receptive fields and functional architecture of monkey striate cortex. *J Physiol*, *195*(1), 215–243.

Hubel, D. H., & Wiesel, T. N. (1974, Dec). Sequence regularity and geometry of orientation columns in the monkey striate cortex. *J Comp Neurol*, *158*(3), 267–293. Available from `http://dx.doi.org/10.1002/cne.901580304`

Huk, A. C., Dougherty, R. F., & Heeger, D. J. (2002, Aug). Retinotopy and functional subdivision of human areas mt and mst. *J Neurosci*, *22*(16), 7195–7205. Available from `http://dx.doi.org/20026661`

Huxley, A. F. (2002, Jan). Hodgkin and the action potential 1935-1952. *J Physiol*, *538*(Pt 1), 2.

Kiebel, S. J., David, O., & Friston, K. J. (2006, May). Dynamic causal modelling of evoked responses in eeg/meg with lead field parameterization. *Neuroimage*, *30*(4), 1273–1284. Available from `http://dx.doi.org/10.1016/j.neuroimage.2005.12.055`

Kiebel, S. J., Garrido, M. I., & Friston, K. J. (2007, Jun). Dynamic causal modelling of evoked responses: the role of intrinsic connections. *Neuroimage*, *36*(2), 332–345.

Available from http://dx.doi.org/10.1016/j.neuroimage.2007.02.046

Kiebel, S. J., Klöppel, S., Weiskopf, N., & Friston, K. J. (2007, Feb). Dynamic causal modeling: a generative model of slice timing in fmri. *Neuroimage*, *34*(4), 1487–1496. Available from http://dx.doi.org/10.1016/j.neuroimage.2006.10.026

Kimmig, H., Greenlee, M. W., Gondan, M., Schira, M., Kassubek, J., & Mergner, T. (2001, Nov). Relationship between saccadic eye movements and cortical activity as measured by fmri: quantitative and qualitative aspects. *Exp Brain Res*, *141*(2), 184–194. Available from http://dx.doi.org/10.1007/s002210100844

Kimmig, H., Greenlee, M. W., Huethe, F., & Mergner, T. (1999, Jun). Mr-eyetracker: a new method for eye movement recording in functional magnetic resonance imaging. *Exp Brain Res*, *126*(3), 443–449.

Knight, B. W. (1972, Jun). Dynamics of encoding in a population of neurons. *J Gen Physiol*, *59*(6), 734–766.

Komatsu, H., & Wurtz, R. H. (1988a, Aug). Relation of cortical areas mt and mst to pursuit eye movements. iii. interaction with full-field visual stimulation. *J Neurophysiol*, *60*(2), 621–644.

Komatsu, H., & Wurtz, R. H. (1988b, Aug). Relation of cortical areas mt and mst to pursuit eye movements. i. localization and visual properties of neurons. *J Neurophysiol*, *60*(2), 580–603.

Krauzlis, R. J. (2004, Feb). Recasting the smooth pursuit eye movement system. *J Neurophysiol*, *91*(2), 591–603. Available from http://dx.doi.org/10.1152/jn.00801.2003

Krauzlis, R. J. (2005, Apr). The control of voluntary eye movements: new perspectives. *Neuroscientist*, *11*(2), 124–137. Available from http://dx.doi.org/10.1177/1073858404271196

Krauzlis, R. J., & Stone, L. S. (1999, Dec). Tracking with the mind's eye. *Trends*

Neurosci, *22*(12), 544–550.

Lee, L., Friston, K., & Horwitz, B. (2006, May). Large-scale neural models and dynamic causal modelling. *Neuroimage*, *30*(4), 1243–1254. Available from http://dx.doi.org/10.1016/j.neuroimage.2005.11.007

Leigh, R., & Zee, D. (2006). *The neurology of eye movements* (4th ed.). New York: Oxford University Press.

Levenberg, K. (1944). A method for the solution of certain problems in least squares. *Quarterly of Applied Mathematics*, *2*, 164-168.

Lisberger, S. G., Morris, E. J., & Tychsen, L. (1987). Visual motion processing and sensory-motor integration for smooth pursuit eye movements. *Annu Rev Neurosci*, *10*, 97–129. Available from http://dx.doi.org/10.1146/annurev.ne.10.030187.000525

Logothetis, N. K., Pauls, J., Augath, M., Trinath, T., & Oeltermann, A. (2001, Jul). Neurophysiological investigation of the basis of the fmri signal. *Nature*, *412*(6843), 150–157. Available from http://dx.doi.org/10.1038/35084005

Lynch, J. C., & Tian, J.-R. (2005). Cortico-cortical networks and cortico-subcortical loops for the higher control of eye movements. *Prog Brain Res*, *151*, 461–501. Available from http://dx.doi.org/10.1016/S0079-6123(05)51015-X

Malsburg, C. von der, & Schneider, W. (1986). A neural cocktail-party processor. *Biol Cybern*, *54*(1), 29–40.

Marquardt, D. (1963). An algorithm for least-squares estimation of nonlinear parameters. *SIAM Journal on Applied Mathematics*, *11*, 431-441.

Marreiros, A. C., Daunizeau, J., Kiebel, S. J., & Friston, K. J. (2008, Aug). Population dynamics: variance and the sigmoid activation function. *Neuroimage*, *42*(1), 147–157. Available from http://dx.doi.org/10.1016/j.neuroimage.2008.04.239

Marreiros, A. C., Kiebel, S. J., & Friston, K. J. (2008, Jan). Dynamic causal modelling for fmri: a two-state model. *Neuroimage*, *39*(1), 269–278. Available from

http://dx.doi.org/10.1016/j.neuroimage.2007.08.019

McAdams, C. J., & Maunsell, J. H. (1999, Jan). Effects of attention on orientation-tuning functions of single neurons in macaque cortical area v4. *J Neurosci*, *19*(1), 431–441.

McKeown, M. J., Hansen, L. K., & Sejnowsk, T. J. (2003, Oct). Independent component analysis of functional mri: what is signal and what is noise? *Curr Opin Neurobiol*, *13*(5), 620–629.

McKeown, M. J., & Sejnowski, T. J. (1998). Independent component analysis of fmri data: examining the assumptions. *Hum Brain Mapp*, *6*(5-6), 368–372.

Mechelli, A., Penny, W. D., Price, C. J., Gitelman, D. R., & Friston, K. J. (2002, Nov). Effective connectivity and intersubject variability: using a multisubject network to test differences and commonalities. *Neuroimage*, *17*(3), 1459–1469.

Mechelli, A., Price, C. J., Noppeney, U., & Friston, K. J. (2003, Oct). A dynamic causal modeling study on category effects: bottom-up or top-down mediation? *J Cogn Neurosci*, *15*(7), 925–934.

Missal, M., & Heinen, S. J. (2001, Nov). Facilitation of smooth pursuit initiation by electrical stimulation in the supplementary eye fields. *J Neurophysiol*, *86*(5), 2413–2425.

Missal, M., & Heinen, S. J. (2004, Aug). Supplementary eye fields stimulation facilitates anticipatory pursuit. *J Neurophysiol*, *92*(2), 1257–1262. Available from http://dx.doi.org/10.1152/jn.01255.2003

Moore, T., & Armstrong, K. M. (2003, Jan). Selective gating of visual signals by microstimulation of frontal cortex. *Nature*, *421*(6921), 370–373. Available from http://dx.doi.org/10.1038/nature01341

Moore, T., Armstrong, K. M., & Fallah, M. (2003, Nov). Visuomotor origins of covert spatial attention. *Neuron*, *40*(4), 671–683.

Moore, T., & Fallah, M. (2004, Jan). Microstimulation of the frontal eye field and its

effects on covert spatial attention. *J Neurophysiol*, *91*(1), 152–162. Available from http://dx.doi.org/10.1152/jn.00741.2002

Motter, B. C. (1993, Sep). Focal attention produces spatially selective processing in visual cortical areas v1, v2, and v4 in the presence of competing stimuli. *J Neurophysiol*, *70*(3), 909–919.

Muggleton, N. G., Juan, C.-H., Cowey, A., & Walsh, V. (2003, Jun). Human frontal eye fields and visual search. *J Neurophysiol*, *89*(6), 3340–3343. Available from http://dx.doi.org/10.1152/jn.01086.2002

Muir, A. (1979, Aug). A simple case of the wilson-cowan equations. *Biophys J*, *27*(2), 267–275. Available from http://dx.doi.org/10.1016/S0006-3495(79)85216-9

Müri, R. M. (2005). Mri and fmri analysis of oculomotor function. *Prog Brain Res*, *151*, 503–526. Available from http://dx.doi.org/10.1016/S0079-6123(05)51016-1

Newsome, W. T., Wurtz, R. H., & Komatsu, H. (1988, Aug). Relation of cortical areas mt and mst to pursuit eye movements. ii. differentiation of retinal from extraretinal inputs. *J Neurophysiol*, *60*(2), 604–620.

Ogawa, S., Lee, T. M., Kay, A. R., & Tank, D. W. (1990, Dec). Brain magnetic resonance imaging with contrast dependent on blood oxygenation. *Proc Natl Acad Sci U S A*, *87*(24), 9868–9872.

Olson, C. R., & Gettner, S. N. (1995, Aug). Object-centered direction selectivity in the macaque supplementary eye field. *Science*, *269*(5226), 985–988.

Pack, C., Grossberg, S., & Mingolla, E. (2001, Jan). A neural model of smooth pursuit control and motion perception by cortical area mst. *J Cogn Neurosci*, *13*(1), 102–120.

Penny, W. D., Stephan, K. E., Mechelli, A., & Friston, K. J. (2004a, Jul). Comparing dynamic causal models. *Neuroimage*, *22*(3), 1157–1172. Available from http://dx.doi.org/10.1016/j.neuroimage.2004.03.026

Penny, W. D., Stephan, K. E., Mechelli, A., & Friston, K. J. (2004b). Mod-

elling functional integration: a comparison of structural equation and dynamic causal models. *Neuroimage*, *23 Suppl 1*, S264–S274. Available from http://dx.doi.org/10.1016/j.neuroimage.2004.07.041

Petit, L., & Haxby, J. V. (1999, Jul). Functional anatomy of pursuit eye movements in humans as revealed by fmri. *J Neurophysiol*, *82*(1), 463–471.

Pinel, J. P. (2000). *Biopsychology* (4th ed.). Needham Heights, MA, USA: Allyn & Bacon.

Polk, T. A., Drake, R. M., Jonides, J. J., Smith, M. R., & Smith, E. E. (2008, Dec). Attention enhances the neural processing of relevant features and suppresses the processing of irrelevant features in humans: a functional magnetic resonance imaging study of the stroop task. *J Neurosci*, *28*(51), 13786–13792. Available from http://dx.doi.org/10.1523/JNEUROSCI.1026-08.2008

Raftery, A. (1995). Bayesian model selection in social research. In P. Marsden (Ed.), *Sociological methodology* (pp. 111–196). Cambridge, MA, USA: Blackwell.

Rayner, K. (1998, Nov). Eye movements in reading and information processing: 20 years of research. *Psychol Bull*, *124*(3), 372–422.

Reynolds, J. H., Chelazzi, L., & Desimone, R. (1999, Mar). Competitive mechanisms subserve attention in macaque areas v2 and v4. *J Neurosci*, *19*(5), 1736–1753.

Reynolds, J. H., Pasternak, T., & Desimone, R. (2000, Jun). Attention increases sensitivity of v4 neurons. *Neuron*, *26*(3), 703–714.

Roelfsema, P. R., Lamme, V. A., & Spekreijse, H. (1998, Sep). Object-based attention in the primary visual cortex of the macaque monkey. *Nature*, *395*(6700), 376–381. Available from http://dx.doi.org/10.1038/26475

Roitman, J. D., & Shadlen, M. N. (2002, Nov). Response of neurons in the lateral intraparietal area during a combined visual discrimination reaction time task. *J Neurosci*, *22*(21), 9475–9489.

Rolls, E., & Deco, G. (2002). *Computational neuroscience of vision* (4th ed.). New

York: Oxford University Press.

Rosano, C., Krisky, C. M., Welling, J. S., Eddy, W. F., Luna, B., Thulborn, K. R., et al. (2002, Feb). Pursuit and saccadic eye movement subregions in human frontal eye field: a high-resolution fmri investigation. *Cereb Cortex*, *12*(2), 107–115.

Schiller, P. H., & Chou, I. (2000). The effects of anterior arcuate and dorsomedial frontal cortex lesions on visually guided eye movements: 2. paired and multiple targets. *Vision Res*, *40*(10-12), 1627–1638.

Schiller, P. H., & Tehovnik, E. J. (2005). Neural mechanisms underlying target selection with saccadic eye movements. *Prog Brain Res*, *149*, 157–171. Available from http://dx.doi.org/10.1016/S0079-6123(05)49012-3

Shadlen, M. N., & Newsome, W. T. (2001, Oct). Neural basis of a perceptual decision in the parietal cortex (area lip) of the rhesus monkey. *J Neurophysiol*, *86*(4), 1916–1936.

Stein, R. B. (1967, Jan). Some models of neuronal variability. *Biophys J*, *7*(1), 37–68. Available from http://dx.doi.org/10.1016/S0006-3495(67)86574-3

Stephan, K. E. (2004, Dec). On the role of general system theory for functional neuroimaging. *J Anat*, *205*(6), 443–470. Available from http://dx.doi.org/10.1111/j.0021-8782.2004.00359.x

Stephan, K. E., Marshall, J. C., Penny, W. D., Friston, K. J., & Fink, G. R. (2007, Mar). Interhemispheric integration of visual processing during task-driven lateralization. *J Neurosci*, *27*(13), 3512–3522. Available from http://dx.doi.org/10.1523/JNEUROSCI.4766-06.2007

Stephan, K. E., Penny, W. D., Marshall, J. C., Fink, G. R., & Friston, K. J. (2005, Dec). Investigating the functional role of callosal connections with dynamic causal models. *Ann N Y Acad Sci*, *1064*, 16–36. Available from http://dx.doi.org/10.1196/annals.1340.008

Stephan, K. E., Weiskopf, N., Drysdale, P. M., Robinson, P. A., & Friston, K. J. (2007,

Nov). Comparing hemodynamic models with dcm. *Neuroimage*, *38*(3), 387–401. Available from `http://dx.doi.org/10.1016/j.neuroimage.2007.07.040`

Tagamets, M. A., & Horwitz, B. (1998, Jun). Integrating electrophysiological and anatomical experimental data to create a large-scale model that simulates a delayed match-to-sample human brain imaging study. *Cereb Cortex*, *8*(4), 310–320.

Tagamets, M. A., & Horwitz, B. (2000). A model of working memory: bridging the gap between electrophysiology and human brain imaging. *Neural Netw*, *13*(8-9), 941–952.

Tanaka, M., & Lisberger, S. G. (2002a, Jun). Role of arcuate frontal cortex of monkeys in smooth pursuit eye movements. i. basic response properties to retinal image motion and position. *J Neurophysiol*, *87*(6), 2684–2699.

Tanaka, M., & Lisberger, S. G. (2002b, Jun). Role of arcuate frontal cortex of monkeys in smooth pursuit eye movements. ii. relation to vector averaging pursuit. *J Neurophysiol*, *87*(6), 2700–2714.

Tehovnik, E. J., Sommer, M. A., Chou, I. H., Slocum, W. M., & Schiller, P. H. (2000, Apr). Eye fields in the frontal lobes of primates. *Brain Res Brain Res Rev*, *32*(2-3), 413–448.

Trappenberg, T. P. (2002). *Fundamentals of computational neuroscience.* Oxford, UK: Oxford University Press.

Tremblay, L., Gettner, S. N., & Olson, C. R. (2002, Jan). Neurons with object-centered spatial selectivity in macaque sef: do they represent locations or rules? *J Neurophysiol*, *87*(1), 333–350.

Treue, S., & Maunsell, J. H. (1999, Sep). Effects of attention on the processing of motion in macaque middle temporal and medial superior temporal visual cortical areas. *J Neurosci*, *19*(17), 7591–7602.

Vallines, I., & Greenlee, M. W. (2006, May). Saccadic suppression of retinotopically localized blood oxygen level-dependent responses in human pri-

mary visual area v1. *J Neurosci*, *26*(22), 5965–5969. Available from http://dx.doi.org/10.1523/JNEUROSCI.0817-06.2006

Wang, Y. (2007). Maximum likelihood computation based on the fisher scoring and gauss-newton quadratic approximations. *Computational Statistics & Data Analysis*, *51*(8), 3776-3787. Available from http://dx.doi.org/10.1016/j.csda.2006.12.037

Wardak, C., Olivier, E., & Duhamel, J.-R. (2002, Nov). Saccadic target selection deficits after lateral intraparietal area inactivation in monkeys. *J Neurosci*, *22*(22), 9877–9884.

Wilson, H. R., & Cowan, J. D. (1972, Jan). Excitatory and inhibitory interactions in localized populations of model neurons. *Biophys J*, *12*(1), 1–24. Available from http://dx.doi.org/10.1016/S0006-3495(72)86068-5

Womelsdorf, T., Anton-Erxleben, K., & Treue, S. (2008, Sep). Receptive field shift and shrinkage in macaque middle temporal area through attentional gain modulation. *J Neurosci*, *28*(36), 8934–8944. Available from http://dx.doi.org/10.1523/JNEUROSCI.4030-07.2008

Wong, K.-F., & Wang, X.-J. (2006, Jan). A recurrent network mechanism of time integration in perceptual decisions. *J Neurosci*, *26*(4), 1314–1328. Available from http://dx.doi.org/10.1523/JNEUROSCI.3733-05.2006

Acknowledgements

In this thesis the work of 5 years is outlined. I thank Prof. Dr. Mark William Greenlee for the opportunity to enter this amazing scientific field, furthermore I also thank him for his patience in these years. Dr. Ignacio Vallines and Dr. Roland Rutschmann helped me to understand fMRI physics and GLM analysis and how to avoid the pitfalls there and they have been a great company in these years. Dr. Oliver Baumann and M.A. Katharina Rosengarth have been dear and valued colleagues who helped to get the first years going by exchanging hints how to operate the MRT scanner during long scanning sessions. Dipl. Psych. Markus Raabe is a true master in designing and implementing experiments and in the art of judging a book not only by its cover, a source of inspiration and a dear friend. Dipl. Math. Volker Fischer joined me in the mission to understand DCM and provided me insights in the deeper mathematical foundations. Prof. Dr. Gustavo Deco was a kind host and allowed me to visit his lab and gave me deep insights in the theories behind neurocomputational approaches. Cand. Psych. Philipp Spachtholz joined me in the last year of this project and is a bright and ambitious student and was a great inspiration in the field of neurocomputational modeling with his questions and ideas.

In the private field my parents, Dipl. Ing. Emmerich Imre Acs and Magdalena Acs, were a source of warm and constant support, always pointing out the importance of keeping the goal focused. My bachelor years were unexpectedly ended by my wife Yinjiao He, who gave me all the support and love she could during the last months of this project, when I condensed the results of five years in these pages.

Thank you all!

Statutory Declaration

Hereby I, Ferenc Acs, born on the 11'th of August 1971 in Zagreb, Croatia, declare that I wrote this dissertation without any help of third parties and without using any other aid than stated, that this dissertation was neither presented in equal not in similar form to another examining board at any other university, and that I cited all sources that were used respecting current academic rules.

Regensburg, 10'th of June 2009

Creative Commons License